Abstract

MILLER, PHILIP ROCCO. Transdermal Electrochemical Sensing and Biosensing with Hollow Microneedles. (Under the direction of Dr. Roger J Narayan.)

Wearable sensors have emerged from a next generation idea to commercially available products that monitor sleep patterns, daily activity, and vital signs. In order for these devices to provide clinical information regarding the state of one's health acquisition and characterization of biological fluid is essential thus necessitating access to the *in vivo* space. Currently, invasive methods provide a means to acquire biological fluid such as the finger pricking method however microneedle technology has proven to be an effective minimally invasive method accessing the intradermal space. This technology was developed for enhancing transdermal drug delivery by creating bores within the skin with microscopic needles for delivering a diverse range of pharmaceuticals, which are normally restricted due to the skin's stratum corneum. As the field has matured new microneedle types have been created to improve drug delivery and the number of successful clinical results has grown, however most of the studies have focused on using microneedles only for drug delivery. Prior to this work, a few groups studied using microneedles for acquiring interstitial fluid within the skin for sensing applications while taking advantage of their minimally invasive nature however these studies focused on using commercially available glucose test strips for detection and measurements were not made on the body and largely were not quantitative.

Using these early microneedle sensing studies as motivation I investigated new fabrication techniques for assembling electrochemical electrodes within hollow microneedle arrays to detect analytes in the skin and obviate the need for extraction of interstitial fluid. Individual electrochemical sensors were placed within single hollow microneedles made via a microstereolithography system and their surface was modified to

selectively detection ascorbic acid and hydrogen peroxide. As the sensing platform became more sophisticated with the introduction of new sensing elements (enzymatic carbon pastes, porous carbon, and porous graphene) and incorporation of microfluidic chips, a range analytes were capable of being selectively detected such as glucose, lactate, pH, and potassium. New biocompatible coatings and a novel hollow microneedle array molding method were created for improved microneedle performance and scalability; and an automated assay was developed for a device that could function without user intervention for detection of a known cardiac biomarker.

Transdermal Electrochemical Sensing and Biosensing with Hollow Microneedles

by
Philip Rocco Miller

A dissertation submitted to the Graduate Faculty of
North Carolina State University
in partial fulfillment of the
requirements for the Degree of
Doctor of Philosophy

Biomedical Engineering

Raleigh, North Carolina

2015

APPROVED BY:

_____	_____
Dr. Oliver Adunka	Dr. Albert Banes
_____	_____
Dr. Nancy Monteiro-Riviere GSR and Committee Member	Dr. Harold Pillsbury
_____	_____
Dr. Roger Narayan Chair	Dr. Ronen Polsky

Dedication

To my family for there never ending love and support!

Biography

Philip Rocco Miller was born on April 23, 1984 in Ann Arbor, Michigan to his loving parents Jane and Sam Miller. As he grew he developed an interest in how things functioned and loved disassembling old appliances in his parent's carport and trying to rebuild them. Sports were another passion of his and following being the starting shortstop for the two time AAU North Carolina state champions he was offered a Division-1 athletic scholarship at NC&T, which is where he began his coursework in mechanical engineering. After transferring to North Carolina State University following his first year to focus on school he pursued internships in aeronautical engineering, naval architecture, and industrial energy assessment prior to working as an undergraduate researcher in Dr. Narayan's lab for testing coatings for medical implant applications. Entering graduate school for biomedical engineering he learned two-photon polymerization utilizing laser direct write during a 6-month stint at the Laser Institute of Hannover in Hannover Germany. The following summer he interned at Sandia National Laboratories in Albuquerque, New Mexico, which brought him to the world of wearable sensors, where he is currently employed.

Acknowledgements

I'd first like to thank my parents for instilling the importance of education and their constant support throughout all the stages of my life. Without you none of this would have been possible. To my sister Alice, you're not only my little sister but my life-long best friend. Thanks for your never end pursuit of getting me to calm down by teasing me. To my brother Sammy who provides me with the motivation and happy memories anytime I need a push, I'll always be your irmão mais velho.

Dr. Narayan, thank you for giving a bored undergrad an opportunity to learn something new. I came to you with an interest to learn, a lot of passion, and not a lot of experience and you gave me an opportunity. I loved my time working in your lab and I'm thankful for you being a never-ending resource. I loved my time in Raleigh, Germany, and at Sandia and without you those experiences wouldn't have been possible. I appreciate everything you've provided me and I hope someday I can provide the same to another young student interested in research.

To my committee members, I appreciate your participation and each of your successes provides an ambitious goal for my own career. As a young graduate student we are taught to fear the prelims, qualifiers, and final defense however in my experience these events while nerve-racking and rigorous has been incredibly rewarding due to your insight, expertise, and experience.

To Ryan and Shelby, you've been excellent friends since the moment we met. I loved the time we spent together in and out of the lab, and I look forward to the future occasions where our paths will cross. They're so many memories I have that make me laugh out loud from our time together. I wish you both the best of luck and look forward to our continued friendship.

Sandia National Laboratories is where I've spent the majority of my time over the last few years and I'm appreciative of many people there. I came to Albuquerque to continue to grow as a researcher and without many expectations and left with great memories, great friends, and a wealth of experience and knowledge. To Thayne Edwards, Matt Moorman, DeAnna Lopez, Dulce Hayes, Igal Brener, Dave Wheeler, Ryan Hess, Darren Branch, Leah Applehans, Xiaoyin Xiao, Steve Casalnuovo, Lisa Garcia, and Kaylee Parchert I'm thankful for your friendship, mentorship, general help and great attitude, and putting up with my messy desk. Ronen, you're a huge part of why I'm so proud of the work in this thesis. I love coming to work every day and love the conversations we have regarding work and life. I'm also hugely appreciative of your wiliness to indulge my crazy ideas and being patient with me over the years. Susan you were like a big sister to me and I'll never forget all the memories I have of you. So many times I walked into your office with the weight of the world on my back I'd get advice on work, relationships, or anything that was on my mind and I'd leave a new person. Thank you.

Last but not least, to my lovely partner Elisa. After thirty years of life I had a fairly pessimistic view of the world and after meeting you, you created a happiness in me that I didn't think was possible. Your patience, love, passion, and good nature make me want to be a better human being and I look forward to a lifetime with you. If you can survive living with me for the last year of my thesis and taking 25hour flight to Bali with me, I think you may just be able to withstand me forever. I love you.

Table of Contents

List of Tables

List of Figures

Chapter 1 Introduction

This dissertation details the design, fabrication, and testing of microneedle-based wearable devices designed to extract biological fluid from the skin, selectively detect biomarkers within the fluid, and report their concentration via electrochemical measurements. This chapter discussion the research areas used to create this interdisciplinary device.

Rapid Prototyping

Rapid prototyping, which originated in the 1980's, is a type of fabrication system developed to create prototypes of a part, product, or design to improve the turn-around time and trouble shoot the final version of the product.[1] Prototypes are first designed with computer-aided design (CAD) software, such as SolidWorks, and then fabricated with a layer-by-layer approach where each layer corresponds to a layer of the computer design, as seen in Figure 1-1. Various rapid prototyping techniques exist and fall into two categories based on their mode for creating the prototype; additive or subtractive. Additive methods are characterized by the addition of materials to a stage or platform for fabrication of the prototype and UV polymerization, laser sintering , and printing are some of the common mechanisms used to deposit or cure the material being used.[2,3,4] With these methods there is a bulk solution of the material that is deposited or selectively cured in the layer-by-layer approach with one of the initiating sources (polymerization, printing, or sintering) transforming the precursors into the material forming each layer. Materials for polymerization methods are limited to polymers since they can be polymerized by free radical polymerization.[5] In this process the resin is made up of monomer units and photoinitiators, which absorb photons from the light source and creative free radicals, which initiate the polymerization process with the surrounding monomers, forming the

polymer chain as seen in Figure 1-3. Inkjet printing is performed in a couple of different modes with thermal deposition and UV-curing being the most common.[6,7] With the thermal deposition method a polymer is heated to its melting point then emitted from the nozzle in the desired location. For the UV curing method, a precursor solution is deposited then exposed to a UV lamp to complete the polymerization process. A diverse range of materials and entities can be deposited with inkjet printing and polymers, conducting polymers, ceramics, nanoparticles, cells, and biomolecules have all been deposited with inkjet printing.[8,9,10,11,12,13] Selective laser sintering operates, as its name suggest, by using a scanning laser to selectively sinter areas of a power, in the form of a polymer or metal, to transform that area into a functional layer of the part. Where inkjet printing is a free-form technique, in that it deposits material where necessary before moving to the next layer, selective laser sintering sinters one layer then drops the stage where the part is fabricated such that a new layer of precursor material (powder) can be spread over the previous layer (Figure 1-2). The process is then repeated until the part is complete.

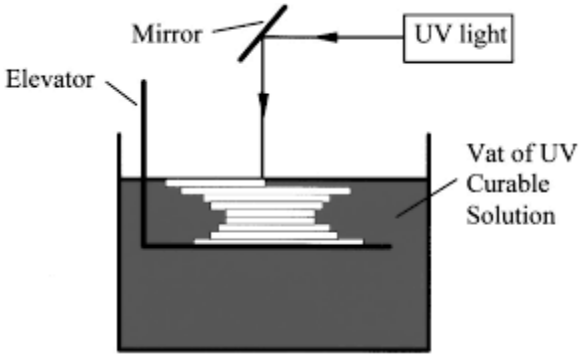

Figure 1-1: Cross-sectional schematic of a UV-based rapid prototyping system. Source: http://xlab.me.berkeley.edu/pdf/10.1063_1.1503410.pdf

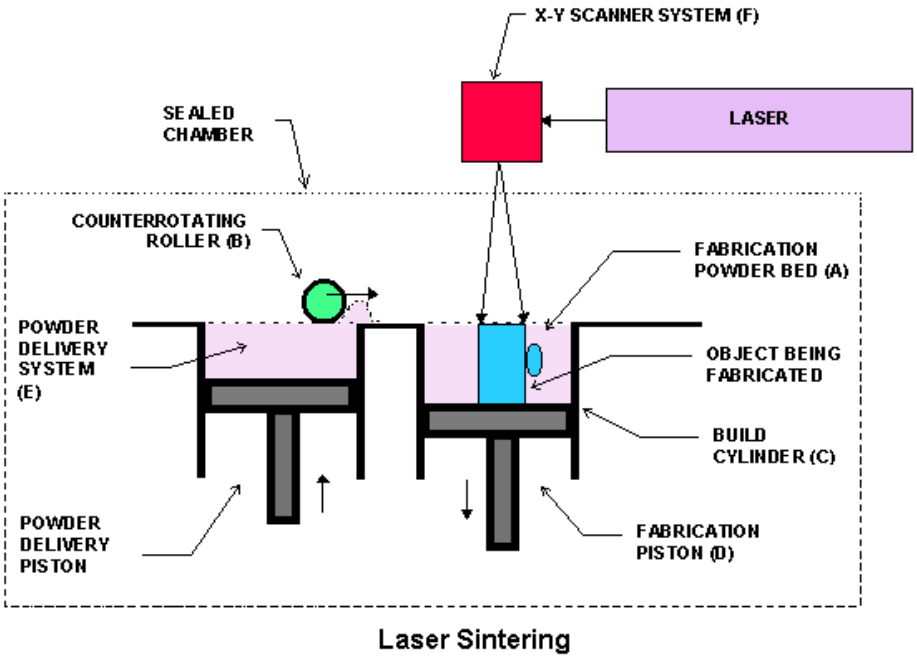

Figure 1-2: Schematic of selective laser sintering. Zoomed in inset shows the layer-by-layer fabrication approach and the adjacent precursor bin is used to provide a new layer of material to sinter to create the next layer. Source: http://www.additive3d.com/sls.htm

Subtractive methods are just the opposite from the additive approach in that prototypes are made from removal of material from a bulk part. Milling is the common method and in this technique the CAD file provides details of what area the mill needs to remove. [14] Additive systems are typically preferred due to their comparative minimum feature size and amount of wasted precursor material. As these technologies has progressed they've gone from creating prototypes that designers, engineers, and technicians can hold and discuss, to fabrication of structures that are capable of being tested and even in some cases used for the final product. As previously stated a diverse range of rapid prototyping systems exist for creation of prototypes however microstereolithography offers a simple system that provides suitable resolution, material biocompatibility, and material strength for making biomedical devices which this thesis will focus on.[15]

Microstereolithograhpy

A deconstruction of the term microstereolithography provides details into its begins and it originates from the German printing method "lithography", which was used to replicate artist's work while allowing them to use conventional means for creating a piece. Adding the Greek term "stereo", which is a reference to a solid item with three-dimensionality, Charles Hull named and created the first stereolithography system and patented the idea throughout the 1980's.[16] Microstereolithography is a continuation of Hulls' invention but is focused on making parts with feature sizes in the micron range using the additive process detailed in the previous section. UV-based radical polymerization is the additive mechanism and is defined in the figure below (Figure 1-3);

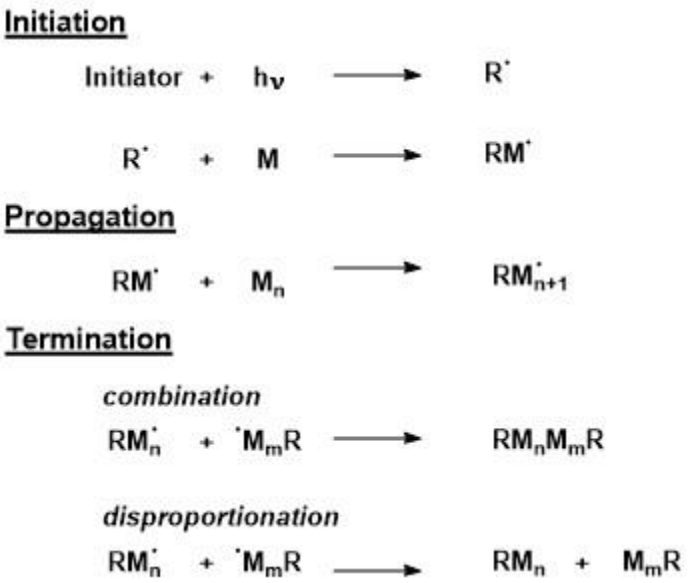

Figure 1-3: Schematic of free radical polymerization. Source: https://en.wikipedia.org/wiki/Photopolymer#/media/File:Free_rad_mech1.jpg

The photoinitiator, "R", absorbs photons from the UV light source "h_v" and creates radicals "R^*", which initiate bonding between adjacent monomer units "M". As more photoinitiators absorb light, more radicals are produced, adding monomers to the polymer chain "RM^*_{n+1}". In order to control the location of the polymerization process masks are used. The masks form a physical barrier that restricts the passage of light into the bulk resin thus

polymerizing certain areas and not others. Creation of 3D parts involves polymerizing in a layer-by-layer fashion such that the mask changes with each layer, depending on the contour of the part for that particular layer. Masks come in a variety of forms and one of the more prevalent and automated systems is the Dynamic Digital Mirror by Texas Instruments (Figure 1-4).[17] This device uses an array of thousands of tiny mirrors (16um x 16um) that are suspended just above a substrate so that they can rotate about one axis. Each mirror also has its own electrical connection such that when an electrical potential is applied the mirror is rotated relative to the substrate. When used in a stereolithography system the mirrors are positioned so they reflect light from the UV source into the resin or reflect the light away for the resin depending on the potential applied, thus not polymerizing the resin at that location. Essentially each mirror acts as a pixel in a 2D mask that changes depending on the design of the layer and can create structures in the micron region. The CAD file defines each of the layers and tells what mirrors to direct the light into the resin. This process has a nice degree of industrial scalability and is used in both research and industry applications and will been used throughout this thesis.

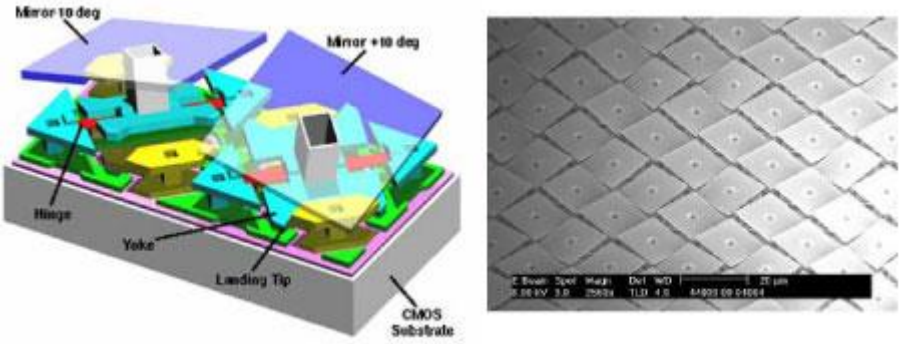

Figure 1-4: Schematic rendering of two digital micromirrors rotated in an "on" and "off" position (left) and a scanning electron micrograph of an array of micromirrors (right). Source: http://www.supernovalifescience.com/proddetail.php?prod=9000

Two-Photon Polymerization

Many commercially available UV-based rapid prototyping systems are designed for macro

scale fabrication and aren't capable of making parts entering the micron or sub-micron range. Even sophisticated, lab-built systems employing UV light have a limited feature size. Due to these issues groups have investigated alternative light sources applied to the methodology of microstereolithography and changing the light source offers unique capabilities a UV systems does not[18]. Using a pulsed Titanium: Sapphire laser, the polymerization process can happen within the resin as opposed to at the surface of the resin as is with the UV-based process (Figure 1-5). This allows the laser beam to travel freely within the resin for creation of the part and reduces a lot of the stage step-height dependence on resulting part resolution. The difference between the light sources is that the Titanium: Sapphire system creates a multi-photon polymerization process as opposed to the single photon process found with UV-based systems. For this process to occur the total energy of the two-photons must be equivalent to the energy of a single photon absorbed by the photoinitiator in the UV region thus the wavelength of the light source is doubled to the near infrared (i.e. 780nm) such that the energy of the doubled wavelength photon is half that of the single photon in the UV region, which is the wavelength that most photoresists absorb. A comparison between the photochemical processes between one and two photon polymerization can be seen in Figure 1-6. There is however a definitive amount of time for the second photon to be absorbed once the first photon is absorbed by the photoinitiator at the intermediate state, which is why the beam is pulsed at an incredible rate (~140fs) and gives this class of lasers their name; "Femtosecond Lasers". Additionally, the beam must be focused to increase the photon density to ensure complete polymerization and locations outside the focal spot are not polymerized, thus allowing the beam to travel through the resin without unintentionally polymerizing in undesired areas as seen in Figure 1-6.

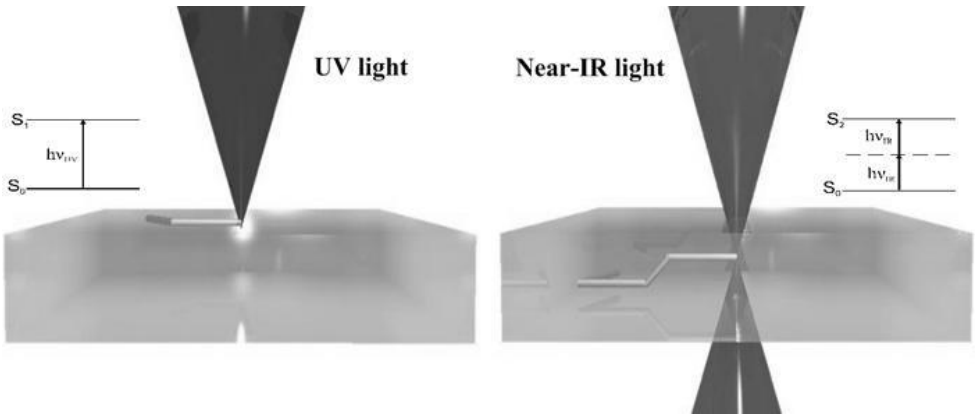

Figure 1-5: Comparison between UV based polymerization (left) and two-photon polymerization operating in the Near infrared region (right). Control of the location of the polymerization is dependent on the type of light source used. Source: http://www.asdn.net/asdn/nanotools/two-photon_polymerization.shtml

Combining these factors allows a highly localized photochemical polymerization to take place in standard UV resins and for creation of 3D parts the laser beam is scanned across the mask in a similar manner to the previously described UV-based approach.

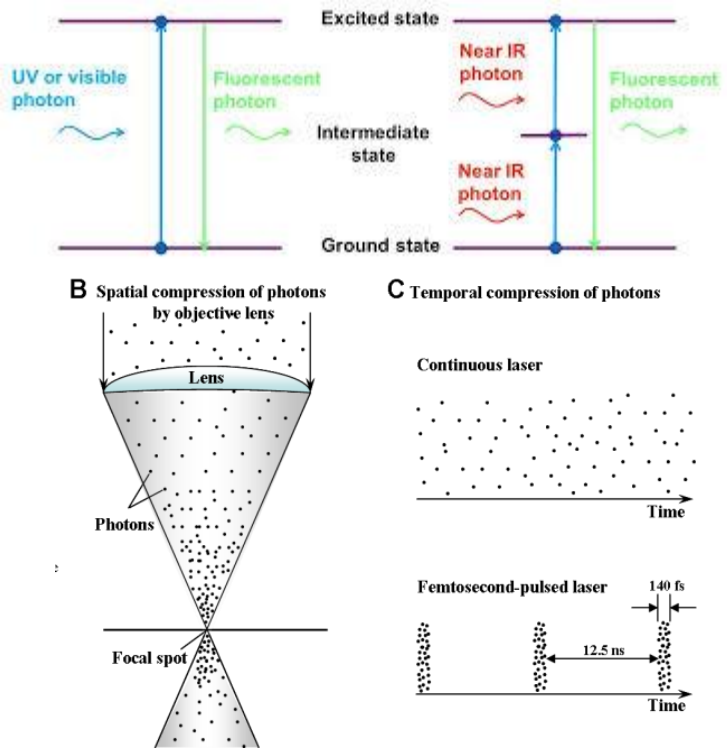

Figure 1-6: Schematic detailing the photochemical process for one and two photon polymerization (top), focal spot influence on polymerization, and comparison of photon spacing for pulsed laser system compared to continuous (bottom right).Source: http://www.intechopen.com/books/updates-in-advanced-lithography/recent-advances-in-two-photon-stereolithography

Electrochemistry

A major aspect to the field of wearable sensors and specifically to this dissertation is the ability to detect biomarkers in a rapid and selective manner and to perform this task electrochemistry will be used. A benefit to using this detection technique, as opposed to optical or acoustic detection, is that the components required for detection can fit within a device small enough to be worn on the body without imposing a significant strain on the user. Micro-potentiostat are available commercially that are about the size of an eraser

head and microelectrodes have been used extensively in-vivo and offer improved signal-to-noise ratios compared to their macro-electrode counterparts.[19]

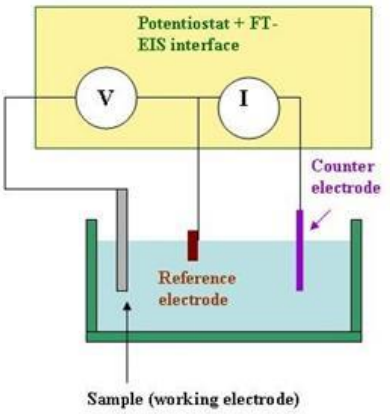

Figure 1-7: Schematic of a three-electrode electrochemical cell containing a working, reference, and counter electrode attached to a potentiostat. Source: http://people.clarkson.edu/~droy/Corrosion_EIS.htm

Electrochemistry is the study of chemical reactions taking place between the surface of an electrode and molecules in a solution.[20] When used for diagnostic measurements, detection of the analyte of interest happens through redox reactions between a molecule in solution and the surface of the electrode or via a byproduct of a biosensor at the surface of the electrode.[21] In a typical electrochemical measurement, three electrodes comprised the electrochemical cell as seen in Figure 1-7. The working electrode is where the measurements take place and its potential is measured against a reference electrode, which provides a stable potential during measurements. The third electrode, the auxiliary or counter electrode, matches the potential of the working electrode and provides a stable current such that the reference electrode doesn't have to provide a comparable potential and current. Two-electrode systems have been used however are more susceptible to noise since both the potential and the current are measured against the reference electrode. The construction and material of each of the electrode in the cell is essential to performing

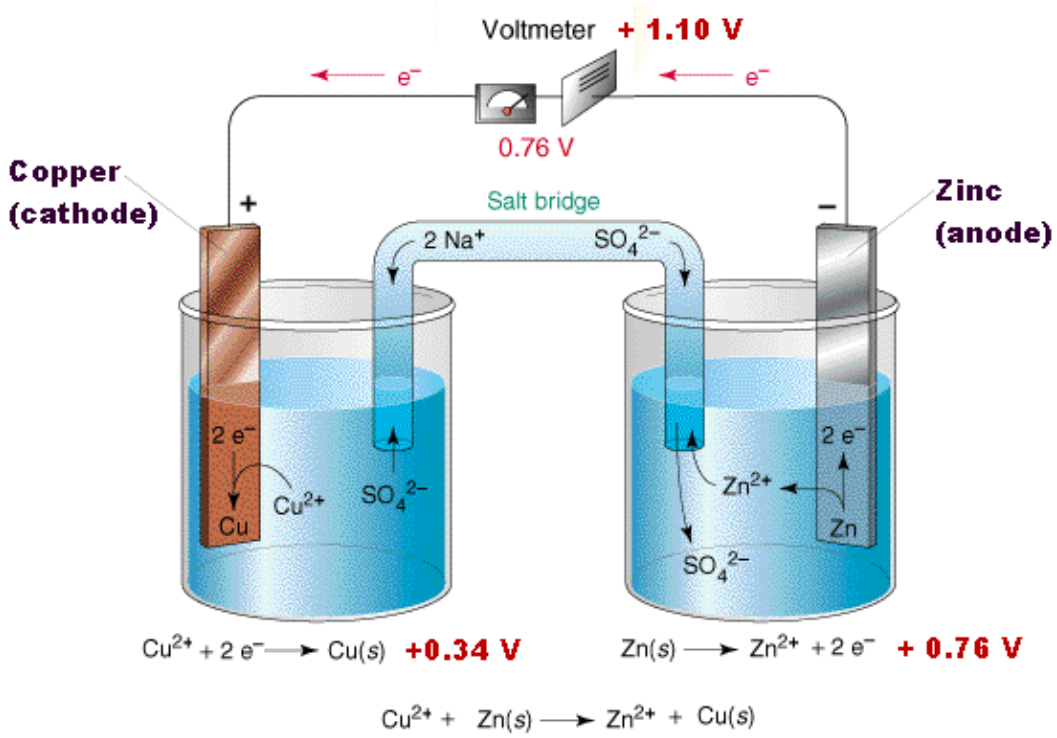

Figure 1-8: Schematic of a galvanic cell detailing each side of the electrochemical cell. A zinc anode and copper cathode are placed in separate solutions with an electrical connector between them and a salt bridge connecting the solutions. A potential difference in generator between the electrodes due to spontaneous redox reactions taking place between the surface of the electrodes and the components of the half cells. Source: http://chemwiki.ucdavis.edu/Analytical_Chemistry/Electrochemistry/Electrochemistry_2%3A_Galvanic_cells_and_Electrodes

accurate measurements however the reference and counter electrodes are generally not changed. The counter electrode must be an inert material such that it doesn't react with the solution and a platinum wire or mesh is considered standard. Additionally, the electrode must have a larger surface area compared to the working electrode such that the half reactions taking place at its surface to balance the redox reactions at the working electrode happen fast enough so as to not impede the reactions at the working electrode. The material choice for a reference electrode is more complex and is generally comprises of multiple components. To understand the design of the reference electrode it can be taught through the example of an electrochemical half-cell or a battery, which is just the complete cell

referred to as a galvanic cell as seen in Figure 1-8.[22] Galvanic cells operate based on spontaneous redox reactions that take place at the surface of an electrode. To generate and control this spontaneous reaction two half-cells are used, each containing two different metals within a solution of its own ion. When the electrodes are connected electrodes flow from the anode to the cathode and allow the continuous oxidation-reduction to take place while a salt bride is placed between the cells to balance the ion fluctuation happening within the cells. Each cell produces a potential difference due to the respected redox reaction and their sum is a reflection of the potential difference across the cell, which remains constant assuming the electrode material and solution don't change. This stable potential is the basis for creation of the reference electrode, which as previously mentioned needs to remain stable while reactions are taking place at the working electrode. The most common reference electrode is the Ag/AgCl reference due to its reliability, ease of fabrication, and lack of toxicity compared to older mercury based reference electrodes.[23] Generation of the AgCl coating on Ag wire performed in many ways however polishing the wire and exposing it to a chloride solution is among the more facile. In this form the wire can be used as a reference electrode however is susceptible to potential drift if the test solution fluctuates significantly in their chloride concentrations, which dissociate chloride from the AgCl layer coating the wire. To avoid this issue the wire is place in a saturated or near saturated (3M) solution of NaCl within a glass capillary that is only exposed to the test solution through a porous frit that limits the passage of ions but allows potential to pass through. Materials used for the working electrode are more diverse and typically depend on the analyte on interest however should have redox reactivity with the analyte and have a large potential window.

For biosensing applications the first consideration is whether the analyte is electrochemically active, meaning the analyte has some detectable redox reaction that can

be performed selectively. For instance, dopamine is a classic analyte detected via oxidation at the working electrode using voltammetry. Voltammetry is an electroanalytical technique where the potential of the working electrode is scanned between two potentials or from one potential to the next while monitoring the resulting current.[24] For instance, using bare carbon fiber electrodes dopamine can be detected and quantified in vivo without any surface modification.[25] When an analyte doesn't offer a selective electrochemical signal or any electrochemical signal, which is true for many proteins, a biosensor must be used. By definition a biosensor is a sensor that incorporates a biological molecule (e.g. enzyme, IgG, etc.) to aid in detection of the analyte.[26] A classic example of a biosensor is a glucose sensor. Glucose has no electrochemical activity, meaning scanning the potential of an electrode will not provide a selective redox reaction in the presence of other known interferon's such as uric acid and acetaminophen, which are known to create false readings due to their similar oxidation potentials.[27] In the glucose biosensor an enzyme is used (glucose oxidase) to create byproducts that are electrochemically detected due to the enzymatic oxidation of glucose into hydrogen peroxide and gluconic acid. Depending on the sensors system hydrogen peroxide is either reduced or oxidized for generation of a signal or aids in cycling an electrochemical mediator to generate a signal.

Microneedles

Microneedles were initially created by Mark Prausnitz and Mark Allen in the late 1990's at Georgia Tech as a means to improve topical drug delivery of large molecular weight compound through the skin, which are normally blocked due to the body's natural barrier (stratum corneum) to its external environment.[28] The skin is a multilayer organ that has a range of roles in maintaining homeostasis including heat regulation, gas exchange, and as mentioned a barrier to harmful substances that may enter the body.[29] While the skin

allows for exchange of fluids in order to assist with hydration and heat regulation it restricts passage of large molecular weight compounds typically above 500Da.[30] This value is a general threshold since transdermal diffusion is a more complex process to characterize due to a range of physiochemical factors that contributing to determine diffusion. Smaller compounds, such as nicotine, had been delivered topically however macromolecules, such as vaccines, would benefit from an alternative delivery route to hypodermic injection, which causes pain to the user, adds to the growing population that has a fear of syringes, and cannot be administered orally due to GI tract degradation.[31,32] The first microneedles (Figure 1-9) sought to puncture the stratum corneum such that temporary access points would exist in the skin for delivery of compounds that would not normally diffuse without the microneedle pretreatment.[28] Using standard silicon microfabrication techniques arrays of solid microneedles were created and applied cadaver human skin. After application and removal of the microneedle arrays a solution of calcein, which is a dye with poor permeability across human skin. Following a period of incubation skin samples were compared for diffusion of the calcein with and without the microneedle treatment and microneedle treated skin was shown to significantly increase the passage compound across the skin.

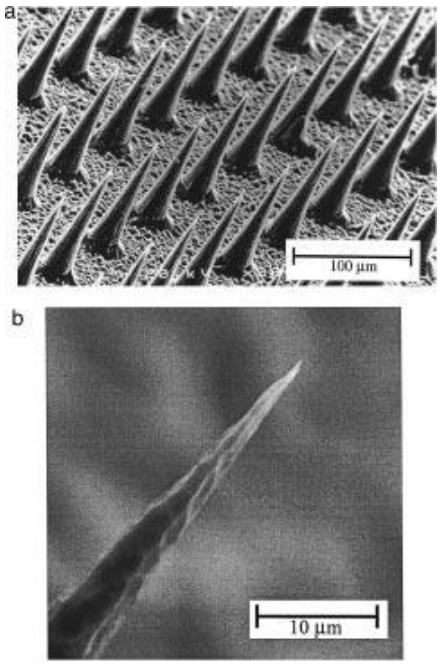

Figure 1-9: Scanning electron micrograph images solid microneedle arrays (a) and single solid microneedle (b) from the first microneedle study. Source: http://www.google.com/patents/US6503231

In follow up papers their collaboration showed that due to the size of the microneedles they didn't cause pain to the users specifically because they were short enough to not interact with deeper layers of the skin that had higher concentrations of nerve endings than layers closer to the surface of the skin.[33] Since those early studies a wealth of studies have been performed on microneedles for drug delivery applications and recently were shown to improve the immune response of mice exposed to the flu with improved immune response to reacquiring the virus.[34,35] While drug delivery is the main area where microneedles are being explored they're becoming used in a few other interesting areas. Multiple groups have shown that they can be used as tissue sutures for minimally invasively bonding of tissue.[36,] Metal microneedles have been used for improved ECG measurements and were shown to have improve signal to noise measurements when compared to commercially available sensors due to their ability to interact with the intradermal space and reduce the resistance found across the skin.[37,38] The Prausnitz group used microneedles years ago for sensing

applications but few other groups have performed similar experiments since then.[39] However a recent increase in interest has brought microneedle sensors back as an appealing method for transdermal sensing.

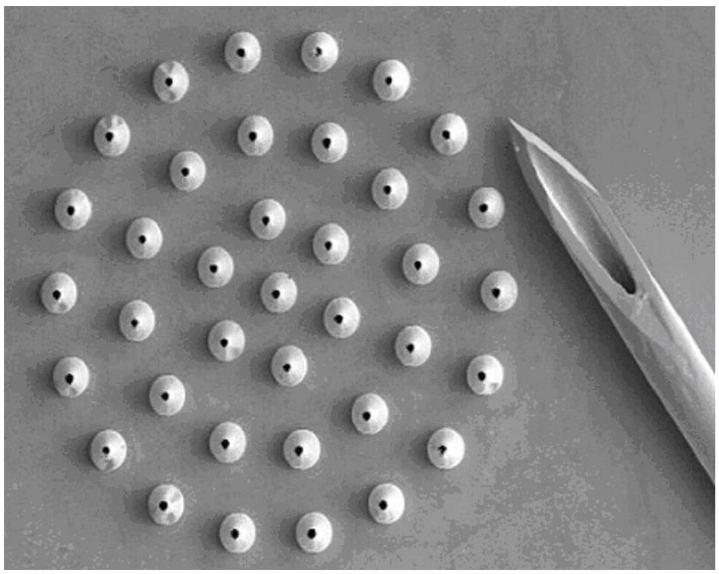

Figure 1-10: Scanning electron micrograph of an array of hollow microneedles compared to a standard syringe tip. Source: http://drugdelivery.chbe.gatech.edu/gallery_microneedles.html

Microneedle-Based Sensing

Transdermal sensing has blossomed into a novel technology for acquiring vital clinical information for point-of-care diagnostic devices.[40] Many techniques and devices have been created for detection, and recently microneedles have been investigated as POC devices.[41] Other transdermal sensing modalities exist such as reverse iontophoresis, which doesn't compromise the integrity of the skin, however is limited to small molecules that can diffuse across the stratum corneum with the external applied force.[42] More invasive techniques can acquire larger biomolecules however are not self-administrable (microdialysis) or create a wound (blister method) compared to affect microneedles have on the skin.[43,44] Other biological fluid sources have been explored for diagnostics, such as tears and saliva; however correlation with clinically accepted blood concentration and

collection of the sample remain some of the challenges.[45,46,47] Multiple mechanisms exist for using microneedles to detect analytes and usually fall within the one of the following methods; extraction of fluid (interstitial or blood) for on-body or off-body analysis, in vivo detection using microneedles as electrodes, or using the microneedles as probes for capturing and extracting circulating entities (Figure 1-11). This literature review will cover the early work in the field and touch on some of the recent studies, including clinical studies that have been performed. Mukerjee et al was one of the first groups to study arrays of microneedles for sensing.[48] Hollow silicon microneedles arrays were fabricated with standard wet etching techniques and arrays were integrated over a microfluidic channel for filling the channels with both biological and non-biological fluids via capillary action. Hollow microneedles heights varied between 250um and 300um with 300um needle-to-needle spacing. Interstitial fluid extraction from human subjects was investigated and bore placement relative to the needle tip was shown to impact fluid extraction. Needles with a "snake-fang" design, where the needle bore was offset from the tip, were shown to extract fluid and were believed to avoid bore occlusion from dermal tissue due to the position of the bore relative to the tip. Microneedles with bores concentric about the needle tip were not capable of extracting fluid when placed against a human subject's ear and were susceptible to clogging of dermal tissue however they were capable of extracting fluid from a blister. Snake-fang needles, when placed against a human subject's ear, extracted interstitial fluid with only capillary action and saturated a commercially available colorimetric glucose strip residing in the fluidic channel, revealing the glucose concentration to be in the 80-120 mg/dl range, which correlated to the concentration of glucose found in the subjects blood at the same time point. Acquisition of interstitial fluid from the subject's ear took 20 minutes to fill the fluidic chamber and saturate the glucose detection strip. Around the same time as the previous study Zimmerman et al created a

hollow microneedle glucose sensor that used an in-device enzyme immobilization technique, which avoided thermal exposure of the enzyme during the wafer bonding process.[49] In their approach, hollow microneedles were theorized to allow interstitial fluid to diffuse through the needle bores and mix with dialysis fluid, which was pumped through a fluidic channel towards downstream electrodes. Prior to the on-chip three-electrode system, a dialysis membrane was placed within the channel to filter large proteins that cause electrode fouling and lessen the lifetime of the sensors. Additionally, an on-chip reservoir containing calibration fluid was integrated such that regular finger pricking wasn't necessary to calibrate the system. Glucose oxidase was immobilized by UV polymerization within a photosensitive polymer (PVA-SbQ) and UV exposure wasn't shown to affect the activity of glucose oxidase. Glucose was measured over a range of physiologically relevant concentrations and flow rate was optimized at 25 ul/min relative to sensor signal generation. When using an array of 8 (200um tall and 40um bore) microneedles on a human subjects finger the diffusion of glucose through the needles wasn't enough to produce a sustainable signal. The group theorized that larger arrays of microneedle would solve this problem. Following these early microneedle sensing studies, Wang et al used single or arrays of solid glass microneedles, made via thermal pulling, as a means to create bores in the skin to collect interstitial fluid in rat and human subjects via vacuum extraction.[50] Needle heights ranged from 700-1500um with tip radiuses of 15-40um. Following needle insertion and removal, a bell-jar connected to a vacuum was used to apply a negative pressure of 200-500 mm Hg to the microneedle treated area for between 2 and 10 minutes. At these operating conditions, 1- 10ul of interstitial fluid was extracted onto the surface of the skin of human subjects through bores created by microneedle application and was not considered a painful process by human subjects. Glucose was measured with commercially available glucose detection strips and

correlations were made with intravenous glucose concentrations taken with traditional finger pricking techniques. Slight lag times were noticed between glucose measurements made with microneedles and the finger pricking method (20 minutes) and these measurements showed good correlations with the Clark Error Grid analysis (95% for 15 rats and 100% for 6 human subjects). Based on the success of these early studies our group investigated incorporating electrochemical sensors and microfluidic chips with hollow microneedles to perform on-body analysis, create sophisticated sensing platforms, and detect entities which commercial strips aren't available or amenable to microsystem integration which will be discussed in detail in later chapters.[51,52,53,54]

Table 1: Microneedle sensing studies performed *in vivo*.

Analyte/Disease	Group	Animal Type and Location	MN Type	Detection Method	Detection Location
Glucose	*Murkerjee et al*[48]	Human ear	Hollow Si	Colorimetric	On-body
Nitric Oxide	*Keum et al*[55]	Mice Colon	PCL/PD/PEDOT	Electrochemical	In-body
Glucose	*Jina et al*[56]	Human forearm	Hollow Si	Electrochemical	On-body
Glucose	*Wang et al*[50]	Human forearm and rat skin	Glass	Electrochemical	Off-body
Dengue Fever Virus NS1	*Muller et al*[61]	Mouse skin	Antibody coated Au/Si solid MNs	Optical ELISA	Off-body
Glucose	*Sakaguchi et al*[57]	Human forearm	Solid PCL	Fluorescence	Off-body

The Kendall group pioneered another approach for using microneedles, which they refer to as microprojection arrays, as immunodiagnostic sensors.[58,59] Instead of extracting fluid from the skin for analysis, microneedle surfaces are functionalized with antigen specific antibodies and when inserted into the skin they selectively captured their antigen

specific biomarker for later off-body analysis. Arrays were created with gold coated silicon needles functionalized with carboxylated thiols and later polycarbonate microneedles were functionalized to explore fabrication techniques outside of the standard silicon processing modalities.[60] Functionality of the arrays was showcased in a mouse model by selectively detecting NS1, an early biomarker for dengue fever, and the detection capability was compared to standard serum assays utilizing ELISA.[61] Detection limit of the in skin acquisition with microneedles was 8 ug/ml, which compares favorably to detection levels of serum based clinical diagnostics assays. Their group has also studied the effect of needle size and application time on the skin for monitoring the effectiveness of a vaccine (Fluvax) and created a multiplexed platform for collection and detection of multiple biomarkers in a mouse model.[62,63] In a method similar to the early Prausnitz study on interstitial fluid extraction, Sakaguchi et al applied solid polycarbonate microneedle to the skin of human subjects with an applicator (applied at 6 m/s) to create bores in the skin and used a either a hydrogel patch or a plastic reservoir filled with a solvent (KCl solution) to collect interstitial fluid once needles were removed from the skin.[64] Calibration of the glucose extraction rates was determined by sodium ions since the rate of fluid uptake varied over the course of sampling. As seen in other microneedle studies, correlations were seen between intravenous glucose levels and interstitial fluid levels.

As previously discussed, hollow microneedles pose fabrication challenges and require unique geometries for extraction of interstitial fluid. In light of these challenges, the Donnelley group has developed hydrogel microneedles that offer unique capabilities for both drug delivery and sensing applications, due to their porous architecture, inherent fluid uptake, and biocompatibility.[65,66] The novelty of these needles for both sensing and delivery is their automatic uptake of interstitial fluid due to the swelling natural of hydrogels, once applied to the skin or a liquid environment, which avoids the need for pumping or

complex needle geometries. In addition these arrays can be fabricated with molding, which simplifies the fabrication process significantly. A clinical perspective study showed the use of these hydrogel microneedles arrays were well tolerated by adolescents for potential disease monitoring application and a human study was also perform for determining the rates of fluid extraction.[67] Utilizing a similar concept the Prausnitz group sought to extract interstitial fluid from mice using microneedles made from hydrogels.[68] Swelling of the cross-linked poly (methyl vinyl-alt-maleic acid) and PEG copolymer hydrogels were studied for their rates of fluid uptake. Methods were created to then collect the fluid from the hydrogel microneedle patches via centrifugation of the patches within the cap of a microcentrifuge tube. Experiments were also performed in live mice and detailed the ability to extract interstitial fluid into the hydrogel microneedles.

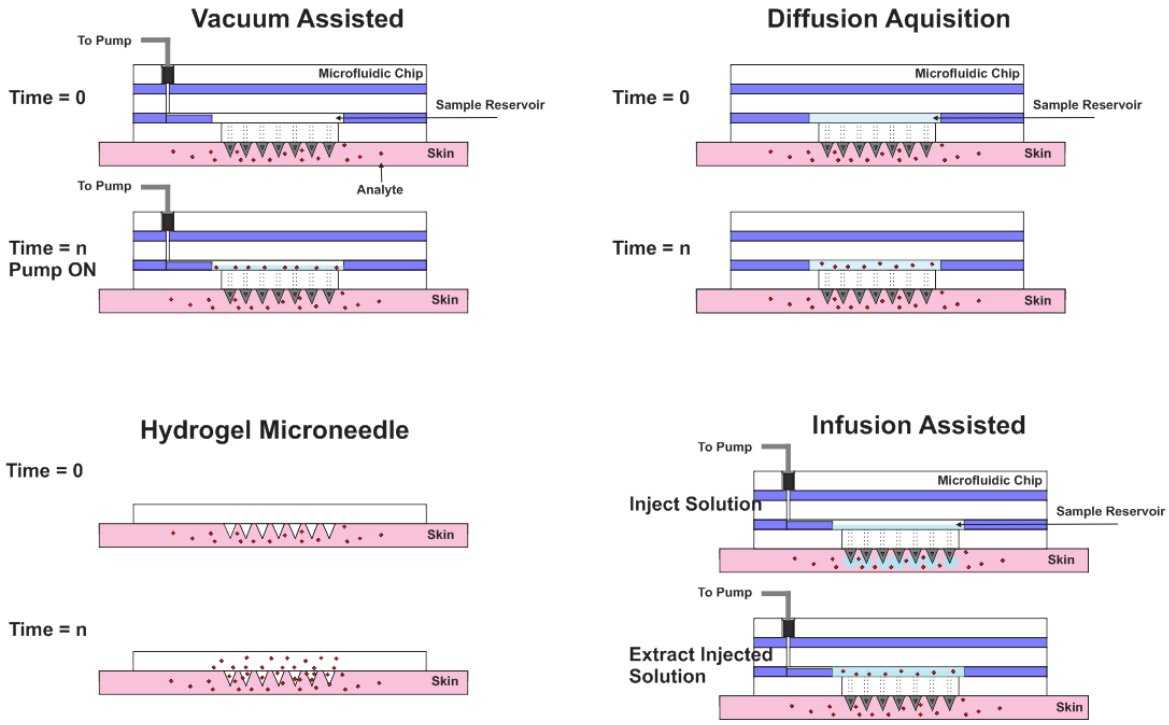

Figure 1-11: Schematic of extraction methods for collecting interstitial fluid using microneedles.

Continuing with the concept of turning microneedles into electrodes, Windmiller et al studied packing carbon pastes within hollow microneedles for creating enzymatic biosensors.[69] Pastes were packed such that they were encased within the bores so that extraction of fluid wasn't necessary. Rhodium on carbon was placed within the bores and was tested initially for reducing peroxide over a range of 0-500uM with a linear response. Using rhodium obviates the need for an electrochemical mediator because of its catalytic effect on peroxide. When an enzyme is added to the paste negative potentials can be used for the reduction of peroxide thus avoiding issues of electrochemical interference from known interferons. Once the pastes were packed with lactate oxidase calibrations were run against a physiological range of lactate and a linear response was achieved from 0 to 8mM. Electrochemical interference was tested against common electro active interferons such as ascorbic acid, uric acid, and acetaminophen with no effect on the resulting signal. Stability of the entrapped enzyme was tested and shown to be stable following a preconditioning step over a course of two hours. Windmiller et al also explored another route for sensing with microneedles by placing solid needles within hollow ones such that they were not exposed beyond the bore.[70] The internal solid needles were turned into electrochemical sensors by sputtering with platinum and electrochemically depositing a conducting polymer and an enzyme. Glutamate oxidase, the entrapped enzyme, was shown to be electrochemically active for oxidizing glutamate over a range of physiologically relevant concentrations. Glutamate is a known neurotransmitter and can be an indicator for a number of ailments such as head injury, Alzheimer's, and ischemic neural injury.[71,72,73] Concealing electrodes within microneedle bores still requires some interstitial fluid uptake and depending on the entrapped mechanism biosensors may be prone to damage or release due to interaction with surrounding tissue. To compensate for this potential issue, Invernale et al created a glucose sensing smart patch out of in-place array of microneedles made via machining

316L SS to entrap glucose oxidase within a conducting polymer.[74] Entrapment was electrochemically performed with PEDOT as the conducting polymer and glucose oxidase as the enzyme. The sensors were shown to detect glucose over a range of physiologically relevant concentrations. Biocompatibility of the metallic transducer was determined over a period of 7 days and compared platinum, stainless steel, and platinum coated stainless steel. Long-term stability of the devices was tested over a seven-day period and compared to both dry and wet environments. Startup companies have begun to develop microneedles into sensing platforms and Arkal Medical created arrays of hollow microneedles for transdermal sensing of glucose.[75] Microneedles were made from silicon and a three electrode system was incorporated into a microfluidic chip residing behind the array. Bore placement and application speed of the needles to skin was investigated. Two microneedle geometries were studied and both designs made with either tapered or straight microneedle walls were capable of puncturing the human skin. This group utilized a unique extraction method for acquiring analytes. Previous studies have focused on extraction of fluid for detection or placing electrodes within the skin for the sensing mechanism however the Arkal group filled their fluidic chip with a buffered solution and once applied to the skin allowed for equilibration of analytes between the device reservoir and skin for detection. Devices were worn on the skin of human subjects and glucose concentrations were monitored relative to intravenous levels. Device concentrations mimicked intravenous ones with only slight lag times. The group also did a clinical trial with successful results over a 72 hour time period in human subjects with minimal irritation of the skin at the insertion sites demonstrating the most advanced microneedle sensing platform to date.[76]

Extraction of interstitial fluid and sensing of this fluid are obvious hurdles in transdermal sensing however other technical challenges exist. Zahn et al created a microneedle with inspiration from the microdialysis world such that downstream

electrochemical electrodes wouldn't be susceptible to fouling due to interactions with large molecular weight compounds found in a real sample.[77] Settling of large molecular compounds onto electrode surfaces disrupt small molecule diffusion (e.g. glucose) and can created incorrect readings. The group created a porous membrane, made from porous polysilicon, on the face of an in-plane microneedle made using silicon wet etching techniques. Diffusion was visually investigated across the polysilicon membranes with a dye and equilibration was seen within 500 seconds. Most reports showcase microneedles ability to extract or interact with interstitial fluid however the Jung group has investigated drawing lithography for creating ultra-high aspect ratio hollow metallic microneedles for extracting blood.[78] In this approach, a resist is pulled between two plates at a controlled rate with the resist spun coated on the lower plate. The upper plate has arrays of pedestals that when pulled from the resist create drawn needles which are then UV cured. Metallization is done with a silver seed layer deposited with Tollen's reaction followed by electroplating with nickel. After cutting with a laser individual hollow microneedles or arrays are possible. The group later incorporated a PDMS reservoir behind a single hollow nickel microneedle as a self-actuating extraction system for acquiring blood from the ears of rabbits. In this approach upwards of ~120ul of blood was extracted at an inlet rate of 8ul/sec.

In conclusion, microneedle-based sensing platforms are becoming an emerging technique for transdermal sensing and clinical success and startup companies featuring this technology is an indicator of their benefit. However, the success of the clinical studies has largely focused on glucose and correlations between other small and large biomolecules with clinically accepted intravenous standards need to be investigated. For disease management, long-term device wearing is foreseeable and effect of microneedle interaction within the skin and bore lifetimes also need to be investigated.

References

[1] Yan, X., & Gu, P. E. N. G. (1996). A review of rapid prototyping technologies and systems. *Computer-Aided Design*, *28*(4), 307-318.

[2] Rosen, D. W. (2008). Stereolithography and rapid prototyping. In*BioNanoFluidic MEMS* (pp. 175-196). Springer US.

[3] Kruth, J. P., Mercelis, P., Van Vaerenbergh, J., Froyen, L., & Rombouts, M. (2005). Binding mechanisms in selective laser sintering and selective laser melting. *Rapid prototyping journal*, *11*(1), 26-36.

[4] Calvert, P. (2001). Inkjet printing for materials and devices. *Chemistry of materials*, *13*(10), 3299-3305.

[5] *Handbook of radical polymerization*. New York: Wiley-Interscience, 2002.

[6] de Gans, B. J., Duineveld, P. C., & Schubert, U. S. (2004). Inkjet printing of polymers: state of the art and future developments. *Advanced materials*, *16*(3), 203-213.

[7] Calvert, P. (2001). Inkjet printing for materials and devices. *Chemistry of materials*, *13*(10), 3299-3305.

[8] Limpanuphap, S., & Derby, B. (2002). Manufacture of biomaterials by a novel printing process. *Journal of Materials Science: Materials in Medicine*, *13*(12), 1163-1166.

[9] Eom, S. H., Park, H., Mujawar, S. H., Yoon, S. C., Kim, S. S., Na, S. I., ... & Lee, S. H. (2010). High efficiency polymer solar cells via sequential inkjet-printing of PEDOT: PSS and P3HT: PCBM inks with additives. *Organic Electronics*, *11*(9), 1516-1522.

[10] Ebert, J., Özkol, E., Zeichner, A., Uibel, K., Weiss, Ö., Koops, U., ... & Fischer, H. (2009). Direct inkjet printing of dental prostheses made of zirconia. *Journal of dental research*, *88*(7), 673-676.

[11] Lee, H. H., Chou, K. S., & Huang, K. C. (2005). Inkjet printing of nanosized silver colloids. *Nanotechnology*, *16*(10), 2436.

[12] Nakamura, M., Kobayashi, A., Takagi, F., Watanabe, A., Hiruma, Y., Ohuchi, K., ... & Takatani, S. (2005). Biocompatible inkjet printing technique for designed seeding of individual living cells. *Tissue engineering*, *11*(11-12), 1658-1666.

[13] Goldmann, T., & Gonzalez, J. S. (2000). DNA-printing: utilization of a standard inkjet printer for the transfer of nucleic acids to solid supports. *Journal of Biochemical and Biophysical methods*, *42*(3), 105-110.

[14] Frank, M. C., Wysk, R. A., & Joshi, S. B. (2004). Rapid planning for CNC milling—A new approach for rapid prototyping. *Journal of Manufacturing Systems*, *23*(3), 242-255.

[15] Zhang, X., Jiang, X. N., & Sun, C. (1999). Micro-stereolithography of polymeric and ceramic microstructures. *Sensors and Actuators A: Physical*, *77*(2), 149-156.

[16] Hull, C. W. (1986). *U.S. Patent No. 4,575,330*. Washington, DC: U.S. Patent and Trademark Office.

[17] Sun, C., Fang, N., Wu, D. M., & Zhang, X. (2005). Projection micro-stereolithography using digital micro-mirror dynamic mask. *Sensors and Actuators A: Physical*, *121*(1), 113-120.

[18] Cumpston, B. H., Ananthavel, S. P., Barlow, S., Dyer, D. L., Ehrlich, J. E., Erskine, L. L., ... & Perry, J. W. (1999). Two-photon polymerization initiators for three-dimensional optical data storage and microfabrication. *Nature*, *398*(6722), 51-54.

[19] Suzuki, A., Ivandini, T. A., Yoshimi, K., Fujishima, A., Oyama, G., Nakazato, T., ... & Einaga, Y. (2007). Fabrication, characterization, and application of boron-doped diamond microelectrodes for in vivo dopamine detection. *Analytical chemistry*, *79*(22), 8608-8615.

[20] Brett, C. M., Brett, A. M. O., & Heinze, J. (1993). *Electrochemistry: principles, methods, and applications* (Vol. 4). Oxford: Oxford university press.

[21] Wang, J. (2006). Electrochemical biosensors: towards point-of-care cancer diagnostics. *Biosensors and Bioelectronics*, *21*(10), 1887-1892.

[22] Linden, D. (1984). Handbook of batteries and fuel cells. *New York, McGraw-Hill Book Co., 1984, 1075 p. No individual items are abstracted in this volume.*, *1*.

[23] Langford, N. J., & Ferner, R. E. (1999). Toxicity of mercury. *Journal of human hypertension*, *13*(10), 651-656.

[24] Compton, R. G., & Banks, C. E. (2007). *Understanding voltammetry* (p. 107). Singapore: World Scientific.

[25] Heien, M. L., Phillips, P. E., Stuber, G. D., Seipel, A. T., & Wightman, R. M. (2003). Overoxidation of carbon-fiber microelectrodes enhances dopamine adsorption and increases sensitivity. *Analyst*, *128*(12), 1413-1419.

[26] Wang, J. (1999). Amperometric biosensors for clinical and therapeutic drug monitoring: a review. *Journal of pharmaceutical and biomedical analysis*, *19*(1), 47-53.

[27] Wang, J. (2008). Electrochemical glucose biosensors. *Chemical reviews*,*108*(2), 814-825.

[28] Henry, S., McAllister, D. V., Allen, M. G., & Prausnitz, M. R. (1998). Microfabricated microneedles: a novel approach to transdermal drug delivery.*Journal of pharmaceutical sciences*, *87*(8), 922-925.

[29] Freinkel, R. K., & Woodley, D. T. (Eds.). (2001). *The biology of the skin*. CRC Press.

[30]Brown, M. B., Martin, G. P., Jones, S. A., & Akomeah, F. K. (2006). Dermal and transdermal drug delivery systems: current and future prospects. *Drug delivery*,*13*(3), 175-187.

[31] Rose, J. E., Herskovic, J. E., Trilling, Y., & Jarvik, M. E. (1985). Transdermal nicotine reduces cigarette craving and nicotine preference. *Clinical Pharmacology & Therapeutics*, *38*(4), 450-456.

[32] Turnage, J. R., & Logan, D. L. (1974). Treatment of a hypodermic needle phobia by in vivo systematic desensitization. *Journal of Behavior Therapy and Experimental Psychiatry*, *5*(1), 67-69.

[33] Kaushik, S., Hord, A. H., Denson, D. D., McAllister, D. V., Smitra, S., Allen, M. G., & Prausnitz, M. R. (2001). Lack of pain associated with microfabricated microneedles. *Anesthesia & Analgesia*, *92*(2), 502-504.

[34] Prausnitz, M. R. (2004). Microneedles for transdermal drug delivery. *Advanced drug delivery reviews*, *56*(5), 581-587.

[35] Sullivan, S. P., Koutsonanos, D. G., del Pilar Martin, M., Lee, J. W., Zarnitsyn, V., Choi, S. O., ... & Prausnitz, M. R. (2010). Dissolving polymer microneedle patches for influenza vaccination. *Nature medicine*, *16*(8), 915-920.

[36] Nayak, A., & Das, D. B. (2013). Potential of biodegradable microneedles as a transdermal delivery vehicle for lidocaine. *Biotechnology letters*, *35*(9), 1351-1363.

[37] Yu, L. M., Tay, F. E. H., Guo, D. G., Xu, L., & Yap, K. L. (2009). A microfabricated electrode with hollow microneedles for ECG measurement.*Sensors and Actuators A: Physical*, *151*(1), 17-22.

[38] Forvi, E., Bedoni, M., Carabalona, R., Soncini, M., Mazzoleni, P., Rizzo, F., ... & Gramatica, F. (2012). Preliminary technological assessment of microneedles-based dry electrodes for biopotential monitoring in clinical examinations.*Sensors and Actuators A: Physical*, *180*, 177-186.

[39] Wang, P. M., Cornwell, M., & Prausnitz, M. R. (2005). Minimally invasive extraction of dermal interstitial fluid for glucose monitoring using microneedles.*Diabetes technology & therapeutics*, *7*(1), 131-141.

[40] Gatzoulis, L., & Iakovidis, I. (2007). Wearable and portable eHealth systems.*Engineering in Medicine and Biology Magazine, IEEE*, *26*(5), 51-56.

[41] El-Laboudi, A., Oliver, N. S., Cass, A., & Johnston, D. (2013). Use of microneedle array devices for continuous glucose monitoring: a review.*Diabetes technology & therapeutics*, *15*(1), 101-115.

[42] Potts, R. O., A Tamada, J., & J Tierney, M. (2002). Glucose monitoring by reverse iontophoresis. *Diabetes/metabolism research and reviews*, *18*(S1), S49-S53.

[43] Ault, J. M., Riley, C. M., Meltzer, N. M., & Lunte, C. E. (1994). Dermal microdialysis sampling in vivo. *Pharmaceutical research*, *11*(11), 1631-1639.

[44] Kool, J., Reubsaet, L., Wesseldijk, F., Maravilha, R. T., Pinkse, M. W., D'Santos, C. S., ... & Heck, A. J. (2007). Suction blister fluid as potential body fluid for biomarker proteins. *Proteomics*, *7*(20), 3638-3650.

[45] Sen, D. K., & Sarin, G. S. (1980). Tear glucose levels in normal people and in diabetic patients. *British journal of ophthalmology*, *64*(9), 693-695.

[46] Moyer, J., Wilson, D., Finkelshtein, I., Wong, B., & Potts, R. (2012). Correlation between sweat glucose and blood glucose in subjects with diabetes. *Diabetes technology & therapeutics*, *14*(5), 398-402.

[47] Srinivasan, V., Pamula, V. K., Pollack, M. G., & Fair, R. B. (2003, October). Clinical diagnostics on human whole blood, plasma, serum, urine, saliva, sweat, and tears on a digital microfluidic platform. In *Proc. μTAS* (pp. 1287-1290).

[48] Mukerjee, E. V., Collins, S. D., Isseroff, R. R., & Smith, R. L. (2004). Microneedle array for transdermal biological fluid extraction and in situ analysis.*Sensors and Actuators A: Physical*, *114*(2), 267-275.

[49] Zimmermann, S., Fienbork, D., Stoeber, B., Flounders, A. W., & Liepmann, D. (2003, June). A microneedle-based glucose monitor: fabricated on a wafer-level using in-device enzyme immobilization. In *TRANSDUCERS, Solid-State Sensors, Actuators and Microsystems, 12th International Conference on, 2003*(Vol. 1, pp. 99-102). IEEE.

[50] Wang, P. M., Cornwell, M., & Prausnitz, M. R. (2005). Minimally invasive extraction of dermal interstitial fluid for glucose monitoring using microneedles.*Diabetes technology & therapeutics*, *7*(1), 131-141.

[51] Miller, P. R., Gittard, S. D., Edwards, T. L., Lopez, D. M., Xiao, X., Wheeler, D. R., ... & Narayan, R. J. (2011). Integrated carbon fiber electrodes within hollow polymer microneedles for transdermal electrochemical sensing.*Biomicrofluidics*, *5*(1), 013415.

[52] Miller, P. R., Skoog, S. A., Edwards, T. L., Lopez, D. M., Wheeler, D. R., Arango, D. C., ... & Narayan, R. J. (2012). Multiplexed microneedle-based biosensor array for characterization of metabolic acidosis. *Talanta*, *88*, 739-742.

[53] Miller, P. R., Skoog, S. A., Edwards, T. L., Wheeler, D. R., Xiao, X., Brozik, S. M., ... & Narayan, R. J. (2012). Hollow microneedle-based sensor for multiplexed transdermal electrochemical sensing. *Journal of visualized experiments: JoVE*, (64).

[54] Miller, P. R., Xiao, X., Brener, I., Burckel, D. B., Narayan, R., & Polsky, R. (2014). Microneedle-Based Transdermal Sensor for On-Chip Potentiometric Determination of K+. *Advanced healthcare materials*, *3*(6), 876-881.

[55] Keum, D. H., Jung, H. S., Wang, T., Shin, M. H., Kim, Y. E., Kim, K. H., ... & Hahn, S. K. (2015). Microneedle Biosensor for Real-Time Electrical Detection of Nitric Oxide for In Situ Cancer Diagnosis During Endomicroscopy. *Advanced healthcare materials*.

[56]Jina, A., Tierney, M. J., Tamada, J. A., McGill, S., Desai, S., Chua, B., ... & Christiansen, M. (2014). Design, Development, and Evaluation of a Novel Microneedle Array-based Continuous Glucose Monitor. *Journal of diabetes science and technology*, *8*(3), 483-487.

[57] Sakaguchi, K., Hirota, Y., Hashimoto, N., Ogawa, W., Sato, T., Okada, S., ... & Nakajima, H. (2012). A minimally invasive system for glucose area under the curve measurement using interstitial fluid extraction technology: evaluation of the accuracy and usefulness with oral glucose tolerance tests in subjects with and without diabetes. *Diabetes technology & therapeutics*, *14*(6), 485-491.

[58] Raphael, A. P., Prow, T. W., Crichton, M. L., Chen, X., Fernando, G. J., & Kendall, M. A. (2010). Targeted, Needle-Free Vaccinations in Skin using Multilayered, Densely-Packed Dissolving Microprojection Arrays. *Small*, *6*(16), 1785-1793.

[59] Corrie, S. R., Fernando, G. J., Crichton, M. L., Brunck, M. E., Anderson, C. D., & Kendall, M. A. (2010). Surface-modified microprojection arrays for intradermal biomarker capture, with low non-specific protein binding. *Lab on a Chip*, *10*(20), 2655-2658.

[60] Yeow, B., Coffey, J. W., Muller, D. A., Grøndahl, L., Kendall, M. A., & Corrie, S. R. (2013). Surface modification and characterization of polycarbonate microdevices for capture of circulating biomarkers, both in vitro and in vivo.*Analytical chemistry*, *85*(21), 10196-10204.

[61] Muller, D. A., Corrie, S. R., Coffey, J., Young, P. R., & Kendall, M. A. (2012). Surface modified microprojection arrays for the selective extraction of the dengue virus NS1 protein as a marker for disease. *Analytical chemistry*, *84*(7), 3262-3268.

[62] Coffey, J. W., Corrie, S. R., & Kendall, M. A. (2013). Early circulating biomarker detection using a wearable microprojection array skin patch. *Biomaterials*,*34*(37), 9572-9583.

[63] Lee, K. T., Muller, D. A., Coffey, J. W., Robinson, K. J., McCarthy, J. S., Kendall, M. A., & Corrie, S. R. (2014). Capture of the circulating Plasmodium falciparum biomarker HRP2 in a multiplexed format, via a wearable skin patch.*Analytical chemistry*, *86*(20), 10474-10483.

[64] Sakaguchi, K., Hirota, Y., Hashimoto, N., Ogawa, W., Sato, T., Okada, S., ... & Nakajima, H. (2012). A minimally invasive system for glucose area under the curve measurement using interstitial fluid extraction technology: evaluation of the accuracy and usefulness with oral glucose tolerance tests in subjects with and without diabetes. *Diabetes technology & therapeutics*, *14*(6), 485-491.

[65] Donnelly, R. F., Majithiya, R., Singh, T. R. R., Morrow, D. I., Garland, M. J., Demir, Y. K., ... & Woolfson, A. D. (2011). Design, optimization and characterisation of polymeric microneedle

arrays prepared by a novel laser-based micromoulding technique. *Pharmaceutical research*, *28*(1), 41-57.

[66] Donnelly, R. F., Mooney, K., Mccrudden, M. T., Vicente-Pérez, E. M., Belaid, L., González-Vázquez, P., ... & Woolfson, A. D. (2014). Hydrogel-Forming Microneedles Increase in Volume During Swelling in Skin, but Skin Barrier Function Recovery is Unaffected. *Journal of pharmaceutical sciences*, *103*(5), 1478-1486.

[67] Mooney, K., McElnay, J. C., & Donnelly, R. F. (2014). Children's views on microneedle use as an alternative to blood sampling for patient monitoring.*International Journal of Pharmacy Practice*, *22*(5), 335-344.

[68] Romanyuk, A. V., Zvezdin, V. N., Samant, P., Grenader, M. I., Zemlyanova, M., & Prausnitz, M. R. (2014). Collection of Analytes from Microneedle Patches.*Analytical chemistry*, *86*(21), 10520-10523.

[69] Windmiller, J. R., Zhou, N., Chuang, M. C., Valdés-Ramírez, G., Santhosh, P., Miller, P. R., ... & Wang, J. (2011). Microneedle array-based carbon paste amperometric sensors and biosensors. *Analyst*, *136*(9), 1846-1851.

[70] Windmiller, J. R., Valdés-Ramírez, G., Zhou, N., Zhou, M., Miller, P. R., Jin, C., ... & Wang, J. (2011). Bicomponent Microneedle Array Biosensor for Minimally-Invasive Glutamate Monitoring. *Electroanalysis*, *23*(10), 2302-2309.

[71]Baker, A. J., Moulton, R. J., MacMillan, V. H., & Shedden, P. M. (1993). Excitatory amino acids in cerebrospinal fluid following traumatic brain injury in humans. *Journal of neurosurgery*, *79*(3), 369-372.

[72]Greenamyre, J. T., & Young, A. B. (1989). Excitatory amino acids and Alzheimer's disease. *Neurobiology of aging*, *10*(5), 593-602.

[73]Choi, D. W. (1989). Methods for antagonizing glutamate neurotoxicity.*Cerebrovascular and brain metabolism reviews*, *2*(2), 105-147.

[74] Invernale, M. A., Tang, B. C., York, R. L., Le, L., Hou, D. Y., & Anderson, D. G. (2014). Microneedle Electrodes Toward an Amperometric Glucose-Sensing Smart Patch. *Advanced healthcare materials*, *3*(3), 338-342.

[75] Chua, B., Desai, S. P., Tierney, M. J., Tamada, J. A., & Jina, A. N. (2013). Effect of microneedles shape on skin penetration and minimally invasive continuous glucose monitoring in vivo. *Sensors and Actuators A: Physical*, *203*, 373-381.

[76] Jina, A., Tierney, M. J., Tamada, J. A., McGill, S., Desai, S., Chua, B., ... & Christiansen, M. (2014). Design, Development, and Evaluation of a Novel Microneedle Array-based Continuous Glucose Monitor. *Journal of diabetes science and technology*, *8*(3), 483-487.

[77] Zahn, J. D., Trebotich, D., & Liepmann, D. (2005). Microdialysis microneedles for continuous medical monitoring. *Biomedical microdevices*, *7*(1), 59-69.

[78] Li, C. G., Lee, C. Y., Lee, K., & Jung, H. (2013). An optimized hollow microneedle for minimally invasive blood extraction. *Biomedical microdevices*,*15*(1), 17-25.

Chapter 2 Integrated Carbon Fiber Electrodes within Hollow Polymer Microneedles for Transdermal Electrochemical Sensing

Philip R. Miller[1], Shaun D. Gittard[1], Thayne L. Edwards[2], DeAnna M. Lopez[2], Xiaoyin Xiao[2], David R. Wheeler[2], Nancy A. Monteiro-Riviere[1,3], Susan M. Brozik[2], Ronen Polsky[2], and Roger J. Narayan[1]

[1] Joint Department of Biomedical Engineering, UNC/NCSU, 911 Oval Drive, Campus Box 7115, Raleigh, North Carolina 27695-7115, USA

[2] Department of Biosensors and Nanomaterials, Sandia National Laboratories, P.O. Box 5800, MS-0892, Albuquerque, New Mexico 87185, USA

[3] Center for Chemical Toxicology Research and Pharmacokinetics, North Carolina State University, Raleigh, North Carolina 27606, USA

The following section is a complete article reprinted from Biomicrofluidics, Volume 5, Philip R Miller, Shaun D Gittard, Thayne L Edwards, DeAnna M Lopez, Xiaoyin Xiao, David R Wheeler, Nancy A Monteiro-Riviere, Susan M Brozik, Ronen Polsky, Roger J Narayan. 013415,

Note: This article has been reformatted. In particular, the location of figures and spacing may have changed. The references are formatted as in the original manuscript.

Abstract

In this study, carbon fiber electrodes were incorporated within the bores of hollow microneedle, which were fabricated using a digital micromirror device-based stereolithography instrument. The carbon fibers underwent chemical and electrochemical modification in order to enable detection of hydrogen peroxide and ascorbic acid; electrochemical measurements were demonstrated using integrated electrode-hollow microneedle devices. Studies involving full-thickness cadaveric porcine skin and trypan blue dye demonstrated that the hollow microneedles remained intact after puncturing the outermost layer of cadaveric porcine skin. Cell proliferation on the acrylate-based polymer used in microneedle fabrication was examined with human dermal fibroblasts and neonatal human epidermal keratinocytes.

Introduction

In vivo sensors may be used to provide real-time detection of physiological processes, such as monitoring of neurotransmitters, medically relevant molecules, cancer biomarkers, and pathogenic microorganisms.[1] Devices for monitoring physiologically relevant compounds such as acetylcholine, dopamine, glutamate, glucose, lactate, and pyruvate have been described in the literature.[2] Stett et al. described the use of a microelectrode array for evaluating physiologic and pathologic activity within a tissue; in particular, they considered the use of biosensors for drug discovery as well as drug screening.[3] Electrochemical biosensors provide several advantages for point-of-care monitors, including small sensor size, low cost, simplicity, rapid response, and sensitivity; in addition, electrochemical methods may enable simultaneous monitoring of several biomarkers. [1,4,5] For example, Wang et al. developed disposable electrodes by means of screen-printing, which contained carbon inks with sol-gel-derived enzymes.[4,5] Disposable glucose oxidase electrodes have been very important in the development and clinical translation of hand-held diagnostic devices, which are used for patient self-management of diabetes.

As described by Mastrototaro and Newman et al., many conventional monitoring methods utilize macroscale systems; these systems are associated with several shortcomings, including transfer of fluids between devices, painful device-tissue interactions, and large sample volumes.[6,7] An ideal sensor should exhibit several properties, including capability of monitoring a variety of biological markers, compatibility with small sample volumes, and minimal tissue damage. An approach for achieving real-time, minimally invasive point-of-care sensing would be the realization of a device that is capable of obtaining biological samples (e.g., interstitial fluid) through the skin while protecting the sensing transducer from biofouling elements.[8,9]

Hollow microneedles have recently been developed for point-of-care transdermal biosensing and drug delivery.[10] McAllister et al. described microneedles as small-scale projections containing either hollow bores or solid bores; these devices exhibit features between 1 and 1000 μm.[11] McAllister et al. described the use of microneedles for minimizing tissue trauma and pain.[12] Gill et al. demonstrated that microneedles with lengths between 480 and 1450 μm were associated with less pain in normal human volunteers than conventional 26-gauge hypodermic needles; this result is attributed to the fact that microneedles have less contact with Pacinian corpuscles, Meissner's corpuscles, and nerve endings located within the dermis than conventional hypodermic needles.[9,13,14] Hollow microneedles are commonly used to create pores in the stratum corneum layer of the epidermis, enabling controlled delivery of one or more pharmacologic agents to deeper layers of the epidermis or to the papillary dermis.[12,13] This approach is particularly useful for delivery of nucleic acid-based agents (e.g., gene delivery agents) and protein-based agents (e.g., insulin) due to the enhanced drug efficiency because of the density of immune cells which comprise the dermal tissue these agents are currently administered using hypodermic needles.[11,12]

To date, the majority of microneedle research activities have involved the use of microneedles as transdermal drug delivery devices. Microneedles have also been considered for use in micrototal analysis systems, which may be used for evaluation of biological samples; microneedle-based monitors provide simplified acquisition and transfer of biological samples to the electrode, reduced patient pain, reduced energy consumption, and smaller device dimensions than conventional monitors.[14,15] Suzuki et al. utilized micromachining for fabrication of a disposable microanalysis device, which contained a microscopic needle, a sampling (pumping) mechanism, and a microglucose sensor; they

demonstrated sensor responses to glucose solutions with concentrations up to 8 mM and 90% response times of 30–40 s.[16] Zimmermann et al. described the fabrication of a device containing an enzyme-based glucose sensor, a porous silicon dialysis membrane, and hollow out-of-plane microneedles; they introduced interstitial fluid to the microneedles and observed a significant sensor response.[17] Mukerjee et al. utilized a device containing a hollow microneedle array and microfluidic channels for measuring the glucose concentration of interstitial fluid, which was extracted from human skin.[18] Tsuchiya et al. described the development of a blood sampling device, which consisted of titanium microneedle with dimensions similar to those of a female mosquito labrum, a shape memory alloy actuator for skin penetration, and a glucose oxidase-based biosensor; they demonstrated that this pumping system was capable of extracting 2 μl/min of whole blood.[19] Zahn et al. noted that large molecular weight compounds (e.g., large molecular weight proteins) have negative effects on sensor function, including altering signal stability and disrupting enzyme function; they discussed the use of a microdialysis microneedle for filtering glucose and other small molecule weight compounds from biological samples.[15] It should be noted that hollow microneedle-based biosensors commonly require the use of pumping systems for sample acquisition and complex microfluidic channels for sample calibration; furthermore, hazardous chemicals may be required for biosensor calibration.[17,18]

As described by McAllister et al., early microneedle fabrication methods were adopted from microelectronics industry-based processes, including lithography-based processes.[20] Due to its compatibility with conventional microfabrication processes, microneedles were initially fabricated out of silicon. For example, Henry et al. utilized reactive ion etching to fabricate 150 μm long solid microneedles out of silicon.[21] Chun et al.

used Bosch deep reactive ion etching to fabricate holes on a silicon substrate; hollow microcapillary arrays were subsequently fabricated on the substrate.[22] Mukerjee et al. described machining a hollow microneedle array with microfluidic channels out of single crystal silicon.[18] Kim et al. fabricated a hollow metallic microneedle array using a multiple step process, which involved backside exposure of SU-8 and conformal electroplating of nickel.[23] Park et al. prepared microneedles out of biodegradable polymers, including polyglycolic acid and polylactic acid, using either electromechanical masking/etching and polydimethylsiloxane (PDMS) micromolding or *in situ* lens-based lithography and PDMS micromolding.[12,24] Pérennès et al. demonstrated fabrication of hollow microneedle arrays out of polymethylmethacrylate using a multiple step process, which utilized a double deep x-ray lithography, electrodeposition, and molding.[25] Wang et al. described the use of conventional drawn glass micropipette methods for preparing hollow microneedles out of borosilicate glass.[26]

Many conventional microneedle fabrication processes are not compatible with preparation of large numbers of devices due to the fact that these processes involve complex, multiple step procedures and/or long fabrication times. In order to overcome these obstacles, rapid prototyping methods have recently been utilized for microneedle fabrication. Rapid prototyping, also known as solid freeform fabrication or layer manufacturing, involves building a structure in an additive manner by means of layer-by-layer, selective joining of material.[27,28,29] Fabrication of the structure is commonly directed by a computer-aided design drawing. In addition, this approach is compatible with low processing costs and high yield; furthermore, a specialized processing environment (e.g., a clean room) is not required.[30] Stereolithography is one rapid prototyping method that is associated with low processing costs as well as short processing times; Tse et al.

demonstrated use of stereolithography for fabricating high aspect ratio three-dimensional microscale structures.[30] Matsuda and Mizutani used a stereolithography apparatus with an ultraviolet light pen to create microneedles out of acrylate-endcapped poly(epsilon-caprolactone-co-trimethylene carbonate) materials.[31] Microneedles loaded with indomethacin, an anti-inflammatory pharmacologic agent, were shown to minimize inflammation in a murine model. Zhang et al. demonstrated that microstereolithography, a process that is capable of creating structures with 1.2 μm resolution, may be used to prepare microscale channels, microcones, and other three-dimensional structures.[32] Choi et al. utilized microstereolithography to create microneedle arrays.[33] Two photon polymerization is another rapid prototyping technology that has been used for microneedle fabrication. In two photon polymerization, selective polymerization of a photosensitive resin is obtained by means of nearly simultaneous absorption of ultrashort laser pulses; the voxel size is dependent on several parameters, including laser power, sensitivity of the resin, and numerical aperture of the objective lens.[10] Ovsianikov et al. recently demonstrated fabrication of poly(ethylene glycol) diacrylate structures with 200 nm features by means of two photon polymerization.[34] Doraiswamy et al. demonstrated fabrication of a microneedle array out of organically modified ceramic (Ormocer®) material using two photon polymerization.[35] Ovsianikov et al. used two photon polymerization to create in-plane microneedles and out-of-plane hollow microneedles.[36] More recently, Gittard et al. fabricated microneedle arrays out of an acrylate-based polymer using two photon polymerization.[37]

A rapid prototyping approach involving use of a digital micromirror device (DMD™), which was originally developed by Texas Instruments, as a dynamic mask was used for selective polymerization of a photosensitive acrylate-based polymer resin into a

microneedle device. In recent years, several investigators have utilized digital micromirror device-based stereolithography to fabricate small-scale devices. For example, Sun et al. used a digital micromirror device-based stereolithography system to prepare three-dimensional microscale structures, including a matrix and a microspring array with minimum feature size of 0.6 μm.[38] Gittard et al. utilized digital micromirror device-based stereolithography to prepare scaphoid and lunate bone prostheses from computed tomography data; the prostheses exhibited ~50-mm-thick layers.[39] In this study, the minimum compressive force to obtain fracture was 1248 N for the lunate prosthesis and 1360 N for the scaphoid prosthesis. Han et al. used digital micromirror device-based stereolithography to create multilayered scaffolds out of a resin containing poly(ethylene glycol) diacrylate and fibronectin; attachment of murine marrow-derived progenitor cells to fibronectin-containing scaffolds was demonstrated.[40] Choi et al. prepared tissue engineered scaffolds with ~100 μm interconnected pores out of poly(propylene fumarate) by means of digital micromirror device-based stereolithography.[41] In more recent work, Choi et al. demonstrated processing of structures containing multiple materials using digital micromirror device-based stereolithography; these materials have potential use as scaffolds in tissue engineering.[42]

A variety of materials have been used for microneedle fabrication, including silicon, glass, metal (e.g., stainless steel and nickel), and resorbable polymers (e.g., polyglycolic acid and polylactic acid).[11,24,26,43] A commercially obtained acrylate-based polymer, e-Shell 200, was utilized for microneedle fabrication. The material is a class-IIa biocompatible, water-resistant material; it has been used in thin-walled hearing aid shells, solid microneedle arrays, as well as nonmedical applications.[44,45] Information provided by the manufacturer (Envisiontec, Gladbeck, Germany) shows that e-Shell 200 contains 0.5%–1.5% weight

phenylbis(2,4,6 trimethylbenzoyl)-phosphine oxide photoinitiator, 15%–30% weight propylated (2) neopentyl glycoldiacrylate, and 60%–80% weight urethane dimethacrylate. Energy-dispersive x-ray spectroscopy indicated that e-Shell 200 contains carbon, oxygen, and titanium; these elements are known to possess excellent biocompatibility. [42] According to technical data supplied by the manufacturer, e-Shell 200 exhibits a water absorption value of 0.12% (D570-98 test method) and a glass transition temperature of 109 °C (E1545-00 test method). It exhibits tensile strength of 57.8 MPa (D638M test method), flexural strength of 103 MPa (D790M test method), and elongation at yield of 3.2% (D638M test method). Gittard et al. showed using nanoindentation that e-Shell 200 exhibits hardness and Young's modulus values of 93.8±7.25 and 3050±90 MPa, respectively.[39] Work by Park et al. suggests that microneedles fabricated out of materials with Young's modulus values greater than ~1 GPa possess fracture forces that exceed skin insertion forces.[24]

Materials and Methods

MTT Assay:

Proliferation of human dermal fibroblasts and neonatal human epidermal keratinocytes on e-Shell 200 surfaces was evaluated using the MTT (3-(4,5-dimethylthiazol-2-yl)2,5-diphenyl tetrazolium bromide) assay, which involves reduction of a yellow tetrazolium salt to a purple formazan dye by mitochondrial succinic dehydrogenase.[46][57] In this study, e-Shell 200 wafers (diameter=15 mm, thickness=2 mm) were compared against glass cover slips (diameter=15 mm). The cover slips and e-Shell 200 wafers were rinsed and sterilized in two 30 min rinses of 70% ethanol; the materials were subsequently rinsed in sterile de-ionized water. The e-Shell 200 wafers were placed in sterile Petri dishes in a laminar flow cabinet and sterilized with ultraviolet B light; both surfaces were exposed to ultraviolet B light. The materials were rotated 90° after a minimum of 2 h light exposure. Polymers were transferred to sterile 24-well culture plates, rinsed twice in sterile Hank's balanced salt solution, and once in the appropriate cell culture medium. The e-Shell 200 wafers were placed in 2 ml of the appropriate cell culture medium and held in the incubator until seeded. Cryopreserved neonatal human epidermal keratinocytes and human dermal fibroblasts were obtained from a commercial source (Lonza, Walkersville, MD). Fibroblast growth media (FGM-2) and keratinocyte growth media (KGM-2) were also obtained from a commercial source (Lonza, Walkersville, MD). The human dermal fibroblasts and neonatal human epidermal keratinocytes were propagated in 75 cm^2 flasks, grown to 75% confluency, and subsequently harvested. The cells were then seeded (concentration=40 000 cells per well) in a 24-well plate on e-Shell wafers 200 (n=4), glass cover slips (n=4), and polystyrene well plates (n=4). Material rinsing and all media changes were performed by moving the test materials from one solution to the other using a forceps. The materials were placed in fresh medium after 48 h; this time point corresponded with 80% confluency for

human dermal fibroblasts and neonatal human epidermal keratinocytes. MTT viability was assessed 24 h later. The materials with cells were rinsed using Hank's balanced salt solution; desorption using isopropyl alcohol and agitation were subsequently performed. Isopropyl alcohol (quantity=100 µl) was transferred to a new 96-well plate. Absorbance was determined (λ=550 nm) with a Multiskan RC plate reader (Labsystems, Inc., Franklin, MA). The mean values for percent viability were calculated. Significant differences ($p<0.05$) were determined using the PROC GLM Procedure (SAS 9.1 for WINDOWS) (SAS Institute, Cary, NC). When significant differences were found, then multiple comparisons were performed using Tukey's Studentized Range HSD (Honestly Significant Difference) test at $p<0.05$ level of significance.

Microneedle Fabrication:

Arrays of hollow microneedles were fabricated from three-dimensional drawings that were created using Solidworks (Dassault Systemes S.A., Velizy, France). Support structures were fabricated from three-dimensional drawings that were created using Magics RP 13 (Materialise NV, Leuven, Belgium). In the tetrahedron-shaped microneedle design, two faces of the microneedle exhibit a vertical orientation with respect to the substrate (Figure 2-1). The microneedle input dimensions included a triangular base with 1.2 mm sides, a height of 1.5 mm, and a vertical cylindrical channel (diameter=400 µm). The needles were arranged into a 2×2 square array with 2 mm inter microneedle spacing. The substrate input dimensions included lateral dimensions of 1 cm×1 cm and a thickness of 500 µm. Rapid prototyping of the microneedle array was performed using a Perfactory III SXGA+instrument (EnvisionTEC GmbH, Gladbeck, Germany). A 150 W halogen bulb was used as the light source for polymerization of liquid e-Shell 200 resin. Selective

polymerization of the resin in the X-Y plane was achieved using DMD optics (Texas Instruments, Dallas, TX), specifically a DMD SXGA+guidance chip with 1280×1024-pixel resolution. This instrument contains a build envelope of 90 mm×67.5 mm. After fabrication, the e-Shell 200 microneedle array was washed in isopropanol in order to remove the unpolymerized material. Post building curing was accomplished using an Otoflash Post Curing System instrument (EnvisionTEC GmbH, Gladbeck, Germany). This system contains two photoflash lamps and provides light exposure over a wavelength range of 300–700 nm.

Imaging:

A Hitachi S-3200 (Hitachi, Tokyo, Japan) variable pressure scanning electron microscope with a Robinson backscattered electron detector was used for imaging the microneedle arrays. The microneedle arrays were coated with 60% gold-40% palladium using a Technics Hummer II instrument (Anatech, Battle Creek, MI) prior to imaging.

Insertion Tests:

Skin penetration testing was performed with full-thickness cadaveric porcine skin since human skin and porcine skin exhibit similar structures. Trypan blue (Mediatech, Inc., Manassas, VA), a toluidine-based dye, was used to assess the transdermal drug delivery functionality of the hollow microneedle arrays.[24, 43, 58] [47]Cadaveric full-thickness weanling Yorkshire/Landrace skin was stored at 3 °C until testing was performed. Hollow microneedle arrays were inserted into full-thickness porcine skin. After removal of the arrays, trypan blue was applied to the insertion site; the site was subsequently washed with isopropanol swabs. The trypan blue-treated skin was subsequently imaged using optical

microscopy. Images of a microneedle device before and after insertion into porcine skin were obtained using optical microscopy.

Electrochemical Electrodes Modifications and Measurements:

7 μm carbon fibers (Alfa Aesar, St. Louis, MO) were activated in a KOH solution (concentration=0.1 M) at a *p*H of 13 and at a potential of 1.3 V for 5 min. *In situ* diazotation of 2-amino-4-nitrophenol was performed by mixing a solution of 8 mM sodium nitrite and 6 mM 2-amino-4-nitrophenol on ice for 5 min to create the corresponding diazonium salt. After 5 min, the activated carbon fibers were inserted. Two cyclic voltammetry (CV) scans were run from 0.4 to −0.8 V at 0.1 V/s to enable the electrochemical grafting of the 2-nitrophenol and subsequent reduction to the aminophenol. The carbon fibers were modified with palladium to enable the detection of hydrogen peroxide. Activated carbon fiber bundles were placed in a solution of 1 mM palladium (II) chloride; Pd was deposited by applying a potential of −0.8 V for 120 s. All electrochemical measurements were obtained using a PGSTAT12 Autolab electrochemical instrument (EcoChemie, Utrecht, The Netherlands). Data were acquired versus an Ag/AgCl reference and a Pt counter electrode.

Results and Discussion

In this study, we report on the use of a digital micromirror device-stereolithography instrument to fabricate hollow microneedles and the integration of carbon fiber electrodes within the bores of these hollow microneedles. Carbon fiber-containing materials have been considered for use in a variety of medical device applications, including joint prostheses, spinal surgery devices, and tumor surgery devices.[48] Wolter described carbon fibers as well as carbon fiber microparticles as having excellent biocompatibility.[49] It should be noted that fragmentation of carbon fibers remains a source of concern. Neugebauer et al. showed that carbon fiber fragments were associated with a small amount of fibrosis as well as a foreign body giant cell reaction; it should be noted that inflammation, tissue necrosis, and toxic effects on tissues were not associated with carbon fiber fragments.[50] Mendes et al. suggest that carbon fibers are biocompatible as long as the fiber structure is preserved.[51] The carbon fibers were chemically modified to enable detection of two medically significant molecules, hydrogen peroxide and ascorbic acid. Electrochemical characterization was performed on the chemically modified electrode-hollow microneedle devices. Hydrogen peroxide (H_2O_2) is a reactive oxygen species that is monitored in many common enzyme-based electrochemical sensors.[5,52] For example, most glucose sensors contain immobilized glucose oxidase. Hydrogen peroxide and gluconolacone are produced in reactions between glucose and glucose oxidase; monitoring of released hydrogen peroxide is used for quantification of glucose. Monitoring of released hydrogen peroxide may also be used for quantification of glutamate in brain dialysate; hydrogen peroxide is produced in reactions between glutamate and glutamate oxidase.[1,53] Glutamate is an excitatory neurotransmitter, which has been linked with aggressive activity.[1,54] Ascorbic acid has recently been described as an indicator of oxidative stress that is experienced by cells.[55] Harrison et al. noted that

ascorbic acid deficiency is associated with obstetric complications, such as preterm labor and premature rupture of the membranes.[56] Deficient levels of ascorbic acid (<14.1 μM) were noted in 6% of individuals in a sample of 200 lactating women; no symptoms of clinical deficiency (e.g., scurvy) were noted in these individuals.[57] Assessment of ascorbic acid levels may be useful for detecting clinically silent ascorbic acid deficiencies in individuals, particularly nursing mothers. Downard et al. described covalent modification of glassy carbon fiber microelectrodes and glassy carbon electrodes with P-phenylacetate groups; these electrodes exhibit excellent resolution between ascorbic acid and dopamine.[58] We anticipate that integrated electrode-hollow microneedle devices fabricated using this approach may be used to provide real-time detection of a wide variety of physiologically relevant biomarkers.

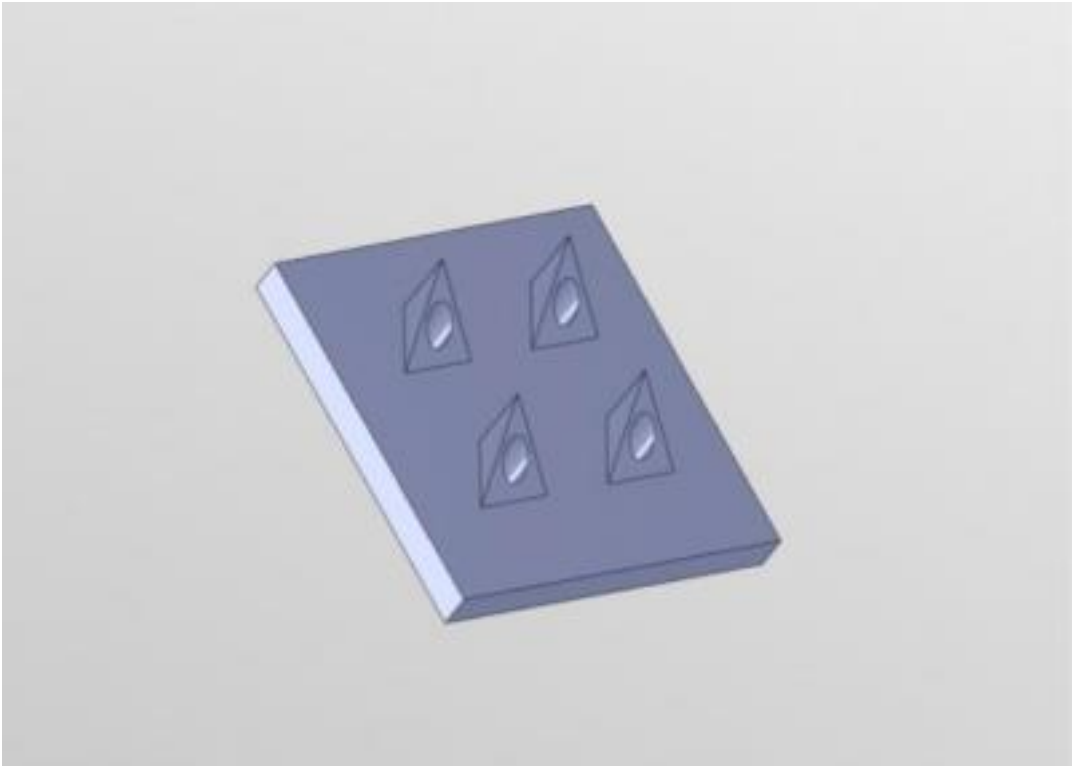

Figure 2-1: Stereolithgraphy file of a 2x2 hollow microneedle created in Solidworks.

The completed microneedle device was comprised of two layers (Figure 2-2). The upper layer consisted of the microneedle array; the lower layer provided support for the carbon fibers and facilitated the alignment of the carbon fibers to the microneedle array. The support component was fabricated from a 1.6 mm thick poly-(methylmethacrylate) (PMMA) piece. An array of holes was laser drilled through the PMMA piece using a Model PLS instrument, consisting of a 6.75 60 W CO_2 laser and a computer-controlled XY stage (Universal Laser Systems, Scottsdale, AZ) [**Error! Reference source not found.**]. The holes were placed in a square pattern with 2 mm spacing. Using a Model HPDFO high power density focusing optics lens (Universal Laser Systems, Scottsdale, AZ), the diameter of the hole at the exit surface was measured at ~45 μm. To control the carbon fiber length beyond the support surface, the support component was placed on top (exit-side down) of a well with a depth of 100 μm. Carbon fiber was manually inserted into each of the holes (entrance side) and allowed to rest at the bottom of the well [Figure 2-2b]. The fibers were secured in place with acrylic adhesive on the entrance side after the desired well depth had been achieved [Figure 2-2c]. shows the optical images of an array of carbon fiber electrodes and a single carbon fiber electrode. The support layer and the microneedle layer were brought together in such a manner that the carbon fibers were positioned within the hollow shafts of the microneedles. The layers were subsequently adhered to each other. Metallic epoxy was applied to the back of the fibers in order to create the connection for the working electrode [Figure 2-2d].

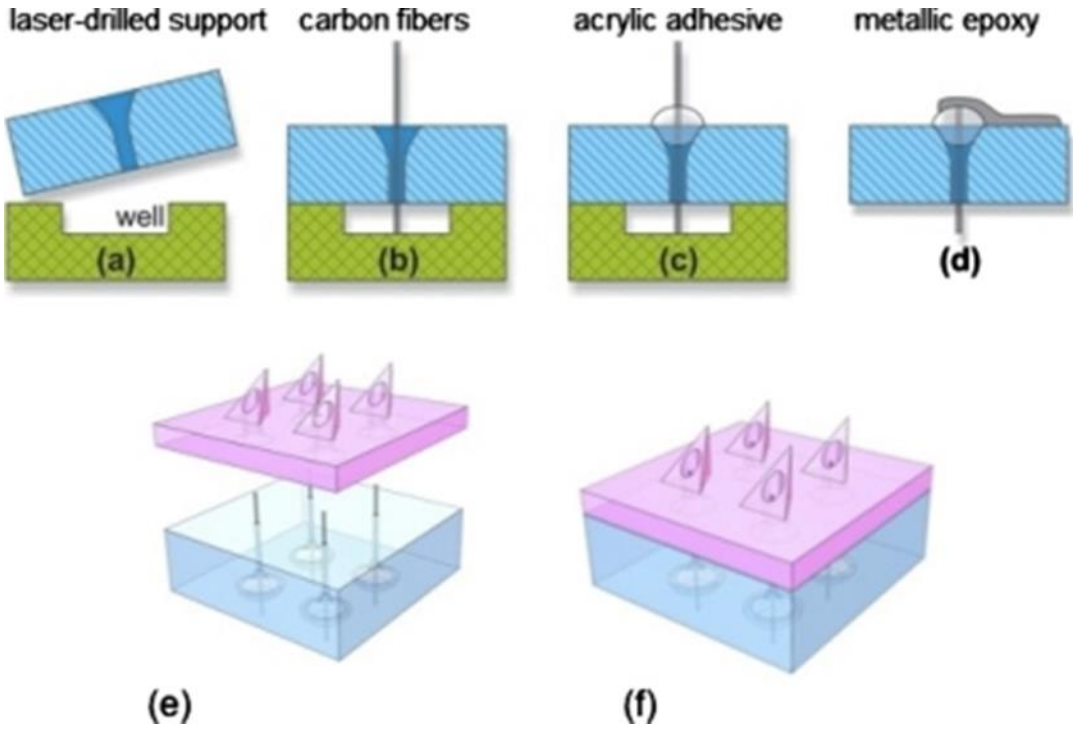

Figure 2-2: Schematic showing steps used for assembly of the microneedle device. CO2 laser cut bores in the microneedle substrate (A), carbon fiber bundles fill bore in the substrate above a pre-defined well (B), adhering the carbon fiber bundles to the substrate

24 h MTT assay data for neonatal epidermal keratinocytes and human dermal fibroblasts are shown in Figure 2-3. The test materials were noted to remain intact in the cell culture media over the course of the MTT assay. The e-Shell 200 and glass materials did not float in the wells; data for each material were fairly consistent. MTT viability of neonatal human keratinocytes was significantly higher for glass than for e-Shell 200 [Figure 2-3A]. MTT viability for human dermal fibroblasts was significantly higher for glass than for e-Shell 200 [Figure 2-3B]. Very slight differences in viability were noted; both neonatal epidermal keratinocytes and human dermal fibroblasts showed a slight decrease on e-Shell 200. Dissimilar responses by neonatal human epidermal keratinocytes and human dermal fibroblasts were attributed to the fact that epithelial cells are derived from ectoderm; on the other hand, fibroblasts are derived from mesoderm.[37] Consequently, these cell types have dissimilar cell receptors and responses to synthetic materials. It should be noted that e-Shell 200 only exhibited a slight but significant decrease in viability, which would not raise concerns regarding potential *in vivo* use in a transdermal medical device.

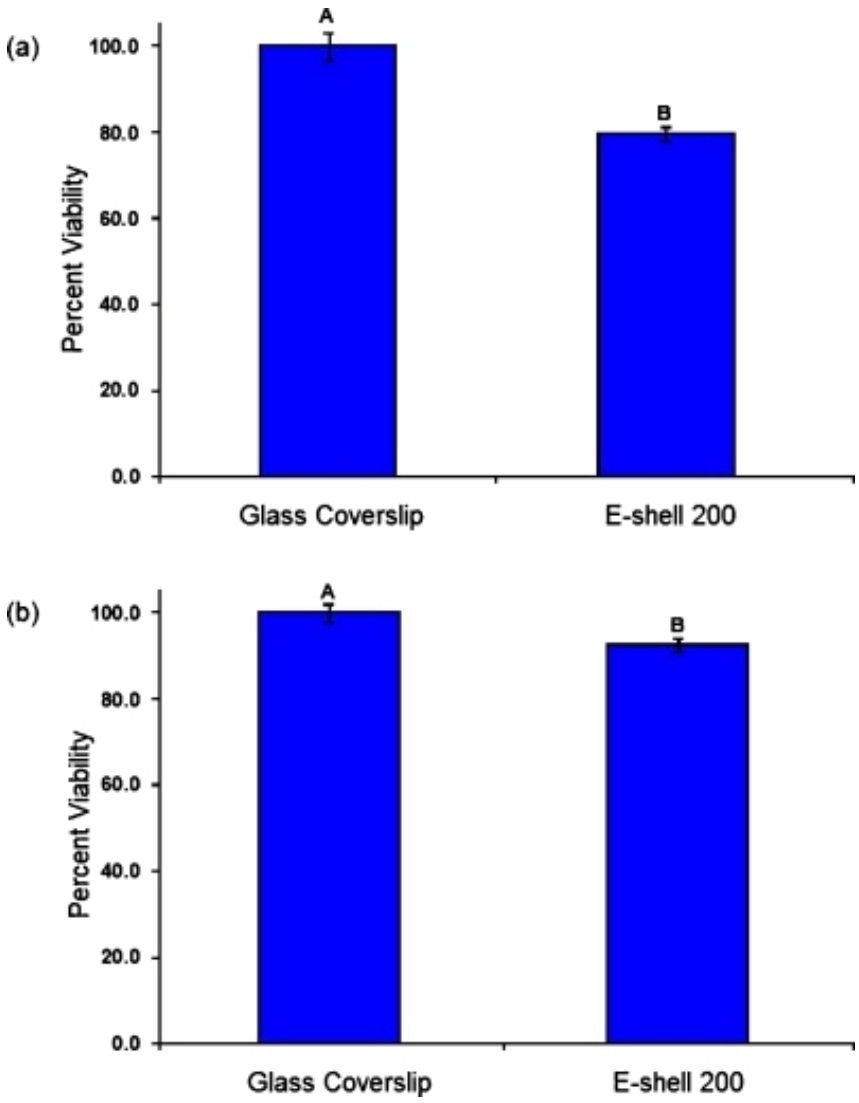

Figure 2-3: MTT viability data for cells grown on e-Shell 200 acrylate-based polymer and glass cover slip. (a) MTT viability of human epidermal keratinocytes grown on e-Shell 200 acrylate-based polymer compared to glass cover slip. A and B denote statistical differences ($p<0.05$) between the polymer and the control. (b) MTT viability of human dermal fibroblasts grown on e-Shell 200 acrylate-based polymer compared to glass coverslip. A and B denote statistical differences ($p<0.05$) between the polymer and the control.

The digital micromirror device-based stereolithography instrument allowed for the fabrication of approximately 200 arrays over a 3 h period. Figure 2-4contains the scanning

electron microscopy (SEM) images of a hollow microneedle array and a single hollow microneedle prior to incorporation of carbon fiber electrodes. Measurements obtained from scanning electron micrographs showed that the microneedles exhibited heights of ~1030 μm, triangular bases with side lengths of ~1120 μm, and bore diameters of ~375 μm. Good microneedle-to-microneedle uniformity was noted among the microneedles in the microneedle array. Differences between input and measured dimensions were attributed to translation of the computer-aided design drawing by the software. Digital micromirror device-based stereolithography and other rapid prototyping techniques involve tessellation, a conversion of the surface of the computer-aided design drawing into a series of polygons. This polygon series is converted into a series of cross-sectional layers, which is subsequently used for layer-by-layer fabrication of the microneedle device. It is not possible to predict how the computer-aided design drawing is manipulated by the software.

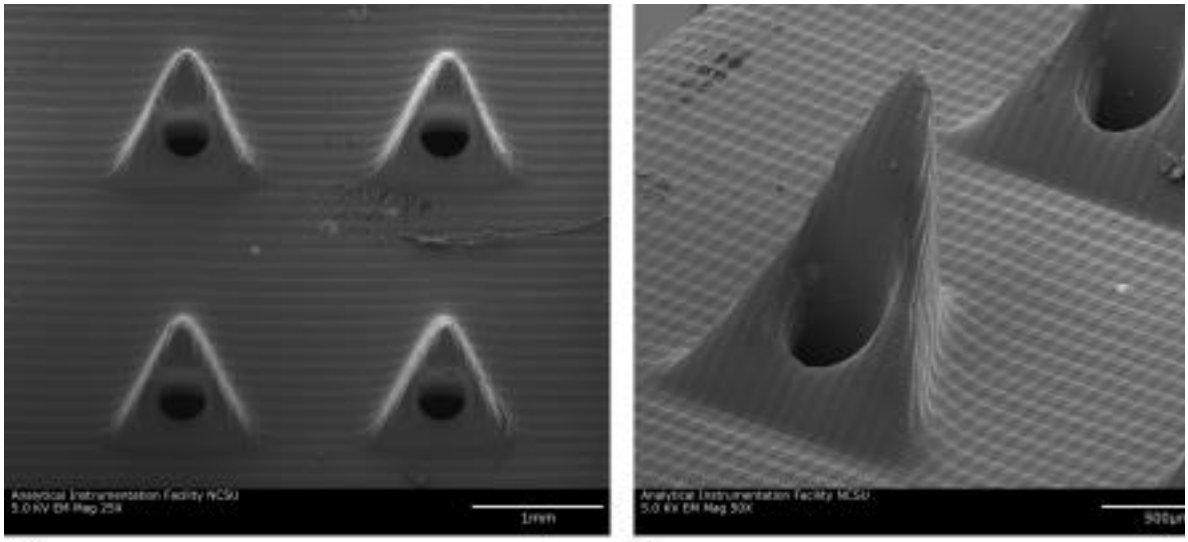

Figure 2-4: Scanning electron microscopy image of hollow microneedles prior to incorporation of carbon fiber electrodes: (a) plan view of hollow microneedle array and (b) isometric view of single hollow microneedle.

Microneedles undergo bending forces, compressive forces, shear forces, and skin resistance during skin insertion; the pressure necessary for human skin penetration exceeds 3.0×10^6 Pa.[21] The skin penetration properties of the microneedle devices were evaluated using cadaveric porcine skin, which has been previously used as a model for assessing microneedle functionality.[12, 43] Figure 2-5 shows the porcine skin after application of the microneedle array, removal of the microneedle array, and application of trypan blue. The trypan blue spots indicate the penetration through the stratum corneum layer (outermost layer) of the epidermis by the microneedle array and the localization of Trypan Blue within the microneedle-generated pores. Figure 2-5 (A-B) show optical micrographs of hollow microneedles before insertion into porcine skin and after insertion into porcine skin, respectively. These images indicate that the microneedles remain intact after skin insertion.

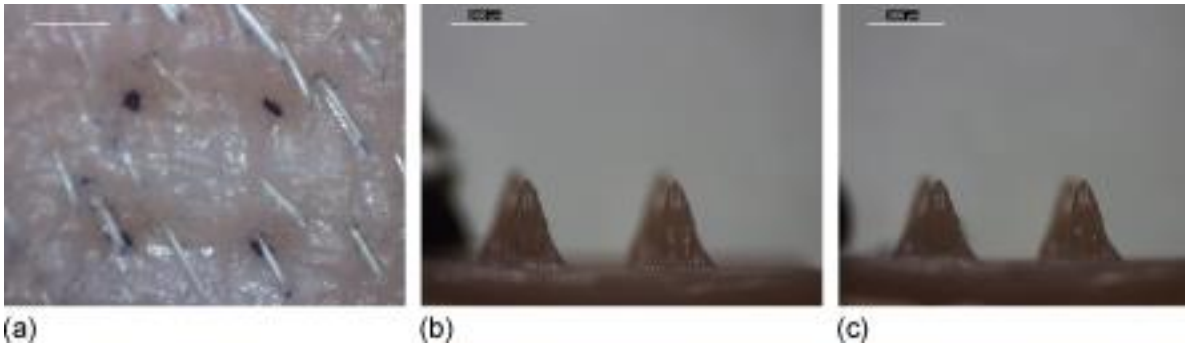

Figure 2-5: Images of microneedle array and cadaveric porcine skin after microneedle insertion. (a) Optical micrograph showing delivery of trypan blue into microneedle-fabricated pores within cadaveric porcine skin (scale bar 1=mm). (b) Optical micrograph showing hollow microneedles before insertion into cadaveric porcine skin. (c) Optical micrograph showing hollow microneedles after insertion into cadaveric porcine skin.

The positioning of the carbon fiber electrodes within the microneedle device should (a) facilitate interactions with the biological sample and (b) minimize carbon fiber exposure to stresses associated with microneedle insertion into skin and movement at the microneedle device-skin interface. To facilitate interactions between the biological sample and the carbon fiber electrodes, the carbon fiber electrodes must be positioned at the centers of the microneedle bores. In addition, dead space between the carbon fiber electrodes and the microneedle sidewalls may allow for infiltration of the biological sample. Figure 2-6 contains the scanning electron microscopy images of a hollow microneedle array and a single hollow microneedle after incorporation of carbon fiber electrodes. Figure 2-6B shows a scanning electron microscopy image of a single hollow microneedle after incorporation of carbon fiber electrodes; this image reveals that the carbon fiber electrodes do not extend beyond the tip of the microneedle bore. Placement of carbon fibers within the microneedle bores necessitated a precise alignment of the microneedle bores and the carbon fibers ; the positions of the laser-ablated holes in the lower layer of the microneedle device were coordinated with the positions of the microneedle bores in the upper layer of

the microneedle device.

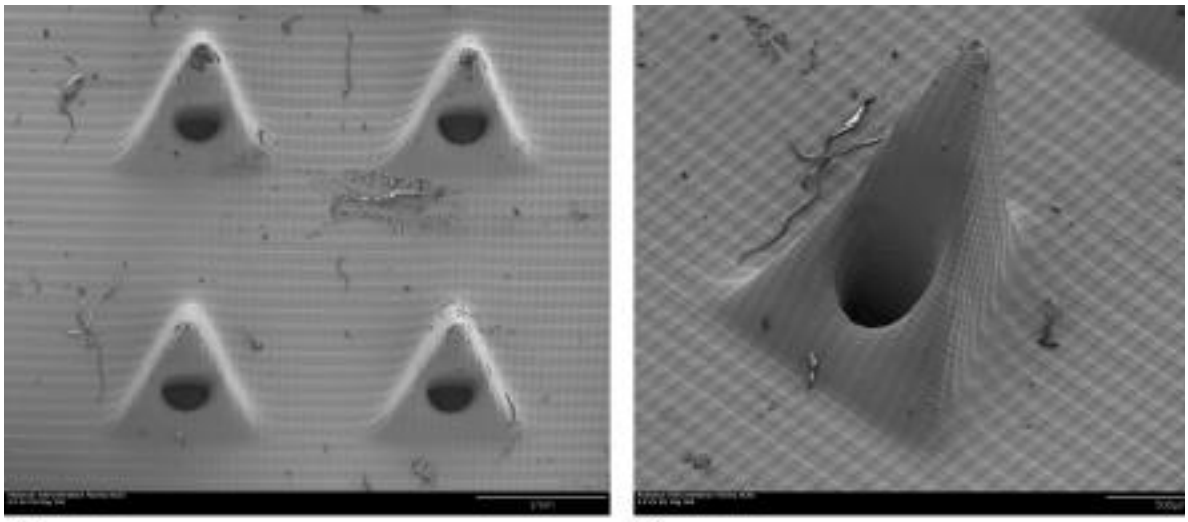

Figure 2-6: Scanning electron microscopy images of hollow microneedles after incorporation of carbon fiber electrodes: (a) plan view of electrode-hollow microneedle array and (b) isometric view of single electrode-hollow microneedle.

The electrochemical response of the carbon fibers within the electrode-hollow microneedle device toward 5 mM $Fe(CN)_6^{3-/4-}$/1 M KCl was evaluated. Figure 2-7 shows a cyclic voltammetric scan of 5 mM ferricyanide in 1 M KCl versus Ag/AgCl and Pt reference counter electrodes, respectively, at a scan rate of 100 mV/s. Well defined oxidation/reduction waves were observed, indicating interaction between the carbon fiber electrodes and the test solution as a result of permeation of the microneedle bore by the test solution. The average formal potential ($E^{0\prime}$) for $Fe(CN)_6^{3-/4-}$ was measured at 220 mV versus Ag/AgCl reference and platinum counter electrodes, respectively. The average peak separation was ΔE_p=125 mV. These results indicate that the carbon fibers within the electrode-hollow microneedle device were capable of providing electrochemical measurements.

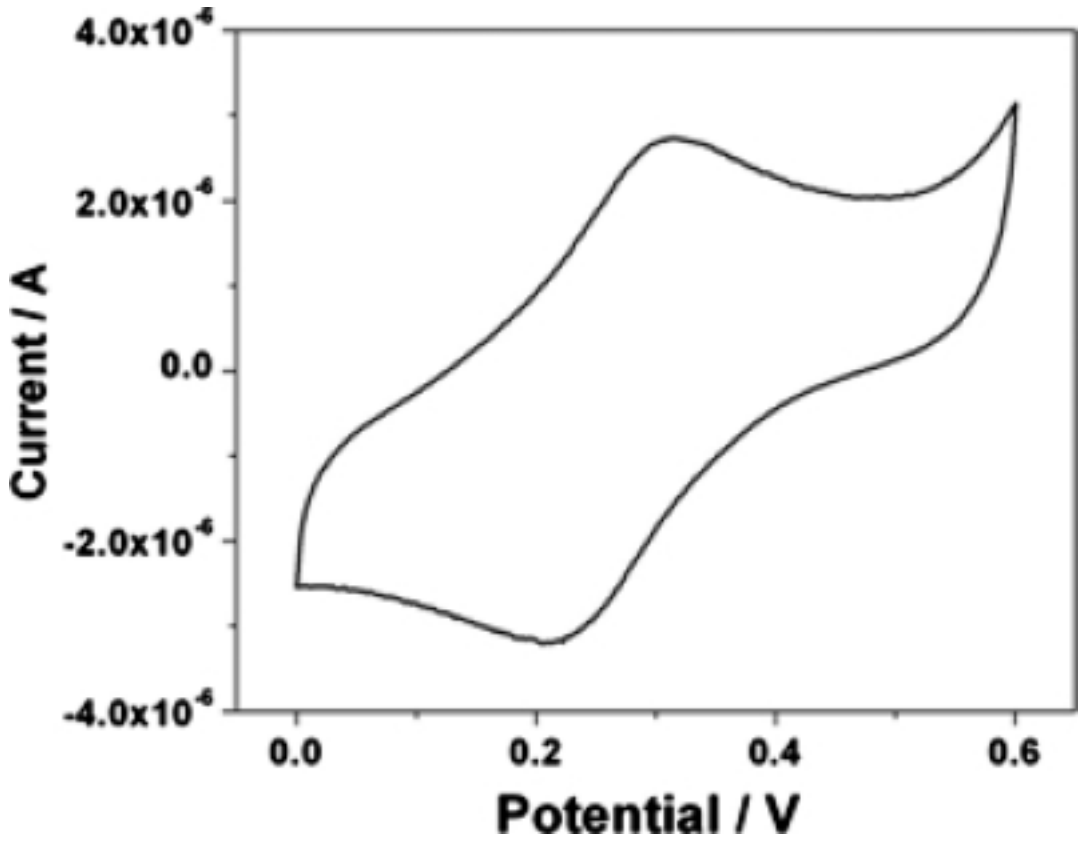

Figure 2-7: Cyclic voltammetric scan of 5 mM ferricyanide in 1 M KCl vs Ag/AgCl and Pt reference counter electrodes, respectively, at a scan rate of 100 mV/s.

Palladium-catalyzed oxidation of hydrogen peroxide on the carbon fibers within the electrode-hollow microneedle devices was also investigated. Palladium was deposited onto the carbon fibers by applying a potential of −0.8 V for 120 s in 1 mM Pd/0.5 M HCl prior to insertion into the microneedle device. Figure8 contains cyclic voltammetric scans of 0, 50, 100, 300, and 500 μM hydrogen peroxide, represented by pink, black, green, blue, and red curves, respectively, versus Ag/AgCl and Pt reference counter electrodes, respectively, at a scan rate of 100 mV/s. This figure shows an increase in reductive currents after additions of 0, 50, 100, 300, and 500 μM hydrogen peroxide, exhibiting a linear range of 100–500 μM and a detection limit of ~15 μM (based on the response of 50 μM hydrogen peroxide; S/N=3).

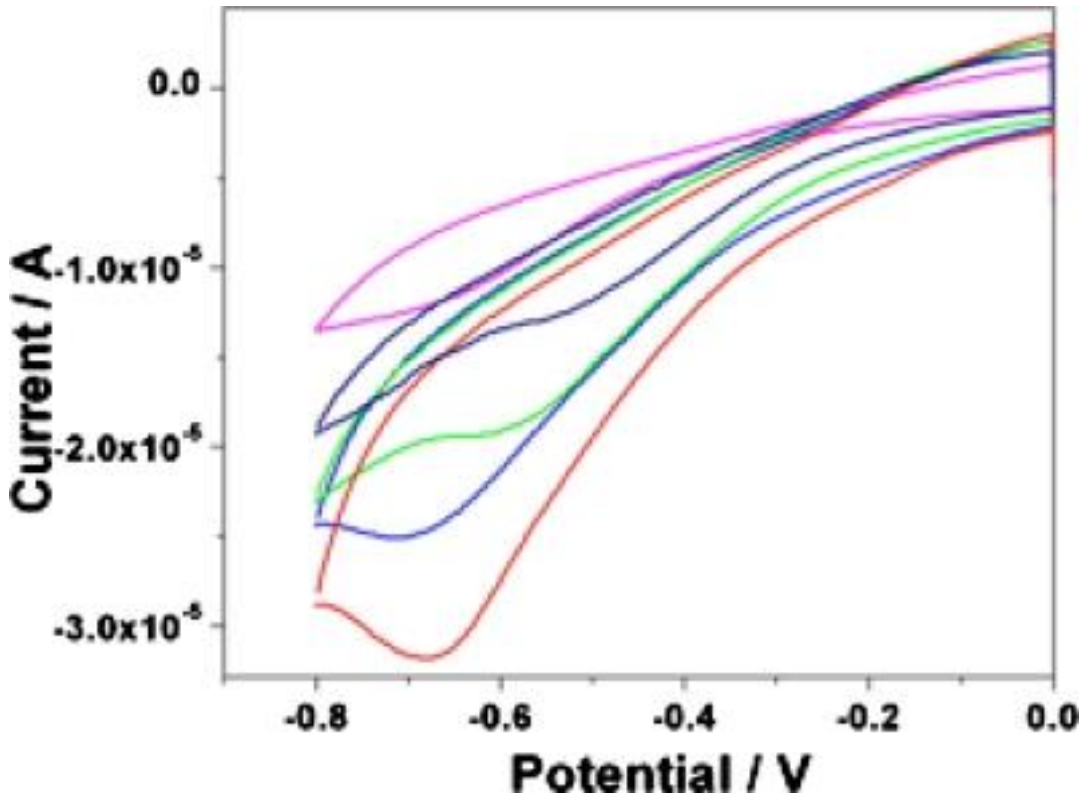

Figure 2-8: Cyclic voltammetric scans of 0, 50, 100, 300, and 500 μM hydrogen peroxide (pink, black, green, blue, and red curves) vs Ag/AgCl and Pt reference counter electrodes, respectively, at a scan rate of 100 mV/s.

Following the examples by Civit et al. and Nassef et al., the carbon fibers were modified with aminophenol (o-AP) groups following *in situ* diazotination and electrografting of the corresponding diazonium salt.[5960] Modification of the carbon fiber electrode with o-AP has been shown to result in electrocatalytic oxidation of ascorbic acid and selective oxidation of ascorbic acid in the presence of common interferon's such as uric and citric acids. Uric acid is a well-known interferon in electrochemical analysis of ascorbic acid, which is attributed to the fact that uric acid and ascorbic acid possess similar oxidation potential values.[61] Linear sweep voltammograms of 100 mM phosphate buffer (blank solution) and 1 mM ascorbic acid in 100 mM phosphate buffer (*p*H=7) versus Ag/AgCl and Pt reference counter electrodes, respectively, at a scan rate of 100 mV/s are shown in Figure 2-9. This result indicates that the carbon fibers within the electrode-hollow

microneedle device are able to detect the ascorbate analyte with the low potential oxidation of ascorbic acid at 195 mV.

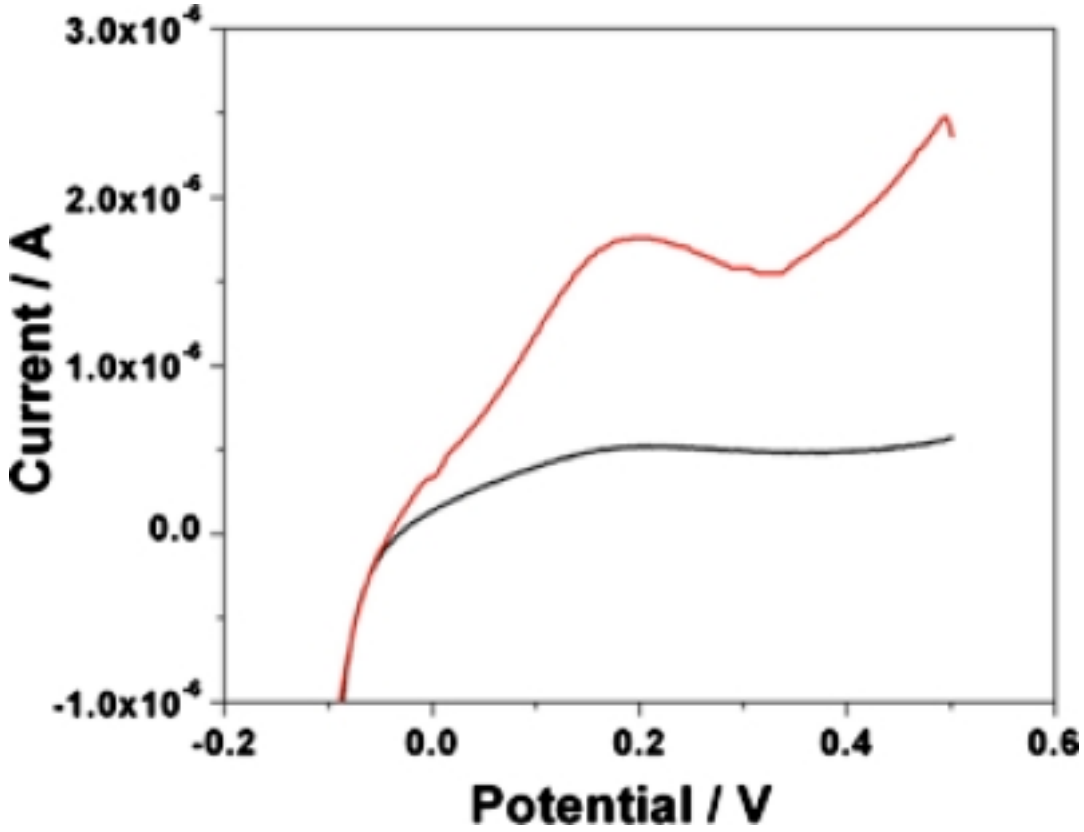

Figure 2-9: Linear sweep voltammograms of 0 mM (black) and 1 mM (red) ascorbic acid in 100 mM phosphate buffer (*p*H=7) vs Ag/AgCl and Pt reference counter electrodes, respectively, at a scan rate of 100 mV/s.

Conclusions

In summary, we have demonstrated that carbon fiber electrodes integrated within hollow microneedles, which were produced using digital micromirror device-based stereolithography, can function as electrochemical transducers. The low cost and high yield offered by the digital micromirror device-based stereolithography process suggest that it is a suitable approach for large-scale production of hollow microneedles. The rapid processing rate offered by the digital micromirror device-based stereolithography process suggests that it is an appropriate approach for tailoring microneedle design. Studies involving

porcine skin demonstrated that the microneedle arrays were able to penetrate the outermost layer of the skin and that the microneedles remained intact after insertion. The MTT assay indicated that the e-Shell 200 only exhibited a slight decrease in viability in a manner that would raise concerns regarding potential *in vivo* use in a non-implantable medical device.

Electrochemical measurements by the carbon fibers within the electrode-hollow microneedle device were demonstrated. In addition, chemical modification of the carbon fibers for selective analytes was shown; detection of hydrogen peroxide and ascorbic acid using these modified carbon fibers was demonstrated. While these experiments used outside reference and counter electrodes, it is envisioned that selective microneedles within the microneedle arrays can be modified to integrate quasi reference and counter electrode components. It is also envisioned that a single microneedle array can include multiple functionalities, including drug delivery and monitoring of several analytes; such a device would be capable of integrated, closed-loop sensing and drug delivery. As mentioned by Wilson et al., biocompatibility issues must be successfully addressed in order achieve continuous *in vivo* monitoring.[2] Decreasing the microneedle length is another important parameter that must be considered in future efforts; Gill et al. demonstrated that microneedle length was positively correlated with pain; patient pain may be reduced by decreasing microneedle length.[13] Use of novel stereolithography-compatible materials, including materials based on vinyl esters, may provide higher cell viability rates.[62][62]

References

[1]Justino, C. I., Rocha-Santos, T. A., & Duarte, A. C. (2010). Review of analytical figures of merit of sensors and biosensors in clinical applications. *TrAC Trends in Analytical Chemistry*, *29*(10), 1172-1183.

[2] Wilson, G. S., & Gifford, R. (2005). Biosensors for real-time in vivo measurements. *Biosensors and Bioelectronics*, *20*(12), 2388-2403.

[3] Stett, A., Egert, U., Guenther, E., Hofmann, F., Meyer, T., Nisch, W., & Haemmerle, H. (2003). Biological application of microelectrode arrays in drug discovery and basic research. *Analytical and bioanalytical chemistry*, *377*(3), 486-495.

[4] Wang, J., Pamidi, P. V., & Park, D. S. (1996). Screen-printable sol-gel enzyme-containing carbon inks. *Analytical Chemistry*, *68*(15), 2705-2708.

[5] Wang, J. (2001). Glucose biosensors: 40 years of advances and challenges.*Electroanalysis*, *13*(12), 983.

[6]Newman, J. D., & Setford, S. J. (2006). Enzymatic biosensors. *Molecular biotechnology*, *32*(3), 249-268.

[7] Mastrototaro, J. J. (2000). The MiniMed continuous glucose monitoring system.*Diabetes technology & therapeutics*, *2*(1, Supplement 1), 13-18.

[8] Vaddiraju, S., Tomazos, I., Burgess, D. J., Jain, F. C., & Papadimitrakopoulos, F. (2010). Emerging synergy between nanotechnology and implantable biosensors: a review. *Biosensors and Bioelectronics*, *25*(7), 1553-1565.

[9] Kaushik, S., Hord, A. H., Denson, D. D., McAllister, D. V., Smitra, S., Allen, M. G., & Prausnitz, M. R. (2001). Lack of pain associated with microfabricated microneedles. *Anesthesia & Analgesia*, *92*(2), 502-504.

[10] Gittard, S. D., Ovsianikov, A., Chichkov, B. N., Doraiswamy, A., & Narayan, R. J. (2010). Two-photon polymerization of microneedles for transdermal drug delivery. *Expert opinion on drug delivery*, *7*(4), 513-533.

[11] McAllister, D. V., Wang, P. M., Davis, S. P., Park, J. H., Canatella, P. J., Allen, M. G., & Prausnitz, M. R. (2003). Microfabricated needles for transdermal delivery of macromolecules and nanoparticles: fabrication methods and transport studies. *Proceedings of the National Academy of Sciences*, *100*(24), 13755-13760.

[12] Park, J. H., Yoon, Y. K., Choi, S. O., Prausnitz, M. R., & Allen, M. G. (2007). Tapered conical polymer microneedles fabricated using an integrated lens technique for transdermal drug delivery. *Biomedical Engineering, IEEE Transactions on*, *54*(5), 903-913.

[13]Gill, H. S., Denson, D. D., Burris, B. A., & Prausnitz, M. R. (2008). Effect of microneedle design on pain in human subjects. *The Clinical journal of pain*,*24*(7), 585.

[14] Gardeniers, H. J., Luttge, R., Berenschot, E. J., De Boer, M. J., Yeshurun, S. Y., Hefetz, M., ... & van den Berg, A. (2003). Silicon micromachined hollow microneedles for transdermal liquid transport. *Microelectromechanical Systems, Journal of*, *12*(6), 855-862.

[15] Zahn, J. D., Trebotich, D., & Liepmann, D. (2005). Microdialysis microneedles for continuous medical monitoring. *Biomedical microdevices*, *7*(1), 59-69.

[16] Suzuki, H., Tokuda, T., & Kobayashi, K. (2002). A disposable "intelligent mosquito" with a reversible sampling mechanism using the volume-phase transition of a gel. *Sensors and Actuators B: Chemical*, *83*(1), 53-59.

[17] Stoeber, B., & Liepmann, D. (2005). Arrays of hollow out-of-plane microneedles for drug delivery. *Microelectromechanical Systems, Journal of*, *14*(3), 472-479.

[18] Mukerjee, E. V., Collins, S. D., Isseroff, R. R., & Smith, R. L. (2004). Microneedle array for transdermal biological fluid extraction and in situ analysis.*Sensors and Actuators A: Physical*, *114*(2), 267-275.

[19] Tsuchiya, K., Nakanishi, N., Uetsuji, Y., & Nakamachi, E. (2005). Development of blood extraction system for health monitoring system. *Biomedical microdevices*, *7*(4), 347-353.

[20] McAllister, D. V., Allen, M. G., & Prausnitz, M. R. (2000). Microfabricated microneedles for gene and drug delivery. *Annual Review of Biomedical Engineering*, *2*(1), 289-313.

[21] Kaushik, S., Hord, A. H., Denson, D. D., McAllister, D. V., Smitra, S., Allen, M. G., & Prausnitz, M. R. (2001). Lack of pain associated with microfabricated microneedles. *Anesthesia & Analgesia*, *92*(2), 502-504.

[22] Chun, K., Hashiguchi, G., & andHiroyuki Fujita, H. T. (1999). Fabrication of array of hollow microcapillaries used for injection of genetic materials into animal/plant cells. *Japanese journal of applied physics*, *38*(3A), L279.

[23] Kim, K., Park, D. S., Lu, H. M., Che, W., Kim, K., Lee, J. B., & Ahn, C. H. (2004). A tapered hollow metallic microneedle array using backside exposure of SU-8. *Journal of Micromechanics and Microengineering*, *14*(4), 597.

[24] Park, J. H., Allen, M. G., & Prausnitz, M. R. (2005). Biodegradable polymer microneedles: fabrication, mechanics and transdermal drug delivery. *Journal of Controlled Release*, *104*(1), 51-66.

[25] Perennes, F., Marmiroli, B., Matteucci, M., Tormen, M., Vaccari, L., & Di Fabrizio, E. (2006). Sharp beveled tip hollow microneedle arrays fabricated by LIGA and 3D soft lithography with polyvinyl alcohol. *Journal of Micromechanics and Microengineering*, *16*(3), 473.

[26] Wang, P. M., Cornwell, M., Hill, J., & Prausnitz, M. R. (2006). Precise microinjection into skin using hollow microneedles. *Journal of investigative dermatology*, *126*(5), 1080-1087.

[27]Bertsch, A., Bernhard, P., Vogt, C., & Renaud, P. (2000). Rapid prototyping of small size objects. *Rapid Prototyping Journal*, *6*(4), 259-266.

[28] Lan, P. X., Lee, J. W., Seol, Y. J., & Cho, D. W. (2009). Development of 3D PPF/DEF scaffolds using micro-stereolithography and surface modification.*Journal of Materials Science: Materials in Medicine*, *20*(1), 271-279.

[29] Melchels, F. P., Feijen, J., & Grijpma, D. W. (2010). A review on stereolithography and its applications in biomedical engineering. *Biomaterials*,*31*(24), 6121-6130.

[30] Tse, L. A., Hesketh, P. J., Rosen, D. W., & Gole, J. L. (2003). Stereolithography on silicon for microfluidics and microsensor packaging. *Microsystem Technologies*, *9*(5), 319-323.

[31] Matsuda, T., & Mizutani, M. (2002). Liquid acrylate-endcapped biodegradable poly (ϵ-caprolactone-co-trimethylene carbonate). II. Computer-aided stereolithographic microarchitectural surface photoconstructs. *Journal of biomedical materials research*, *62*(3), 395-403.

[32] Zhang, X., Jiang, X. N., & Sun, C. (1999). Micro-stereolithography of polymeric and ceramic microstructures. *Sensors and Actuators A: Physical*, *77*(2), 149-156.

[33] Choi, J. W., Park, I. B., Ha, Y. M., Jung, M. G., Lee, S. D., & Lee, S. H. (2006, October). Insertion force estimation of various microneedle array-type structures fabricated by a microstereolithography apparatus. In *SICE-ICASE, 2006. International Joint Conference* (pp. 3678-3681). IEEE.

[34] Ovsianikov, A., Malinauskas, M., Schlie, S., Chichkov, B., Gittard, S., Narayan, R., ... & Haverich, A. (2011). Three-dimensional laser micro-and nano-structuring of acrylated poly (ethylene glycol) materials and evaluation of their cytoxicity for tissue engineering applications. *Acta biomaterialia*, *7*(3), 967-974.

[35] Doraiswamy, A., Jin, C., Narayan, R. J., Mageswaran, P., Mente, P., Modi, R., ... & Chichkov, B. (2006). Two photon induced polymerization of organic–inorganic hybrid biomaterials for microstructured medical devices. *Acta Biomaterialia*, *2*(3), 267-275.

[36] Ovsianikov, A., Chichkov, B., Mente, P., Monteiro-Riviere, N. A., Doraiswamy, A., & Narayan, R. J. (2007). Two photon polymerization of polymer–ceramic hybrid materials for transdermal drug delivery. *International journal of applied ceramic technology*, *4*(1), 22-29.

[37] Gittard, S. D., Miller, P. R., Boehm, R. D., Ovsianikov, A., Chichkov, B. N., Heiser, J., ... & Narayan, R. J. (2011). Multiphoton microscopy of transdermal quantum dot delivery using two photon polymerization-fabricated polymer microneedles. *Faraday discussions*, *149*, 171-185.

[38] Sun, C., Fang, N., Wu, D. M., & Zhang, X. (2005). Projection micro-stereolithography using digital micro-mirror dynamic mask. *Sensors and Actuators A: Physical*, *121*(1), 113-120.

[39] Gittard, S. D., Narayan, R., Lusk, J., Morel, P., Stockmans, F., Ramsey, M., ... & Chichkov, B. N. (2009). Rapid prototyping of scaphoid and lunate bones.*Biotechnology journal*, *4*(1), 129-134.

[40] Han, L. H., Mapili, G., Chen, S., & Roy, K. (2008). Projection microfabrication of three-dimensional scaffolds for tissue engineering. *Journal of Manufacturing Science and Engineering*, *130*(2), 021005.

[41] Choi, J. W., Wicker, R., Lee, S. H., Choi, K. H., Ha, C. S., & Chung, I. (2009). Fabrication of 3D biocompatible/biodegradable micro-scaffolds using dynamic mask projection microstereolithography. *Journal of Materials Processing Technology*, *209*(15), 5494-5503.

[42] Choi, J. W., MacDonald, E., & Wicker, R. (2010). Multi-material microstereolithography. *The International Journal of Advanced Manufacturing Technology*, *49*(5-8), 543-551.

[43] Gill, H. S., & Prausnitz, M. R. (2007). Coated microneedles for transdermal delivery. *Journal of controlled release*, *117*(2), 227-237.

[44] Technical Data: EnvisionTEC e-Shell 200 Series, http://www.envisiontec.de/fileadmin/pdf/matsheet_eshell200_en_s.pdf. Retrieved 27 January 2011.

[45] Gittard, S. D., Ovsianikov, A., Monteiro-Riviere, N. A., Lusk, J., Morel, P., Minghetti, P., ... & Narayan, R. J. (2009). Fabrication of polymer microneedles using a two-photon polymerization and micromolding process. *Journal of diabetes science and technology*, *3*(2), 304-311.

[46] Bader, R., Steinhauser, E., Rechl, H., Siebels, W., Mittelmeier, W., & Gradinger, R. (2003). [Carbon fiber-reinforced plastics as implant materials]. *Der Orthopade*, *32*(1), 32-40.

[47] Wolter, D. (1983). Biocompatibility of carbon fibre and carbon fibre microparticles. *Aktuelle Probleme in Chirurgie und Orthopädie*, *26*, 28.

[48] Bader, R., Steinhauser, E., Rechl, H., Siebels, W., Mittelmeier, W., & Gradinger, R. (2003). [Carbon fiber-reinforced plastics as implant materials]. *Der Orthopade*, *32*(1), 32-40.

[49] Wolter, D. (1983). Biocompatibility of carbon fibre and carbon fibre microparticles. *Aktuelle Probleme in Chirurgie und Orthopädie*, *26*, 28.

[50] Neugebauer, R., Helbing, G., Wolter, D., Mohr, W., & Gistinger, G. (1981). The body reaction to carbon fibre particles implanted into the medullary space of rabbits. *Biomaterials*, *2*(3), 182-184.

[51] Chakraborty, S., & Raj, C. R. (2007). Mediated electrocatalytic oxidation of bioanalytes and biosensing of glutamate using functionalized multiwall carbon nanotubes-biopolymer nanocomposite. *Journal of Electroanalytical Chemistry*,*609*(2), 155-162.

[52] Jacobs, C. B., Peairs, M. J., & Venton, B. J. (2010). Review: Carbon nanotube based electrochemical sensors for biomolecules. *Analytica Chimica Acta*,*662*(2), 105-127.

[53] Grano, A., & De Tullio, M. C. (2007). Ascorbic acid as a sensor of oxidative stress and a regulator of gene expression: the Yin and Yang of vitamin C.*Medical hypotheses*, *69*(4), 953-954.

[54] Babu, G. N., Bawari, M., Mathur, V. N., Kalita, J., & Misra, U. K. (1998). Blood glutamate levels in patients with motor neuron disease. *Clinica chimica acta*,*273*(2), 195-200.

[55] Salmenperä, L. (1984). Vitamin C nutrition during prolonged lactation: optimal in infants while marginal in some mothers. *The American journal of clinical nutrition*, *40*(5), 1050-1056.

[56] Harrison, F. E., Meredith, M. E., Dawes, S. M., Saskowski, J. L., & May, J. M. (2010). Low ascorbic acid and increased oxidative stress in gulo (−/−) mice during development. *Brain research*, *1349*, 143-152.

[57] Mosmann, T. (1983). Rapid colorimetric assay for cellular growth and survival: application to proliferation and cytotoxicity assays. *Journal of immunological methods*, *65*(1), 55-63.

[58] Downard, A. J., Roddick, A. D., & Bond, A. M. (1995). Covalent modification of carbon electrodes for voltammetric differentiation of dopamine and ascorbic acid. *Analytica chimica acta*, *317*(1), 303-310.

[59] Verbaan, F. J., Bal, S. M., Van den Berg, D. J., Groenink, W. H. H., Verpoorten, H., Lüttge, R., & Bouwstra, J. A. (2007). Assembled microneedle arrays enhance the transport of compounds varying over a large range of molecular weight across human dermatomed skin. *Journal of Controlled Release*, *117*(2), 238-245.

[60] Nassef, H. M., Radi, A. E., & O'Sullivan, C. (2007). Simultaneous detection of ascorbate and uric acid using a selectively catalytic surface. *Analytica chimica acta*, *583*(1), 182-189.

[61] Bravo, R., Hsueh, C., Brajter-Toth, A., & Jaramillo, A. (1998). Possibilities and limitations in miniaturized sensor design for uric acid. *Analyst*, *123*(7), 1625-1630.

[62] Heller, C., Schwentenwein, M., Russmueller, G., Varga, F., Stampfl, J., & Liska, R. (2009). Vinyl esters: low cytotoxicity monomers for the fabrication of biocompatible 3D scaffolds by lithography based additive manufacturing.*Journal of Polymer Science Part A: Polymer Chemistry*, *47*(24), 6941-6954.

Chapter 3 Multiplexed Microneedle-Based Biosensor Array for Characterization of Metabolic Acidosis

Philip R Miller[1], Shelby Skoog[1], Thayne L Edwards[2], Deanna M Lopez[2], David R Wheeler[2], Dulce C Arango[2], Xiaoyin Xiao[2], Susan M Brozik[2], Joseph Wang[3], Ronen Polsky[2], Roger J Narayan [1*]

[1] Joint Department of Biomedical Engineering, University of North Carolina and North Carolina State University, Raleigh, NC 27695-7115, USA

[2] Department of Biosensors and Nanomaterials, Sandia National Laboratories, Albuquerque, NM 87185, USA

[3] Department of NanoEngineering, University of California at San Diego, La Jolla, CA 92093-0448, USA

The following section a complete article reprinted from Talanta, Volume 88, Philip R Miller, Shelby A Skoog, Thayne L Edwards, Deanna M Lopez, David R Wheeler, Dulce C Arango, Xiaoyin Xiao, Susan M Brozik, Joseph Wang, Ronen Polsky, Roger J Narayan, 739-742,

Note: This article has been reformatted. In particular, the location of figures and spacing may have changed. The references are formatted as in the original manuscript.

Abstract

The development of a microneedle-based biosensor array for multiplexed in situ detection of exercise-induced metabolic acidosis, tumor microenvironment, and other variations in tissue chemistry is described. Simultaneous and selective amperometric detection of pH, glucose, and lactate over a range of physiologically-relevant concentrations in complex media is demonstrated. Furthermore, materials modified with a cell-resistant (Lipidure®) coating were shown to inhibit macrophage adhesion; no signs of coating delamination were noted over a 48-hour period.

Introduction

Pathologic conditions and exercise are associated with alterations in the chemical environment. For example, vigorous exercise can result in metabolic acidosis [1]. In addition to increased fluid pressure and decreased oxygen concentration, alterations in the tissue microenvironment are noted with many tumors [2]. The hypoxic environment of cancer cells along with the Warburg effect (aerobic glycolysis and lactate production by cancer cells) create a microenvironment that is characterized by low glucose concentrations, high lactate concentrations, and low pH levels [3,4]. Although low pH values are a well-established characteristic of tumor microenvironments [5], the basis of extracellular acidosis is not completely understood. Lactate production is considered to be a main contributor; however, CO_2 production, bicarbonate depletion, ATP hydrolysis, and glutaminolysis may also be contributing factors [6,7,8,9]. In addition, the dynamic nature of cancer cells leads to alterations in metabolism such that cancer cells may rapidly cycle between lactate-producing and lactate-consuming states [10]. While this complex relationship between neoplastic cell proliferation, metabolism, and tumor microenvironment is not entirely understood, this association is observed at the earliest stages of tumor progression [11]. Several areas of study, including genomics, proteomics and metabolomics, can provide insight into signaling pathways and metabolic control of proliferating cancer cells. Furthermore, sensors that enable real time simultaneous detection of multiple biomarkers within the tumor microenvironment may provide additional insight into metabolic acidosis associated with cancer. Novel bioanalytical tools for simultaneous detection of multiple biomarkers may be useful for addressing issues regarding tumor microenvironment and other medically-relevant conditions.

We report the first demonstration of microneedle arrays that have individually addressable

sensing microneedles for simultaneous detection of pH, glucose, and lactate. Microneedles offer a novel approach for minimally invasive detection of physiologically-relevant analytes. Initially developed for painless transdermal delivery of pharmacologic agents and vaccines, recent work has shown that hollow microneedle arrays may be used to house microelectrodes for highly sensitive and selective electrochemical detection of physiologically-relevant analytes [12,13,14,15,16,17,18]. For example, previous studies have involved the use of hollow microneedle-based devices for electrochemical detection of individual analytes such as ascorbic acid, hydrogen peroxide, lactate, and glucose [12,13,14]. Owing to the arrayed nature of these microneedle structures, specific target analytes can be detected by each constituent of the array and multiplexed sensing operations can be realized. The multiplexed addressable microneedle array technology that is reported in the present work could lead to a new generation of diagnostic tools for simultaneous detection of a variety of physiologically-relevant analytes.

Materials and Methods

Reagents:

All reagents were used without modification or purification unless stated. 4-Benzoylamino-2,5-dimethoxybenzenediazonium chloride hemi(zinc chloride) salt Azoic Diazo No. 24 (Fast Blue RR salt), lactate oxidase from *Pediococcus sp.* (E.C. 1.13.12.4), glucose oxidase from *Aspergillus niger* (E.C. 1.1.3.4), mineral oil (0.870 g/m^3), polyethyleneimine, graphite powder, rhodium on carbon with 5 wt. % loading, D-(+)-glucose , L-(+)-lactic acid, sodium phosphate monobasic, sodium phosphate dibasic, phosphoric acid, 2-propanol (99.5%), and acetonitrile (99.8%) were obtained from a commercial vendor (Sigma-Aldrich, St. Louis, MO). Unless noted, ultrapure nanofiltered deionized water was used (18.2 MΩ•cm).

Electrochemical Measurements:

Electrochemical measurements were performed on a PGSTAT12 Autolab® Potentiostat (EcoChemie, Utrecht, the Netherlands); control of experiments and acquisition of data were performed with the accompanying software. To complete the cell, an Ag/AgCl reference electrode and a Pt wire counter electrode were used.

Microneedle Fabrication:

Hollow microneedles were fabricated with a Perfactory® III SXGA instrument and an Otoflash® Post Curing System instrument (EnvisionTEC GmbH, Gladbeck, Germany). Fabrication was based on computer aided design files that were created using Solidworks®

(Dassault Systemes SA, Velizy, France) and support structures that were created using Magics® RP 13 (Materialise NV, Leuven, Belgium). A photo-sensitive polymer that may be polymerized using ultraviolet radiation, E-shell 300 (Envisiontec GmbH, Gladbeck, Germany), was utilized in this study. Upon completion of the build process using the Perfactory® III SXGA instrument, the microneedles were washed in isopropanol to remove unpolymerized resin and dried. After drying, the microneedles were placed in the Otoflash® Postcuring System (EnvisionTEC GmbH, Gladbeck, Germany) for 50 seconds to ensure complete polymerization of the structures. Microneedle shape was based on a previous microneedle array design with an alteration to the bottom row of the 2 x 2 array of microneedles; these microneedles were offset by 45° to facilitate placement over electrode cavities. In addition, vents were placed in the substrate around the microneedles to facilitate fluid flow through the microneedles. The light source for the micro-stereolithography system (z-step height=50 mm) was a 150 W halogen bulb, which was operated at 180 mW.

SEM Imaging:

Imaging of the microneedle arrays was performed with a S-3200 variable pressure scanning electron microscope (Hitachi, Tokyo, Japan), which was equipped with a Robinson backscattered electron detector. Prior to imaging, the microneedle arrays were coated with a 60% gold-40% palladium layer using a Technics Hummer II instrument (Anatech, Battle Creek, MI).

Synthesis of Glucose Oxidase and Lactate Oxidase Pastes:

Pastes were made using previously-described protocols. For glucose detection, 10 mg of glucose oxidase was added to 2.2 mg of polyethyleneimine and thoroughly mixed. To this mixture, 100 mg of paste made from 60 % rhodium on carbon and 40% mineral oil w/w was added and combined until a homogeneous mixture was obtained.

For lactate detection, 2.5 mg of lactate oxidase was mixed with 2.5 mg of rhodium on carbon; this mixture underwent 5 cycles that involved alternation between sonicating in an ice bath and vortexing for five minutes each [3]. 31.25 mg of mineral oil and 3.75 mg of polyethyleneimine were added to the mixture and combined with a mortar and pestle for an hour. Pastes were prepared prior to testing and stored at 3 ^{o}C when not in use.

Chemical Modification to Carbon Pastes for pH Detection:

70% (w/w) graphite powder was mixed with 30% (w/w) mineral oil until a homogeneous paste was obtained. The paste was then applied to the electrode cavity; the surface was cleaned by gently scraping with the edge of a weight boat. A solution of 0.5 M phosphoric acid and 10 mM Fast Blue RR salt was applied to the carbon paste and allowed to deposit for 30 minutes. The sensor was then cleaned with deionized water.

Electrode Strip and Sensor Assembly:

Three-inch, 10-conductor, 0.5 mm spacing, flat flexible cable assemblies (Molex, Lisle, IL) were used to prepare the sensor devices. Two sensor devices were fabricated from each flat flexible cable assembly. Laser ablation was used to create openings in the polyester insulating layer to the tin-plated copper conductors. A Model 6.75 60W CO_2

raster/vector laser system (Universal Laser Systems, Inc., Scottsdale, AZ), which was operated in vector mode, was used to produce alignment marks. After the laser was aligned to the flat flexible cable, the hole-array pattern (hole diameter=500 μm) was raster ablated from the flat flexible cable. This pattern and subsequent patterns were designed using CorelDraw® software (Corel, Ottawa, ON); these patterns were directly transferred to the laser system via the printer driver. The residue on the metal from the ablation process was removed with acetone that was sprayed from an air brush (Anest Iwata, West Chester, OH) using a pressure of approximately 40 psi; this structure was subsequently rinsed with isopropanol and water. The ablated and cleaned flat flexible cable was then cut into two pieces at the midpoint. A CO_2 vector laser was subsequently used for ablation of a 0.003 inch layer of Melinex® (DuPont Teijin, Chester, VA) piece that was coated on a single side with an ultra-clean acrylic-based laminating adhesive (3M, Minneapolis, MN); these materials were obtained from a commercial vendor (Fralock, San Carlos, CA). The perimeter of this piece was identical to that of the microneedle array base. The hole pattern was identical to that of the previous step except that the hole diameter was slightly larger (hole diameter=750 μm). This layer was adhered to the flat flexible cable and pressed together under a pressure of 3000 psi for 2 minutes. This layer provided a smooth working surface for application of carbon paste; a spatula and a squeegee were used to create a smooth electrode surface and to remove excess paste from the Melinex® surface. Fluidic microchannels were vector cut using a carbon dioxide laser into a 0.004 inch Melinex® layer that was coated on both sides with an acrylic-based laminating adhesive; this structure was adhered to the first Melinex® layer and pressed together as previously described. Assembly of paste electrodes initially involved creation of the pH selective electrode. Once the solution containing Fast Blue RR salt and phosphoric acid was deposited and washed away, the two modified pastes were applied to their respected cavities with

care to avoid contaminating one paste with another. An identical layer of ablated tape was adhered to the top of the previous tape such that the patterns of the two tape layers exhibited precise matching. The microneedle array was then attached to this assembly with parafilm.

Cell-Resistant Coating:

Lipidure® (NOF America Corporation, White Plains, NY) 0.5 w/w% was dissolved in ethanol by alternating between sonicating and vortexing. E-shell 300 chips were prepared by molding with a 1 mm thick, 1 cm circular aluminum disk. The mold was created by adhering the aluminum disk to a glass slide, applying polydimethylsiloxane to cover the disk, and heating the construct at 150 ^{o}C to polymerize the polydimethylsiloxane. The polydimethylsiloxane mold was filled with E-shell 300 resin and a glass slide was placed over the cavity to ensure that no air was trapped within the E-shell 300 resin. A 50 s treatment in the Autoflash® postcuring system was used to polymerize the resin. The chips were washed with isopropanol, washed with deionized water, dried, and placed in 12 well plates. 2 ml of the Lipidure® solution was added to each of the wells and allowed to dry in a vacuum desiccator. Once dried, the samples were removed from the well plates, rinsed with 2-propanol, rinsed with deionized water, and dried. The samples were then placed in sterile 6-well plates and seeded with RAWRGTAPCP cells (gift from Bryan Carsons of Sandia National Laboratories) at a density of 300,000 cells/well in 3 mL of Dulbecco's Modified Eagle Medium (10% FBS, 1% Pen/Strep); G418-sulfate (400 mg/ml) and Hygromycin B (400 ml/50 ml) (Mediatech Cellgro, Manassas, Virginia) were added to the medium. The cells were cultured in a 5% CO_2 incubator at a temperature of 37 ^{o}C. The samples were removed at predetermined time points of 2, 24, and 48 hours. A 200M Axiovert inverted

microscope (Carl Zeiss, Oberkochen, Germany) was used to image the samples. Transmission images were obtained of the E-shell 300 substrates in the well plates. After imaging, the substrates were removed from the wells and twice rinsed in 1X phosphate buffered saline solution to remove any unattached cells. The substrates were then immersed in 1X phosphate buffered saline solution. Fluorescence images were obtained for comparing cell attachment on Lipidure®-coated and uncoated materials.

Results and Discussion

In this study, microneedle sensors were comprised of a hollow microneedle array that was aligned with strategically placed wells on a commercially-obtained flexible flat cable. Each well had been filled with carbon paste material that was tailored to detect pH, glucose, or lactate. Microneedle arrays were fabricated with a dynamic light micro-stereolithography system using an approach that has been previously described; the microarray design was defined using commercially-obtained computer-aided design software Figure 3-1a.[12] CO_2 laser ablation was used to create openings in the top insulation layer of the flexible flat cable, exposing the underlying conductors. A layer of single-sided polyester tape was also laser ablated with well patterns that corresponded to the flexible flat cable openings; this structure was aligned and adhered to the flexible flat cable. These wells were subsequently filled with carbon paste (Figure 3-1b). This method allowed for each electrode to be addressed by one conductor of the flexible flat cable, which readily interfaced with a circuit board through a low-insertion force connector. A second layer of laser-ablated, double-sided, adhesive-coated tape was used to attach the microneedle array to the flexible flat cable; this structure also served as a fluidic microchannel for the sample. Use of rhodium-modified carbon pastes for detection of glucose and lactate has previously been described [13,14,19]. Microneedle paste electrodes for detection of pH were created by chemically depositing Fast Blue RR diazonium salt; the electrodes were subsequently washed with deionized water [20]. Calibration of chemically modified carbon pastes for detecting alterations in pH was performed in 0.1 M phosphate buffer over a 5.0-8.0 pH range at intervals of 0.5 pH units. Cyclic voltammetric scans were performed from -0.7 V to 0.8 V at 100 mV/s against external Ag/AgCl reference and Pt counter electrodes. The pH response was measured by evaluating the shift of the anodic peak potential position of the

quinone moiety on the immobilized Fast Blue RR salt. Figure 3-2 shows the calibration curve for chemically modified carbon paste strips. Increasing buffer acidity caused a negative shift in the anodic peak potential; a highly linear relationship over the entire tested pH region (R^2=99%) demonstrated that the sensors within the integrated carbon paste microneedle platform were capable of pH monitoring.

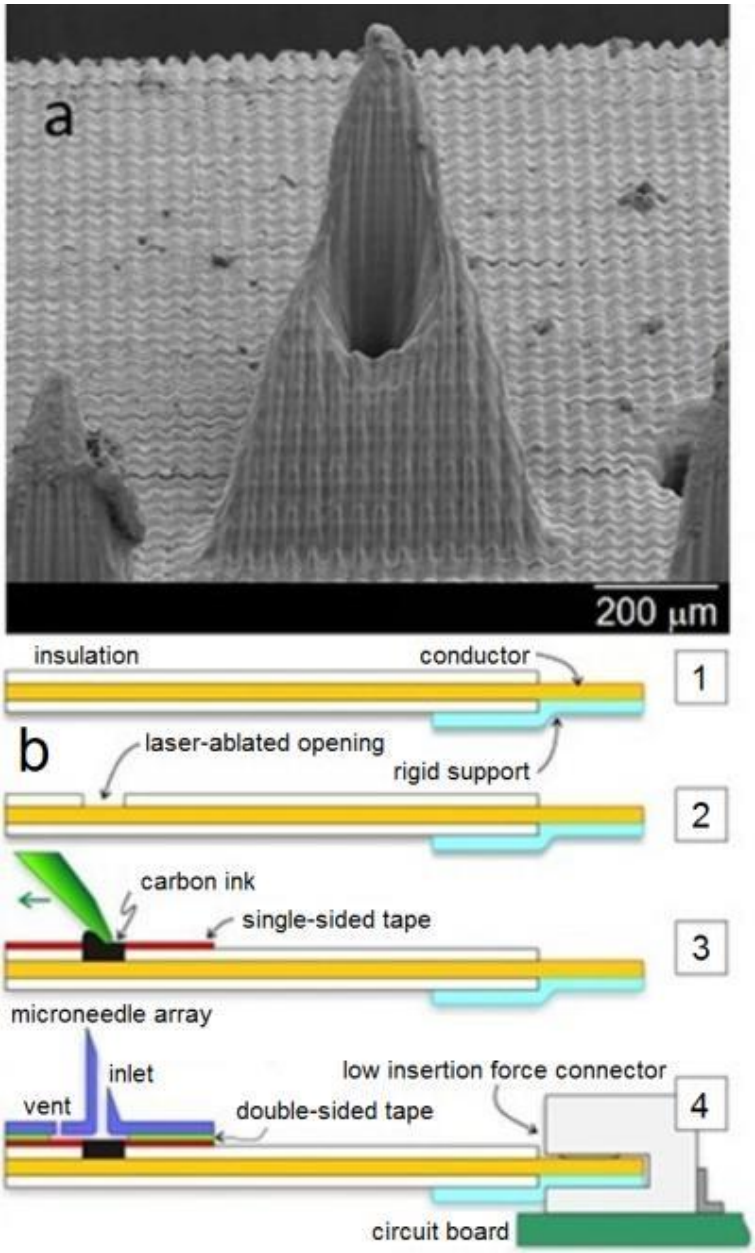

Figure 3-1: Scanning electron micrograph of a single microneedle (A) and schematic of the microneedle-biosensor assembly (B).

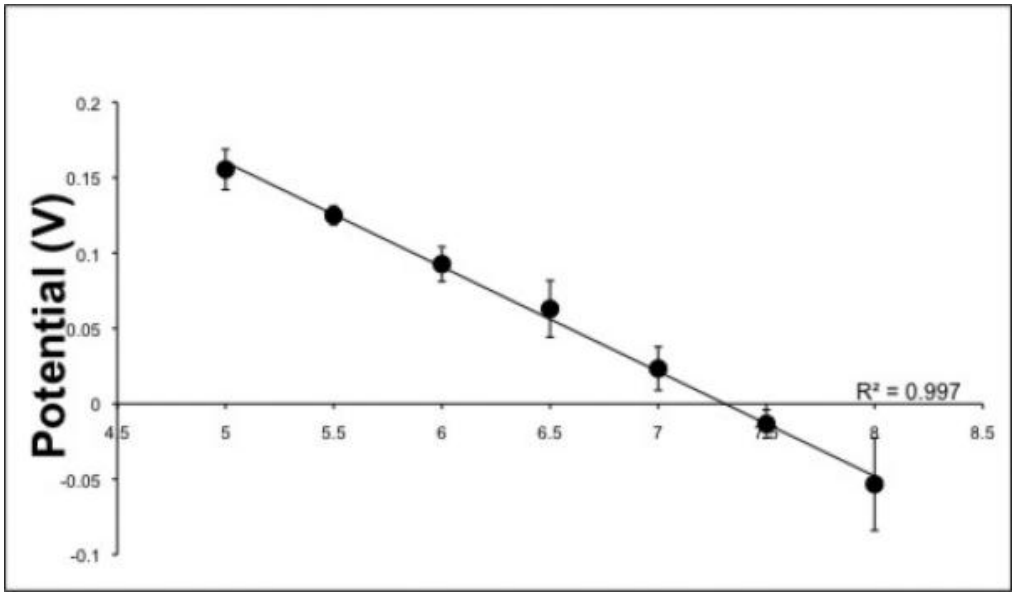

Figure 3-2: Calibration curves of a chemically modified carbon paste electrode in 0.1 M phosphate buffer (pH 5.0-8.0 at 0.5 intervals) against an outside Ag/AgCl and Pt reference and counter electrode, respectively.

The responses for individual wells tailored for glucose and lactate detection were assessed in 0.1 M phosphate buffer. Testing for pH values of 5, 6, 7, and 7.5 against an outside Ag/AgCl reference and Pt counter electrode was performed. This pH range included normal physiological levels for interstitial fluid[11]; pathologic (increased acidity) levels were also evaluated. The chronoamperometric detection potentials for glucose and lactate sensing were selected because they were previously shown to catalytically reduce enzymatically-produced peroxide while minimizing responses of common interfering electroactive species such as ascorbic acid, uric acid, and acetaminophen[19]. For glucose, a fixed detection potential of -0.05 V was used. Figure 3-3 shows calibration curves generated from chronoamperometric scans for each of the pH regions. The responses were linear from 2 mM to 12 mM for each buffer pH; the magnitude of the current response could readily be distinguished, indicating fingerprint detection of glucose is possible for specific pH values. Lactate analysis was performed using a detection potential of -0.15 V. Linear responses were noted over physiologically-relevant concentration values; responses characteristic of

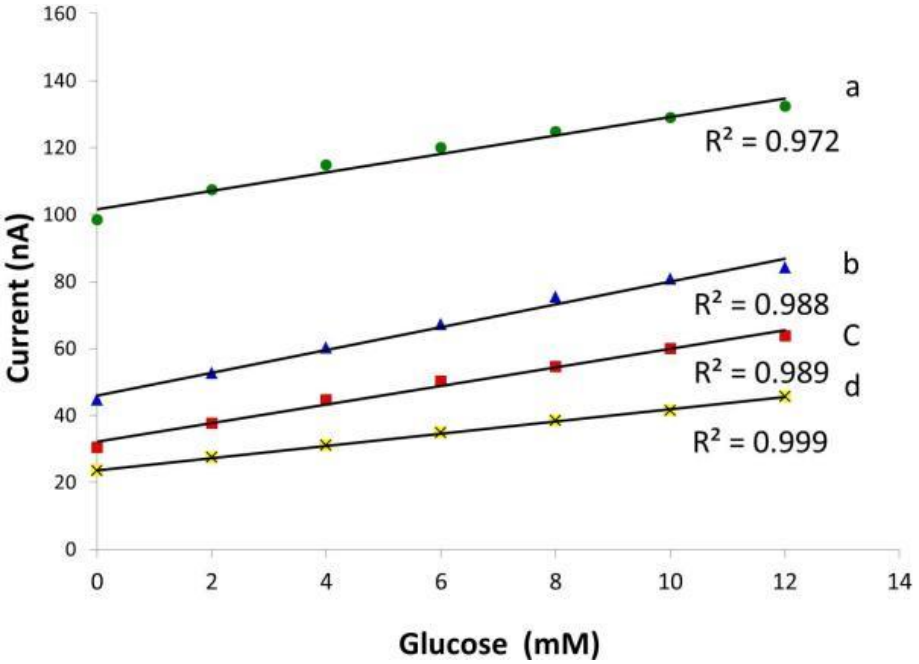

Figure 3-3: Calibration curves of carbon paste containing glucose oxidase in 0.1 M phosphate buffer (pH 5.0, 6.0, 7.0 and 7.5 are indicated by a, b, c, and d, respectively) against an outside Ag/AgCl and Pt reference and counter electrodes with a detection potential of -0.05 V. Data were obtained from the current response after 5 seconds.

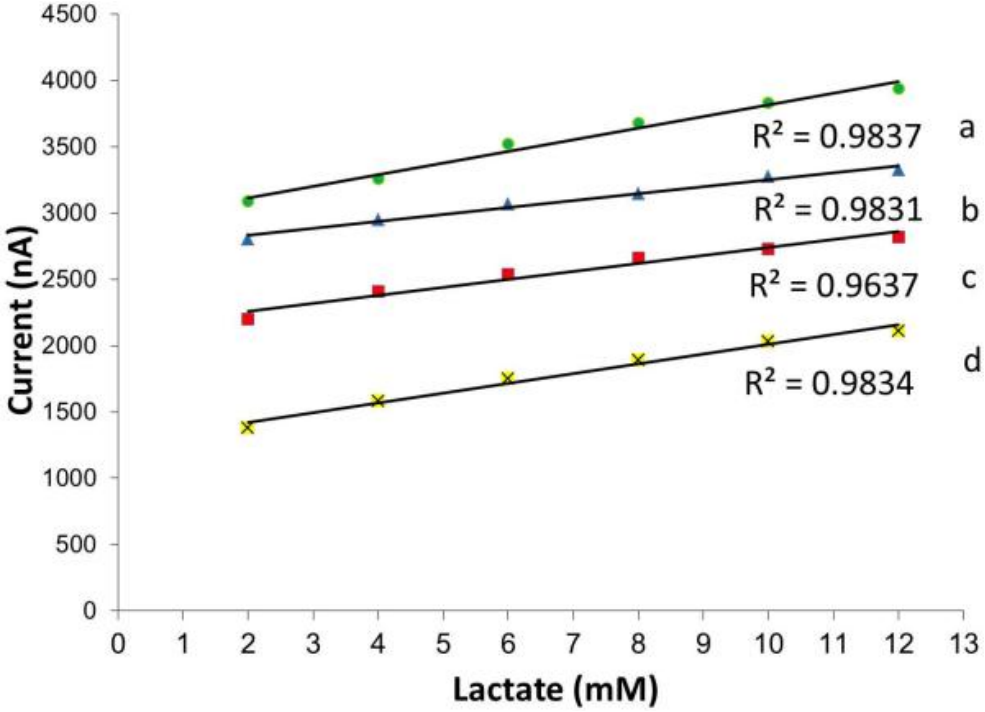

Figure 3-4: Calibration curves of carbon paste-containing lactate oxidase in 0.1 M phosphate buffer (pH 5.0, 6.0, 7.0 and 7.5 are indicated by a, b, c, and d, respectively) against an outside Ag/AgCl and Pt reference and counter electrode with a detection potential of -0.15 V.

each of the pH values were observed (Figure 3-4).

Multiplexed real time detection mandates investigation into whether simultaneous analysis of several markers can be performed with a high degree of accuracy and with minimal cross-talk. We performed analysis of mixtures containing glucose and lactate at a fixed pH value with the integrated carbon paste microneedle platforms. Figure 3-5 shows the response from the lactate microneedle portion of the array before and after addition of glucose (as indicated by green and red curves, respectively). The addition of 4 mM glucose had no effect on the response of the lactate oxidase-modified paste. Subsequent addition of 4 mM lactate produced a current response of ~38 nA, which is consistent with the expected value for a solution with a pH of 7 (based on Figure 3-4). The pH value was simultaneously confirmed from the on-array response of the Fast Blue RR-modified microneedle (inset).

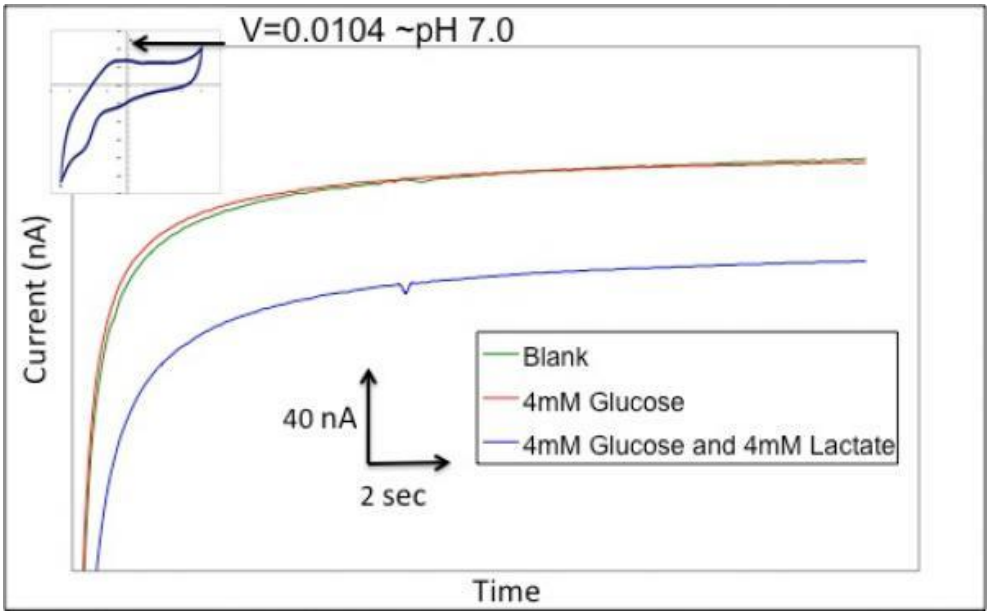

Figure 3-5: Selectivity of the lactate electrode. Figure shows three scans in the order of a blank solution, 4 mM glucose, and 4 mM lactate. Inset: Cyclic voltammogram of Fast Blue-modified carbon paste microneedle.

In this same solution, the glucose oxidase-modified microneedle was tested from its fixed potential chronoamperometric response (Figure 3-6). After stabilizing to a steady state current, the addition of 4 mM lactate resulted in no response on the electrode.

Subsequently, a 4 mM addition of glucose created an increase in reduction current (~10 nA), which corresponded to the expected value for the glucose concentration based on Figure 3-3. This data confirmed that each of the electrodes in the array is capable of performing analyte-specific detection in a complex environment.

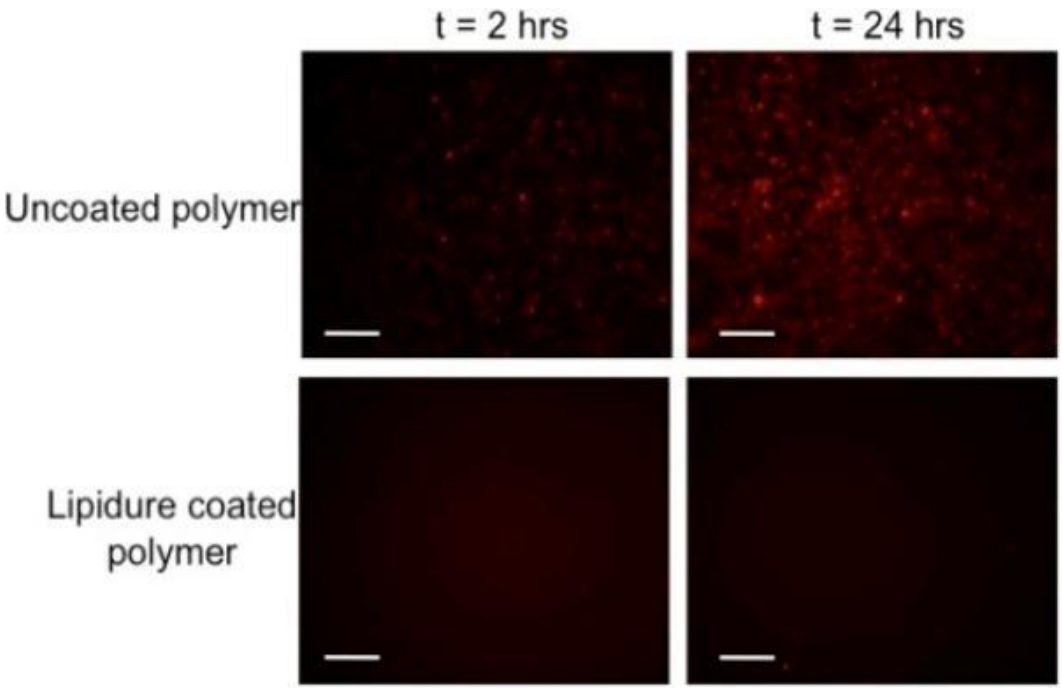

Figure 3-6: Fluorescent images of macrophage adhesion to uncoated and Lipidure®-coated E-shell 300 acrylate-based polymer at 2 and 24 hours post seeding (200 μm scale bar).

In previous work, the E-shell 300 acrylate-based polymer used for microneedle fabrication showed suitable cytotoxicity against both human epidermal keratinocytes and human dermal fibroblasts[21]. Many implantable continuous monitoring systems succumb to biofouling, which is associated with protein, macrophage, and fibroblast adhesion as well as tissue encapsulation at the implantation site[22]. We investigated whether a passive coating could limit adhesion of macrophages to the acrylate-based polymer used for microneedle fabrication. Lipidure®, a copolymer of butyl methacrylate and 2-methacryloyloxyethyl phosphorylcholine, was chosen as the coating material; this material has been previously shown to reduce the adherence of fibroblasts on poly(ethylene telephthalate) in

comparison with uncoated material.[23] In previous work, Mang et al. and Ayaki et al.[24,25] showed using in vitro studies that Lipidure® materials provide good cytocompatibility. To determine the effectiveness of Lipidure®-coated E-shell 300 materials in preventing macrophage adhesion, we examined uncoated materials and coated materials (n=3) at 2 hours, 24 hours, and 48 hours (data not shown) after seeding. Following each time point, the materials were imaged in growth medium with a fluorescent microscope. Figure 3-7 shows macrophage-material interaction at 2 and 24 hours post seeding for both coated and uncoated materials. Uniform macrophage coverage was noted on the uncoated materials; on the other hand, the coated materials displayed little to no cell attachment. The few cells located on the coated materials demonstrated bunched morphologies, indicating poor adhesion. This trend continued through the subsequent time points; the uncoated material maintained a similar number of adherent cells while the coated material contained little to no adherent cells. All of the images showed that the coating did not delaminate from the E-shell 300 substrate for each tested time point; adhesion is a critical factor that determines coating functionality. These results indicate that the Lipidure® coating showed adhesion to E-shell 300 and resistance to macrophage adhesion over the tested time period. Future studies need to be performed to evaluate the relationship between coating thickness and cell attachment as well as the relationship between skin insertion force and coating adhesion.

Conclusions

In conclusion, we have developed a microneedle-based sensor array that is capable of simultaneously detecting multiple analytes in physiologically-relevant tissue environments. The modified microneedles selectively detected changes in pH, lactate, and glucose, indicating potential use for characterizing complex biological environments such as those seen in vigorous exercise and tumor microenvironments. The devices showed suitable performance when tested over physiologically-relevant concentration ranges for each analyte; in addition, the devices showed no signs of adverse responses in complex solutions. Furthermore, the acrylate-based polymer used for microneedle fabrication was coated with a material that limited macrophage adhesion over a 48-hour period. We envision that this sensor technology could be useful to both biomedical research and clinical medicine communities.[26]

References

[1] Robergs, R. A., Ghiasvand, F., & Parker, D. (2004). Biochemistry of exercise-induced metabolic acidosis. *American Journal of Physiology-Regulatory, Integrative and Comparative Physiology*, *287*(3), R502-R516.

[2] Rofstad, E. K. (2000). Microenvironment-induced cancer metastasis. *International journal of radiation biology*, *76*(5), 589-605.

[3] Vander Heiden, M. G., Cantley, L. C., & Thompson, C. B. (2009). Understanding the Warburg effect: the metabolic requirements of cell proliferation. *science*, *324*(5930), 1029-1033.

[4] Warburg, O., Wind, F., & Negelein, E. (1927). The metabolism of tumors in the body. *The Journal of general physiology*, *8*(6), 519-530.

[5] Evelhoch JL. In: The Tumour Microenvironment: Causes and Consequences of Hypoxia and Acidity (Novartis Foundation Symposium 240) Goode JA, Chadwick DJ, editors. John Wiley & Sons; Chichester, UK: 2008. pp. 68–84.

[6] Helmlinger, G., Sckell, A., Dellian, M., Forbes, N. S., & Jain, R. K. (2002). Acid production in glycolysis-impaired tumors provides new insights into tumor metabolism. *Clinical Cancer Research*, *8*(4), 1284-1291.

[7] Vaupel, P., Kallinowski, F., & Okunieff, P. (1989). Blood flow, oxygen and nutrient supply, and metabolic microenvironment of human tumors: a review. *Cancer research*, *49*(23), 6449-6465.

[8] Tannock, I. F., & Rotin, D. (1989). Acid pH in tumors and its potential for therapeutic exploitation. *Cancer research*, *49*(16), 4373-4384.

[9] Medina, M. Á., Márquez, J., & Núñez, I. (1992). Interchange of amino acids between tumor and host. *Biochemical medicine and metabolic biology*, *48*(1), 1-7.

[10] Semenza, G. L. (2008). Tumor metabolism: cancer cells give and take lactate. *The Journal of clinical investigation*, *118*(12), 3835.

[11] Cardone, R. A., Casavola, V., & Reshkin, S. J. (2005). The role of disturbed pH dynamics and the Na+/H+ exchanger in metastasis. *Nature Reviews Cancer*, *5*(10), 786-795.

[12] Miller, P. R., Gittard, S. D., Edwards, T. L., Lopez, D. M., Xiao, X., Wheeler, D. R., ... & Narayan, R. J. (2011). Integrated carbon fiber electrodes within hollow polymer microneedles for transdermal electrochemical sensing. *Biomicrofluidics*, *5*(1), 013415.

[13] Windmiller, J. R., Zhou, N., Chuang, M. C., Valdés-Ramírez, G., Santhosh, P., Miller, P. R., ... & Wang, J. (2011). Microneedle array-based carbon paste amperometric sensors and biosensors. *Analyst*, *136*(9), 1846-1851.

[14] Windmiller, J. R., Valdés-Ramírez, G., Zhou, N., Zhou, M., Miller, P. R., Jin, C., ... & Wang, J. (2011). Bicomponent Microneedle Array Biosensor for Minimally-Invasive Glutamate Monitoring. *Electroanalysis*, *23*(10), 2302-2309.

[15] Ricci, F., Moscone, D., & Palleschi, G. (2008). Ex vivo continuous glucose monitoring with microdialysis technique: The example of GlucoDay. *Sensors Journal, IEEE*, *8*(1), 63-70.

[16] Zimmermann, S., Fienbork, D., Flounders, A. W., & Liepmann, D. (2004). In-device enzyme immobilization: wafer-level fabrication of an integrated glucose sensor. *Sensors and Actuators B: Chemical*, *99*(1), 163-173.

[17] Henry, S., McAllister, D. V., Allen, M. G., & Prausnitz, M. R. (1998). Microfabricated microneedles: a novel approach to transdermal drug delivery. *Journal of pharmaceutical sciences*, *87*(8), 922-925.

[18] Prausnitz, M. R. (2004). Microneedles for transdermal drug delivery. *Advanced drug delivery reviews*, *56*(5), 581-587.

[19] Wang, J., Chen, L., & Liu, J. (1997). Critical comparison of metallized and mediator-based carbon paste glucose biosensors. *Electroanalysis*, *9*(4), 298-301.

[20] Makos, M. A., Omiatek, D. M., Ewing, A. G., & Heien, M. L. (2010). Development and characterization of a voltammetric carbon-fiber microelectrode pH sensor. *Langmuir*, *26*(12), 10386-10391.

[21] Gittard, S. D., Miller, P. R., Boehm, R. D., Ovsianikov, A., Chichkov, B. N., Heiser, J., ... & Narayan, R. J. (2011). Multiphoton microscopy of transdermal quantum dot delivery using two photon polymerization-fabricated polymer microneedles. *Faraday discussions*, *149*, 171-185.

[22] Anderson, J. M., Rodriguez, A., & Chang, D. T. (2008, April). Foreign body reaction to biomaterials. In *Seminars in immunology* (Vol. 20, No. 2, pp. 86-100). Academic Press.

[23]Ishihara, K., Ishikawa, E., Iwasaki, Y., & Nakabayashi, N. (1999). Inhibition of fibroblast cell adhesion on substrate by coating with 2-methacryloyloxyethyl phosphorylcholine polymers. *Journal of Biomaterials Science, Polymer Edition*, *10*(10), 1047-1061.

[24] Ayaki, M., Iwasawa, A., & Niwano, Y. (2011). Cytotoxicity assays of new artificial tears containing 2-methacryloyloxyethyl phosphorylcholine polymer for ocular surface cells. *Japanese journal of ophthalmology*, *55*(5), 541-546.

[25] Mang, A., Pill, J., Gretz, N., Kränzlin, B., Buck, H., Schoemaker, M., & Petrich, W. (2005). Biocompatibility of an electrochemical sensor for continuous glucose monitoring in subcutaneous tissue. *Diabetes technology & therapeutics*, *7*(1), 163-173.

[26] Brizel, D. M., Scully, S. P., Harrelson, J. M., Layfield, L. J., Bean, J. M., Prosnitz, L. R., & Dewhirst, M. W. (1996). Tumor oxygenation predicts for the likelihood of distant metastases in human soft tissue sarcoma. *Cancer research*, *56*(5), 941-943.

Chapter 4 Microneedle-Based Transdermal Sensor for On-Chip Potentiometric Determination of K^+

Philip R Miller[1,2], Xiaoyin Xiao[1], Igal Brener[1], D Bruce Burckel[1], Roger J Narayan[2*], Ronen Polsky[1*]

[1] Joint Department of Biomedical Engineering, University of North Carolina and North Carolina State University, Raleigh, NC 27695-7115, USA
[2] Department of Biosensors and Nanomaterials, Sandia National Laboratories, Albuquerque, NM 87185, USA

The following section a complete article reprinted from Advanced Healthcare Materials, Volume 3, Philip R Miller, Xiaoyin Xiao, Igal Brener, D Bruce Burckel, Roger Narayan, Ronen Polsky,876-881,Copyright 2014.

Note: This article has been reformatted. In particular, the location of figures and spacing may have changed. The references are formatted as in the original manuscript.

Abstract

The determination of electrolytes is invaluable for point of care diagnostic applications. An ion selective transdermal microneedle sensor is demonstrated for potassium by integrating a hollow microneedle with a microfluidic chip to extract fluid through a channel towards a downstream solid-state ion-selective-electrode (ISE). 3D porous carbon and 3D porous graphene electrodes, made via interference lithography, are compared as solid-state transducers for ISE's and evaluated for electrochemical performance, stability, and selectivity. The porous carbon K^+ ISE's show better performance than the porous graphene K^+ ISE's, capable of measuring potassium across normal physiological concentrations in the presence of interfering ions with greater stability. This new microfluidic/microneedle platform shows promise for medical applications.

Introduction

Point of care diagnostic (POC) devices promise to advance health monitoring scenarios by shrinking laboratory-scale equipment to portable systems, which are aided by advances in microfluidics, lab-on-chip methodologies, and miniaturization.[1] The move away from centralized testing laboratories is expected to have many benefits, such as decreasing the amount of time patients spend in clinics and emergency rooms as well as allowing results to be obtained by non-specialists. Wearable sensors are a new paradigm in POC devices, allowing for minimally invasive monitoring of physiological functions and elimination of biological fluid transfer between subject and device; these devices are capable of providing real-time analysis of a patient's condition.[2] Novel epidermal electronic devices consisting of printed flexible circuits that can be stretched and bent to mimic skin elasticity can perform electrophysiological measurements such as measuring temperature and hydration as well as monitoring electrical signals from brain and muscle activity.[3] Temporary tattoos integrated with screen printed electrodes directly attached to the skin were recently reported to measure lactate through sweat.[4]

Microneedle-enabled analysis systems are capable of minimally-invasive interrogation due to their ability to puncture the skin's stratum corneum and access interstitial fluid while not interacting with deeper layers of the skin, which contains tissues that are associated with pain, blood flow, or sensation.[5,6] For example, glass microneedle arrays were used to create pores in the skin in order to extract interstitial fluid by means of a vacuum bell jar for glucose detection with commercially available glucose strips.[7] A strong correlation was shown between intravenous glucose concentrations and those within dermal tissue. In another study, the surfaces of solid gold microneedles were functionalized with antibodies, which were used to collect nonstructural protein-1 (an early marker for dengue virus infection) in mice. When inserted in the skin, the functionalized

microneedles bound the protein and remained attached; once the needles were removed from the animal, further ex vivo analysis was performed.[8] Several examples involving microneedles and electrochemical detection have also been recently reported, including packing of hollow microneedles with enzyme filled carbon pastes to amperometrically detect glucose or glutamate, and use of a multiplexed microneedle device to simultaneously measure glucose, lactate, and pH.[9,10]

Electrolytes are important for maintaining cell signaling, kidney function, homeostasis, and body fluid balance.[11] Electrolyte levels can fluctuate due to exercise, diet, disease, poisoning, and organ failure, making their monitoring invaluable for healthcare assessment. Solid-state ion selective electrodes (ISE) that incorporate H^+ ionophores and solvent polymeric membranes have been shown to be efficacious for metal cation determination.[12] In contrast to liquid-based ISEs, solid-state ISEs require less maintenance and are compatible with microfabrication and array construction methods. Buhlmann and Stein introduced the use of 3D macroporous carbon electrodes, which were prepared from colloidal sphere templating (3DOM), as a solid contact for PVC-doped valinomycin sensing membrane-based K^+ detection.[13] The highly ordered 3D porous carbon structures provided high capacitance and a large interfacial area, which resulted in excellent performance and long-term stability of the sensor compared to non-porous carbon analogues. Herein, we report on the use of novel interferometric lithographically-fabricated 3D porous carbon electrodes integrated into a microfluidic channel for the construction of a K^+ microneedle sensor. As far as, we are aware this is the first example of an ISE microneedle sensor.

Materials and Methods

Porous Carbon Fabrication:

Porous carbon substrates were prepared using an interference lithography method. In this method, negative tone NR-7-coated substrates were exposed to a frequency-tripled 355 nm line of Q-switched Nd:YAG laser. The laser beam was expanded and split so it could be interfered with at 32° between the planewave propagation vectors. The plane of incidence contained both propagation vectors as well as the angle bisector of the propagation vectors, which was tilted with respect to the sample surface normal by 45°. Creation of the porous architecture was achieved by rotating the sample 120° following each exposure and repeating the process three times to ensure proper exposure dosages. Silicon substrates were prepared by spinning an anti-reflecting coating of iCON-7 (Brewer Science, Rolla, MO) at 3000 rpm, followed by baking on a vacuum hotplate at 205 °C for 60 s. An adhesion layer was created by spinning NR7 100P (≈100 nm) at 3000 rpm; this layer was flood exposed and baked at 130 °C on a vacuum hotplate. The layer to be patterned was subsequently spun; NR7–6000P was spun at 3000 rpm (6 μm) and soft-baked at 130 °C. Following the patterning exposure, substrates were baked at 85 °C for 2 min on a vacuum hot plate and then puddle developed for 120 s using RD-6 (Futurrex, Inc.). Spinning drying was used to remove any residual developer from the structures. Substrates were then baked on a hotplate at 180 °C for 30 min and pyrolyzed at 1100 °C for 1 h.

Electrode Preparation:

Porous carbon (PC) electrodes were cut into ≈8 mm × ≈14 mm pieces from bulk Si substrates with a diamond scribe. This electrode size was consistent throughout the experiments; eight pieces were obtained from one bulk Si wafer. PC substrates were cleaned by washing with isopropanol and DI H20; drying with nitrogen was subsequently

performed. Potassium selective membranes were prepared by creating a cocktail solution by mixing 1% valinomycin, 0.3% KTFPB, 66% o-NPOE, and 32.8% PVC in THF at 15 wt%. PC electrodes were coated by pipetting 100 µL of the ISE cocktail onto the substrates; this material was allowed to dry for 24 h. Conditioning of the PC/K^+ ISE's was performed overnight in 10×10^{-3} M KCl. The electrodes were stored in this solution when not in use. A 3-mm glassy carbon disc (BASi) electrode was used as a planar electrode for comparison. The planar carbon electrodes were prepared by first hand polishing with 0.3 and 0.05 µm alumina polish with sanitation in DI H_2O after each round of polishing. Creation of the K^+ selective membrane was performed by using the same ISE cocktail solution that was used with the PC substrates; 20 µL was pipetted onto the cleaned electrodes and allowed to dry for 24 h. Planar carbon ISE's were conditioned in 10×10^{-3} M KCl for 24 h prior to use and stored in the same solution. A pseudo Ag/AgCl reference electrode was used for microfluidic experiments and was prepared by first exposing an Ag wire to a flame to clean the surface of the wire. The wire was then washed with ethanol and then placed in bleach until a chloride layer was formed, which was associated with a color change of the wire to a dark purple.

Microfluidic Chip Fabrication:

Microfluidic chips were made in a layer by layer manner from PMMA sheets and Melinex double-sided adhesive layers. A CO_2 laser was used to ablate patterns into the PMMA and the adhesive layers that were used in formation of the fluidic channels. Layers were assembled with a gig and pressed at 500 psi in order to remove air bubbles from the adhesive layers. O-rings were used between the PMMA layers in order to connect PEEK tubing for flow through experiments and for future vacuum connections involving

interstitial fluid extraction. Ports were laser cut in the chip so that an Ag/AgCl wire and Pt counter could be used as a reference and counter electrode, respectively.

Optimization of the laser energy to avoid resin burning/bubbling and over-polymerization (clogging) of the microneedle bore or sub-optimal laser output energies, which is associated with partial polymerization between the layers (Supporting Information). Based on these results, larger (>25 μm) step heights (write distance between layers) were obtained with the 4× objective. Overpolymerization of hollow microneedle bores was common with energies above 60 mW (measured at the stage); optimal operating energies for hollow microneedle fabrication around 50 mW were chosen to avoid laser power fluctuations. Thus, a 440 μm × 1450 μm × 165 μm microneedle (width, height, and triangular bore) was fabricated and added into the microfluidic manifold. Integration of the hollow microneedle with a microfluidic chip was achieved by writing a hollow microneedle onto a substrate which fit within a recess on the microfluidic chip (Figure 4-7). Previous work by our group utilized 2PP to write both the substrate and the microneedle however this technique is time consuming and only the microneedle requires the fabrication resolution that 2PP offers.[14][14] Initial experimental showed that writing Eshell 300 hollow microneedles directly onto the PMMA microfluidic chip created a weak bond; the microneedles tended to shear when placed into the skin. To circumvent this issue, we created the substrates from the same material as the microneedles so the bonds would be the same. Additionally, preformed substrates allowed for facile integration within the microfluidic chip. To create the fluidic pathway from the microneedle to the microfluidics, a bore was created in the Eshell 300 substrate using a CO_2 laser. Laser cutting speeds were altered while parameters for power, *z*-height, resolution, and gas flow were maintained. Exit bores on the substrates were measured since this side of the bore had a smoother surface for writing needles and was smaller than the entrance bore due to thermal effects of the laser. Bore sizes needed

to be smaller than the base of the microneedle but larger than the bore of the microneedle; a substrate bore of approximately 150 μm was used in this study. A range of laser cutting speeds was examined with 10 mm × 10 mm × 2 mm Eshell 300 substrate. These were measured using a digital microscope. The optimal laser cutting speed for producing exit bores in the Eshell 300 substrates were at 7 (arbitrary units).

EMF Measurements:

A CH Instruments multi-channel potentiostat was used to measure zero potential measurements of PC and PG/K^+ ISE membranes. In-solution measurements used an Ag/AgCl reference electrode and a Pt wire counter. A VoltaLab potentiostat was used for chronopotentiometric measurements. In these experiments, an Ag/AgCl reference and Pt wire counter electrode were used. Activity coefficients were calculated using the extended Debye-Hückel equation.

Microneedle Fabrication:

Hollow microneedles were prepared using a laser direct write system utilizing two-photon polymerization. First, a CAD file was created in the desired shape and dimensions of the microneedle and was uploaded to the LDW operating software (GOLD3D). The software sliced the CAD file and assigned laser and "writing" parameters such that the fabrication process can be optimized. The two photon polymerization effect is achieved with the help of Ti:Sapphire laser, which was operated at 800 nm, 150 fs, and 76 MHz. A 4× objective was used to focus the beam; write settings of 150 μm s^{-1} write speed, 2 μm *x*- and *y*-axis rastering, as well as 25 μm *z*-step height were used in this study. Eshell 300 was used as the resin for both the hollow microneedles and the substrates.

Substrates were created in PDMS molds made by laser cutting PMMA to 10 mm × 10 mm × 2 mm pieces and molding them with PDMS. Eshell 300 was then placed in the molds and cured with a UV lamp. In order to make a fluidic connection between the microfluidic chip and the hollow microneedle, a bore was cut into the substrates with a CO_2 laser such that the bore diameter was around 150 μm. Bore patterns were designed in CorelDraw and a single 100 μm circle (or array or circles) was drawn and uploaded to the laser cutting software. A well was made on top of the bore-containing substrate such that a microneedle could be written onto the substrate. The well was created with parafilm; once filled with resin, a glass cover slip was placed on top of the spacer. A vacuum was pulled from the bottom of the substrate such that a small amount of resin was pulled into the bore in order to remove air.

Results and Discussion

A scanning electron micrograph of the interferometric lithographically-fabricated pyrolyzed carbon (PC) electrode is shown in Figure 4-1A. The electrodes resemble the colloidal crystal-templated 3DOM carbon prepared by Buhlman and Stein with slightly larger pore sizes and higher long-range order. It is also similar in composition, as we previously showed, consisting of an amorphous glassy carbon material. As the 3DOM was shown to be an improvement over planar solid-state ISE electrodes, due to the open porous structure which facilitates penetration of the ionophore-containing membrane, we tested this novel ordered carbon electrode for its potential as a solid-state ISE along with a porous graphene analog (PG). We have previously shown that such a highly ordered periodic porous carbon structure produces a high surface area/high mass transport environment, which is suitable for electrochemical applications and for use as a scaffold for a variety of material modifications.[15]

The conversion of the PC to PG occurred after nickel coating and annealing as previously described.[16] As can be seen in the SEM of the PG electrode (Figure 4-1B), there is an

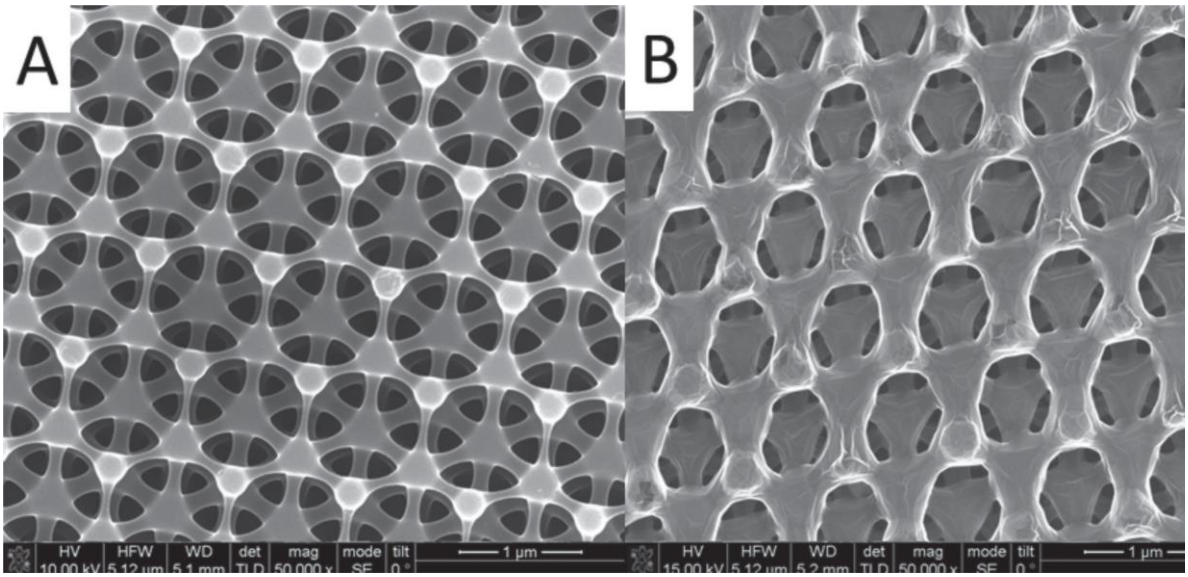

Figure 4-1: SEM of A) porous carbon, and B) porous graphene.

increase in overall arm diameter after conversion, which indicates a concomitant decrease in pore size. The surface roughness also changes dramatically, transitioning from near atomic smoothness[14] to a wrinkled graphene surface. After modification with K+ membrane cocktail (described in the experimental section), reversed chronopotentiometric scans were performed to determine capacitance and stability of the polymeric membrane-modified electrodes in comparison to a planar glassy carbon electrode that was prepared in an identical manner (shown in Figure 4-2). The curves generated are a reflection of the resistance of the membrane and the ability of the membrane to adjust to changes in solution ion concentrations. The very small change in potential upon reverse biasing for the PC and PG electrodes versus the glassy carbon is indicative of increased stability. Resistance values of 12.75 and 12.69 MΩ were calculated for the PC and PG K^+/ISE electrodes, respectively, for the response of the potential jump compared to 37.75 MΩ for the GCE. These resistance numbers are similar to both carbon nanotubes and graphene solid-state ISE transducers.[17,18] The potential drift of the membranes was calculated to be 0.212 mV s^{-1} for the PC/K^+ ISE and 0.211 for the PG/K^+ ISE.

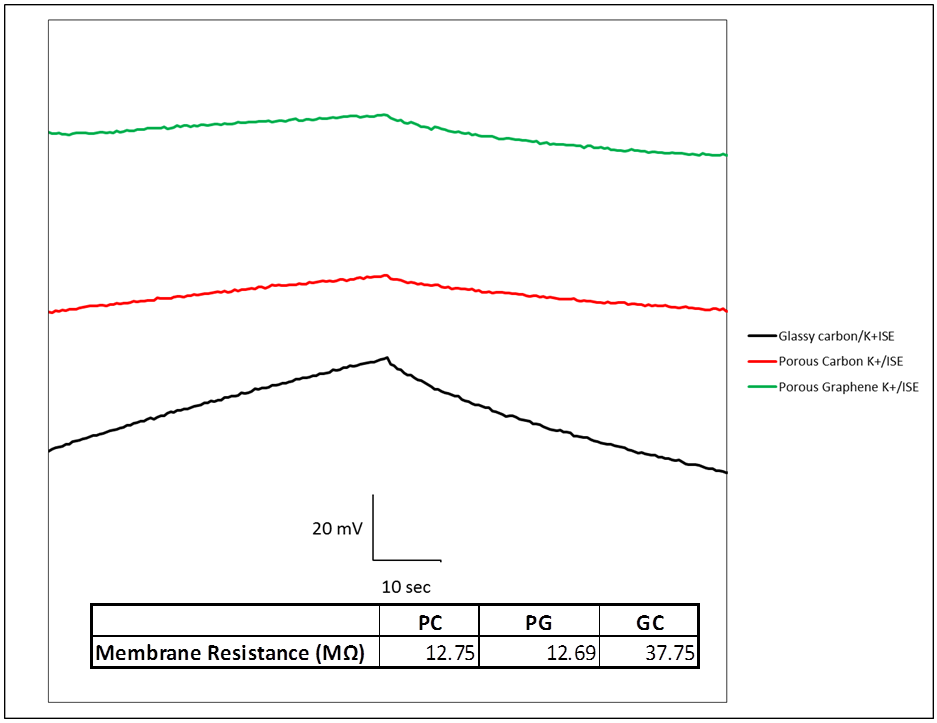

	PC	PG	GC
Membrane Resistance (MΩ)	12.75	12.69	37.75

Figure 4-2: Reversed chronopotentiometric scans of PC and PG K^+/ISE electrodes versus a planar carbon substrate prepared identically (red, green, and black respectively). Initial scan of -1 nA for 60 s followed by a switch to +1 nA for 60 s. Measurements tested against an Ag/AgCl reference electrode and a platinum wire counter electrode in 10×10^{-3} m KCl.

Figure 4-3 and 4-4 show electromotor force (EMF) measurements of the PC and PG/K^+ISE for increasing concentrations of potassium. Potentials in ISE measurements are related to the ionic activity of the ion being detected and the behavior of the potential as a function of the Nernst equation. For the PC/K^+ISE, potential stabilization was rapid for each K^+ spike (approximately 20 s, (inset in Figure 4-3a) and was comparable to other carbon-based transducers.[19] The potential response was near Nernstian (57.9 mV per decade), and the linear range was 10^{-5} M to 10^{-2} M with a detection limit of $10^{-5.65}$ M. The PG produced similar response times with a comparable linear range; however, large potential drifts were observed after each spike before a stable baseline was reached. Fierke et al. showed previously how increasing oxidation of 3DOM electrodes led to a systematic decrease in performance and stability due to formation of an aqueous layer and possible partial delamination of the membrane.[20] Pyrolyzed photoresist is known to possess extremely low

O/C ratios.[21] Previous comparisons between the PC and PG showed much higher electrochemical activity and electron transfer kinetics at PG which were attributed to a higher number of edge defects and functional groups which would likely explain the decreased stability for the PG/ISE electrode. Therefore, the PC electrodes were chosen for their superior stability over PG and used for integration into a microneedle ISE sensor.[15] SEM images of cross sections of the bare PC and membrane-treated PC in Figure 4-5 A and B show that the ISE membrane penetrates completely into the porous structure of the PC down to bottom layers. The complete filling of the pores and conformal coating of the membrane likely contributes to the excellent stability of the sensor, over a surface film, while the 3D nature leads to higher sensitivity by increasing surface area over a planar electrode.

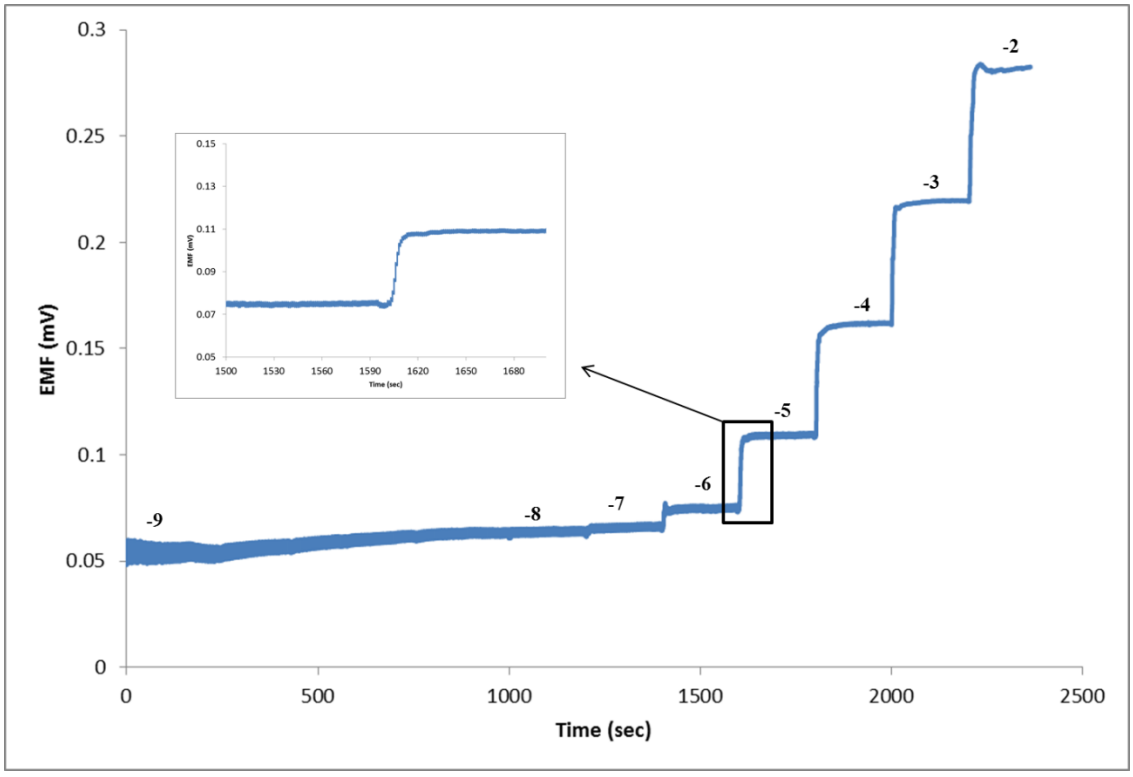

Figure 4-3: EMF measurements from porous carbon potassium ion selective electrode to increasing KCl concentrations in solution tested against an Ag/AgCl reference electrode and a Pt wire counter electrode. Inset shows zoomed in image of EMF response to a single KCl spike. Number on each potential step corresponds to Log of each concentration spike.

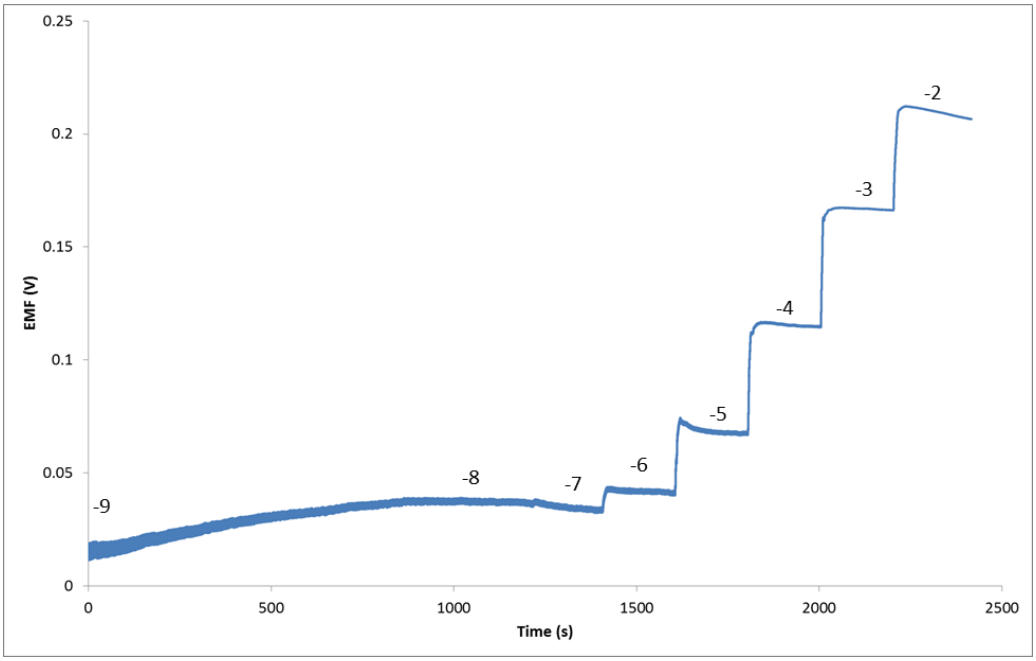

Figure 4-4: EMF measurements from porous graphene potassium ion selective electrode to increasing KCl concentrations in solution tested against an Ag/AgCl reference electrode and a Pt wire counter electrode. Number on each potential step correspond to Log of each concentration spike.

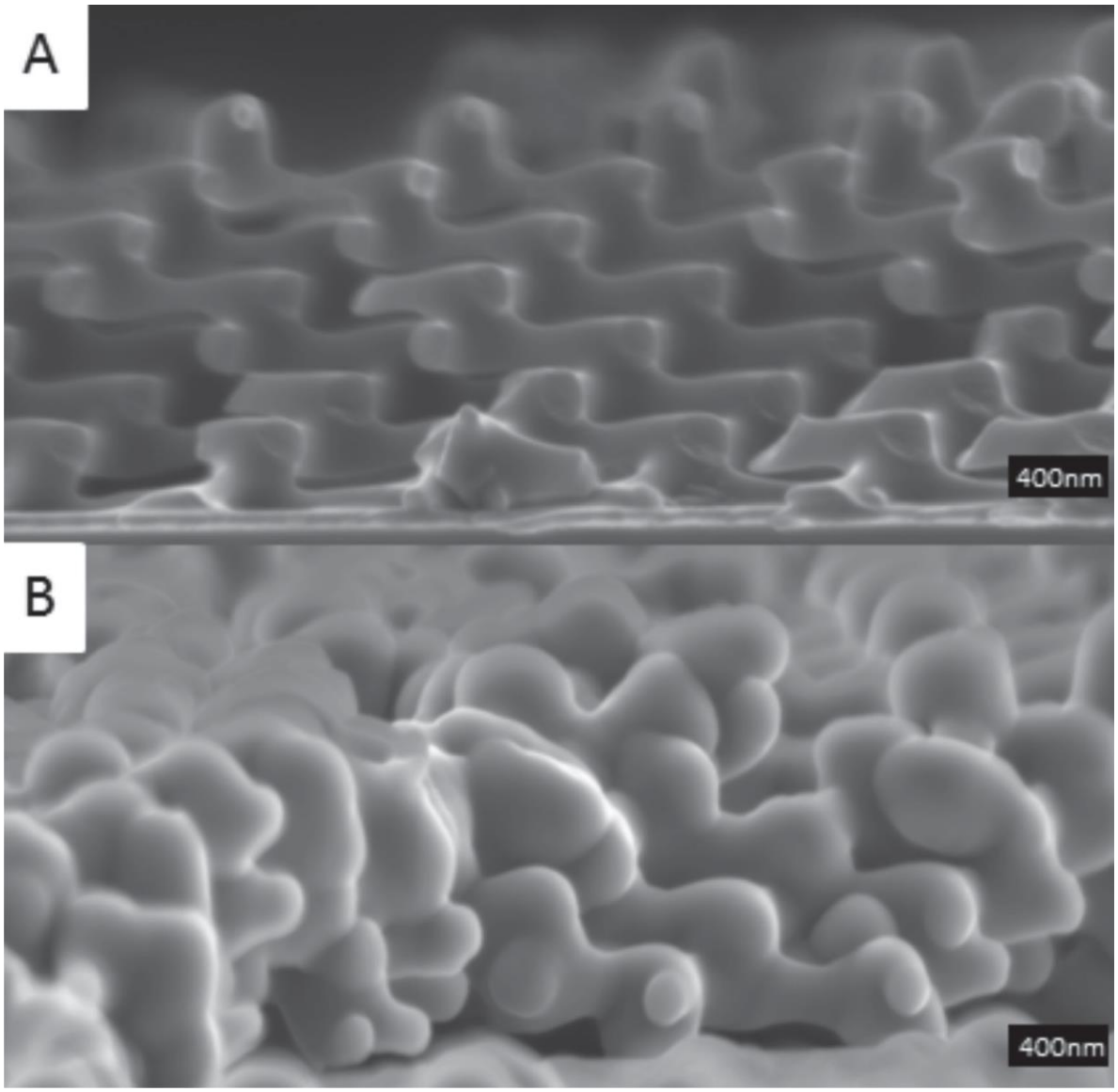

Figure 4-5: Cross-section images of A) porous carbon and B) ISE membrane porous carbon showing filling of membrane inside open porous structure.

Figure 4-6 shows EMF measurements at the PC/K^+ISE for alternating spikes of potassium and sodium in order to determine the influence of ion interference in a mixed solution. Both anions and cations can cause some level of interference with potassium ISE's. Of the known interferon's sodium levels are particularly high in the body and are prone to fluctuations. Normal physiological potassium levels are between 3×10^{-3} and 6×10^{-3} M and normal sodium levels are between 135×10^{-3} and 145×10^{-3} M; spikes were chosen to

represent expected physiological fluctuations. Arrows in Figure 4-6 shows alternating 5 × 10^{-3} M KCl spikes and 10 × 10^{-3} M NaCl spikes. Throughout this scan, the PC/K^+ISE rapidly responded to the KCl spikes; no influence was observed for additions of NaCl. These results indicate that the PC/K^+ISE was not significantly affected by the addition of a prevalent interfering ion and remained selective only to K^+.

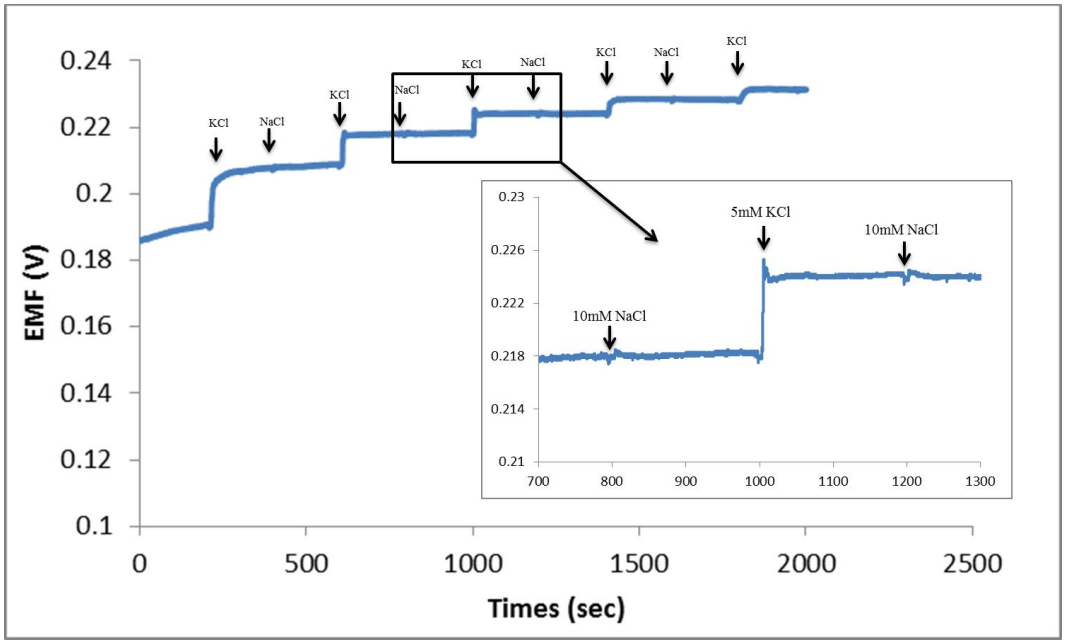

Figure 4-6: EMF response to alternating spikes of 5 × 10^{-3} m KCl and 10 × 10^{-3} M NaCl on porous carbon potassium ion selective electrodes in solution tested against an Ag/AgCl reference and a Pt counter electrode. Red dots signify 10 × 10^{-3} m NaCl spikes while blue dots signify 5 × 10^{-3} m KCl. Inset shows zoomed in view of three spikes.

Integration of nanomaterials into microfluidic platforms can be extremely beneficial.[22] An advantage of using a lithographic approach for creation of a porous carbon ISE contact is the ability to photopattern the carbon electrode, which is useful for miniaturizing and integrating the electrode within a microfabricated device. Eshell 300, a Class 2a biocompatible material commonly used for hearing aid implants, was used to fabricate the microneedle; we previously demonstrated compatibility of this material with two-photon lithography as well as evaluated growth of human epidermal keratinocytes and human epidermal fibroblasts on this material. Integration of the microneedle with a

microfluidic chip was achieved by writing a hollow microneedle onto a removable substrate which could fit within a pre-defined recess on the microfluidic chip shown in Figure 4-7A. A fluidic channel (870 µm width) was cut into the adhesive layer and an opening for the placement of PC/K⁺ISE and microneedle was cut into a 1.5-mm thick PMMA substrate via CO_2 laser machining. A 8 mm × 13 mm cut piece of lithographically patterned PC/K⁺ISE was adhered into the channel reservoir with the double-sided adhesive used for microfluidic chip assemble. A plastic Melinex adhesive plate was placed over the top to complete the channel. Figure 4-7 shows an optical image of an integrated microneedle with a PC/K⁺ISE in a microfluidic chip.

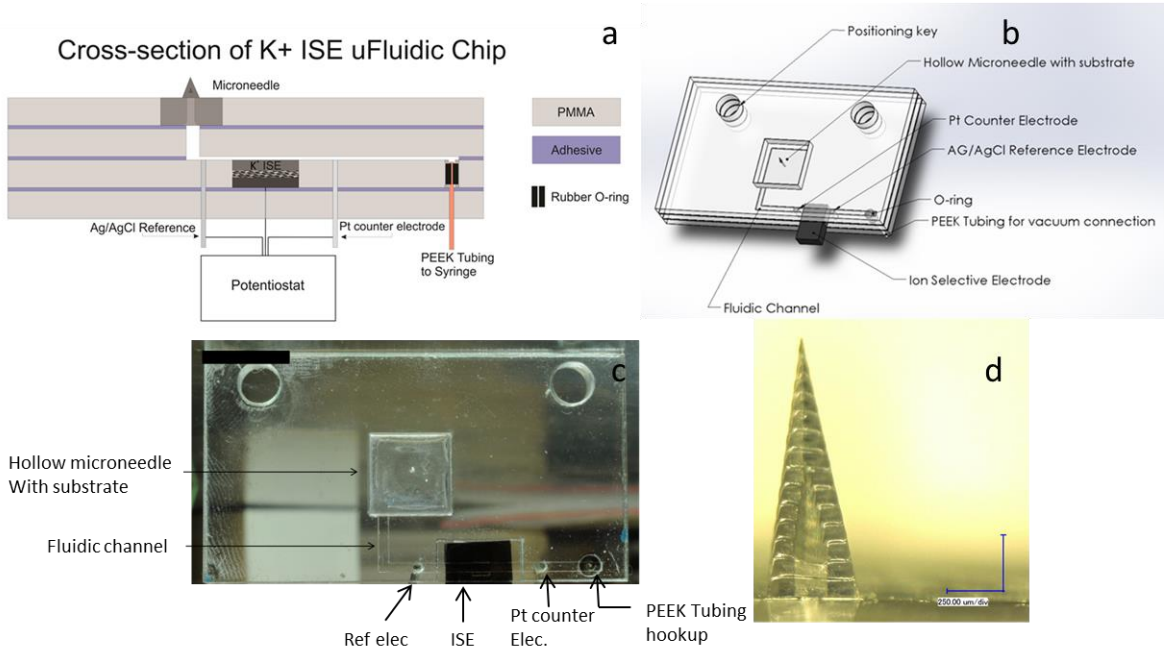

Figure 4-7: a) CorelDraw rendering of a cross-section of the K⁺ ISE microfluidic chip. b) Solidworks drawing of K⁺ ISE microfluidic chip. c) Image of microfluidic chip with on chip reference and counter electrodes (scale bar = 10 mm) and d) optical image of single hollow microneedle made with two-photon lithography (scale bar = 250 = µm).

For on-chip measurements, KCl solutions were flowed through the chip and measured downstream at the PC/K⁺ ISE shown in Figure 4-8. Measurements from the PC/K⁺ ISE were obtained versus an Ag/AgCl wire reference and Pt counter electrode, respectively, that were also integrated into the fluidic channel. The inset in Figure 4-8 shows a

calibration curve generated from the K^+ spikes introduced to the fluidic chip. A linear response was observed for the tested values; however, the response was super Nernstian, which is attributed to the Ag/AgCl reference wire. Ag/AgCl reference wires can be susceptible to fluctuations in potential when varying concentrations of chloride are introduced into the sample due to dissociation of chloride ions on the surface of the electrode. Subtracting the influence of ionic dissociation due the Ag/AgCl wire from the measured values can be used to compensate and plot an ideal Nernstian response. The on chip response of the PC/K^+ ISE after fluidic introduction of K^+ through the microneedle fluidic channel was sensitive to physiological potassium levels, indicating the chip is capable of rapidly and selectively measuring clinically relevant samples corresponding to normal and abnormal concentrations.

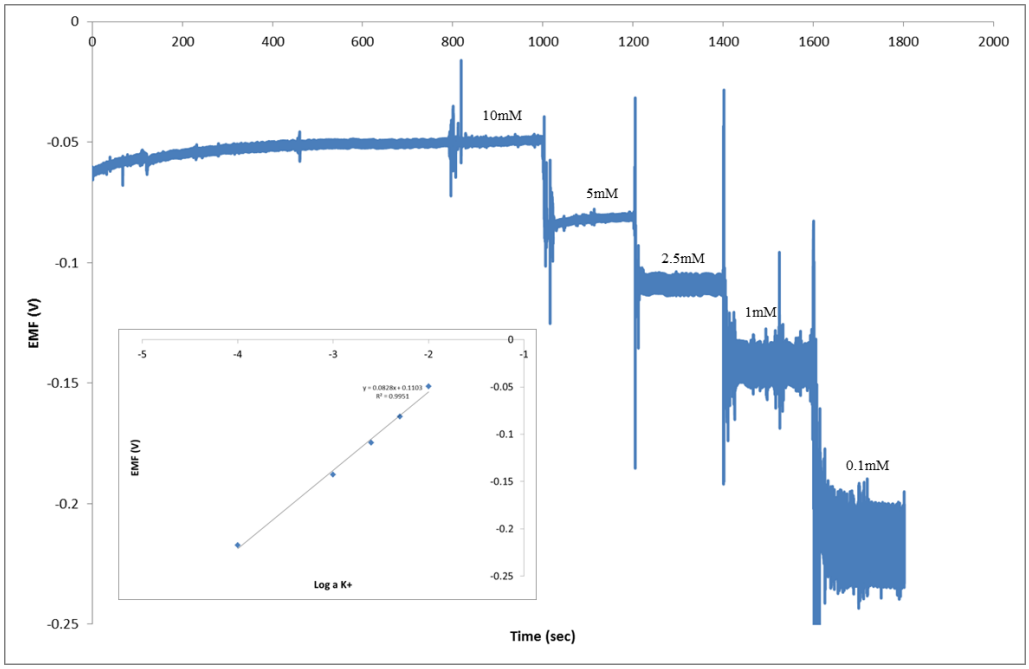

Figure 4-8: On-chip calibration of varying physiologically relevant concentrations of KCl with on-chip Ag/AgCl reference wire and Pt wire counter electrode. Solutions were flown through channel via a syringe and allowed to stabilize for 200 s. Inset shows calibration curve generated from potassium spikes on-chip.

Conclusion

We created a transdermal sensing device designed to measure physiologically relevant concentrations of potassium. As far as we are aware, this is the first demonstration of a microneedle ISE sensor. Porous carbon and porous graphene electrodes were tested as transducers for ISE's. While both were capable of lowering the membrane resistance of the ISE's when compared to glassy carbon electrodes, the porous carbon electrodes showed better electrochemical performance. Porous carbon K^+ ISE's exhibited a detection range from 10^{-5} to 10^{-2} M with a near Nernstian slope of 57.9 mV per decade and rapid stabilization (≈20 s). Porous graphene K^+ ISE's also exhibited rapid EMF changes to potassium spikes however showed instability due to higher concentration of edge defects and oxygen functional groups, which likely result in poor membrane adhesion. Porous carbon K^+ ISE's showed no response to interfering Na^+ ions. The solid-state ISE was incorporated into a fluidic chip along with a hollow microneedle. The method allows for a hollow microneedle to draw fluid over a three-electrode system within a microfluidic chip, which provides an attractive platform for an on-body sensing system for monitoring potassium and can easily be expanded to a host of relevant physiological markers for next generation point of care diagnostic device.

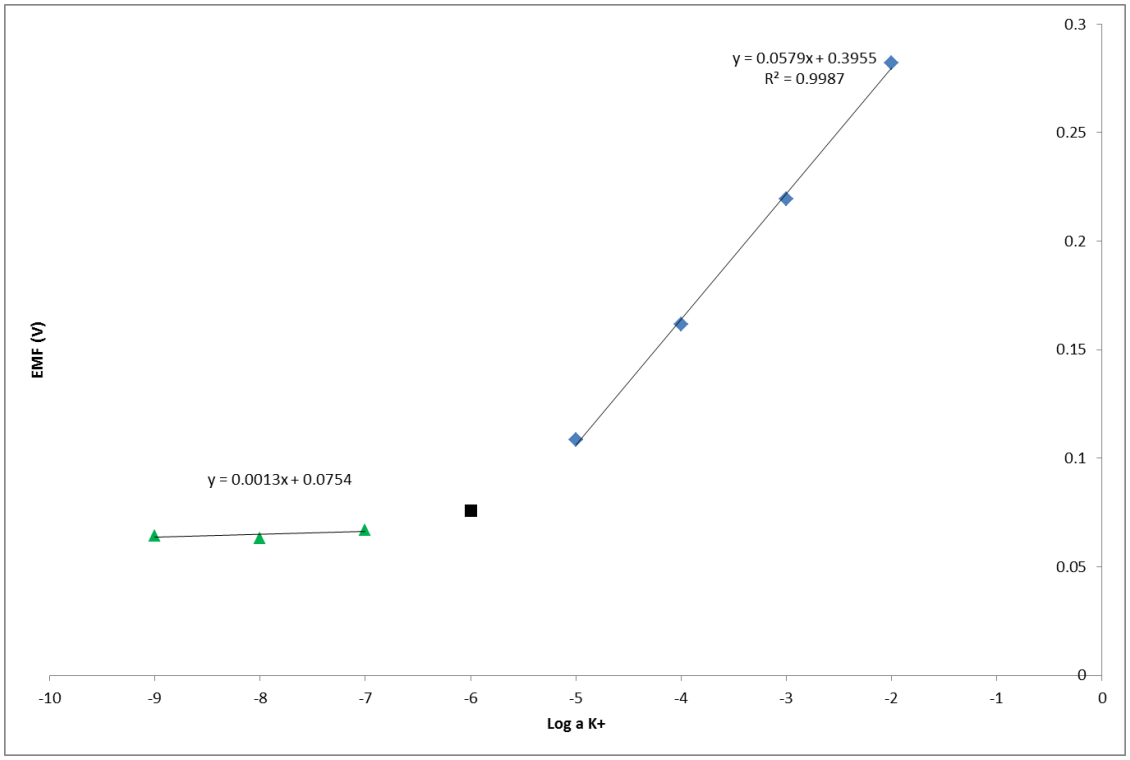

Figure 4-9: Calibration curve of porous carbon potassium ion selective electrodes generated from varying concentrations of KCl tested against an Ag/AgCl reference electrode and a Pt wire counter electrode. The limit of detection was calculated at the intersection of the two lines shown in the figure.

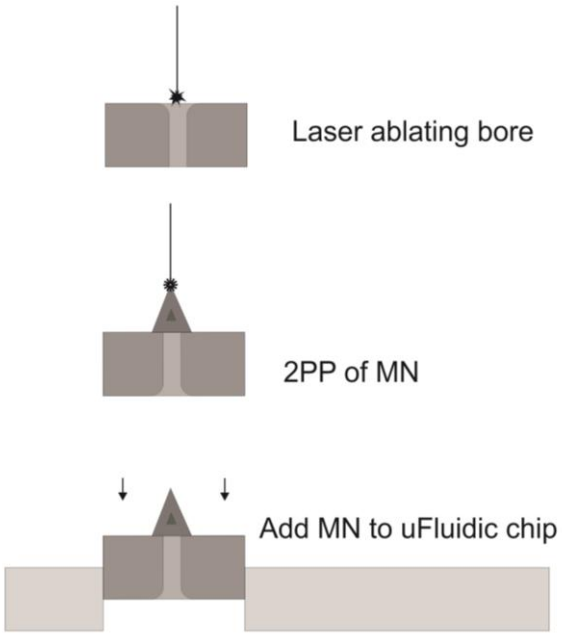

Figure 4-10: Schematic of assembly process for integrating hollow microneedles within the microfluidic chip. First bores are laser cut into Eshell 300 substrates to create a fluidic pathway between the hollow microneedle and the microfluidic chip. Hollow microneedles are then fabricated over the exit side of laser ablated bores. Finally, the microneedle with substrate was added to the top layer of the microfluidic chip and help in place with the underlying double sided adhesive.

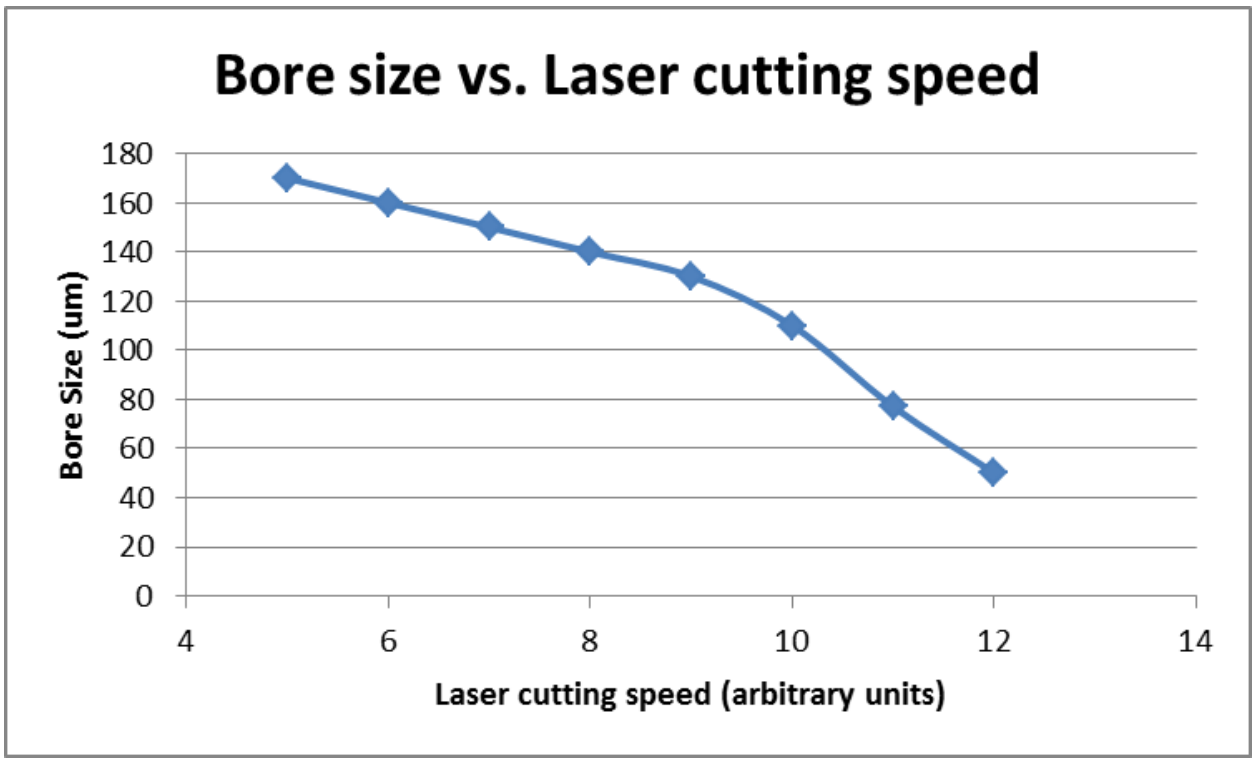

Figure 4-11: Relation between laser cutting speed and exit bore sizes in 2 mm thick Eshell300 substrates. Laser cutting speeds were altered while power, resolution, gas flow rate, and z-height were held constant.

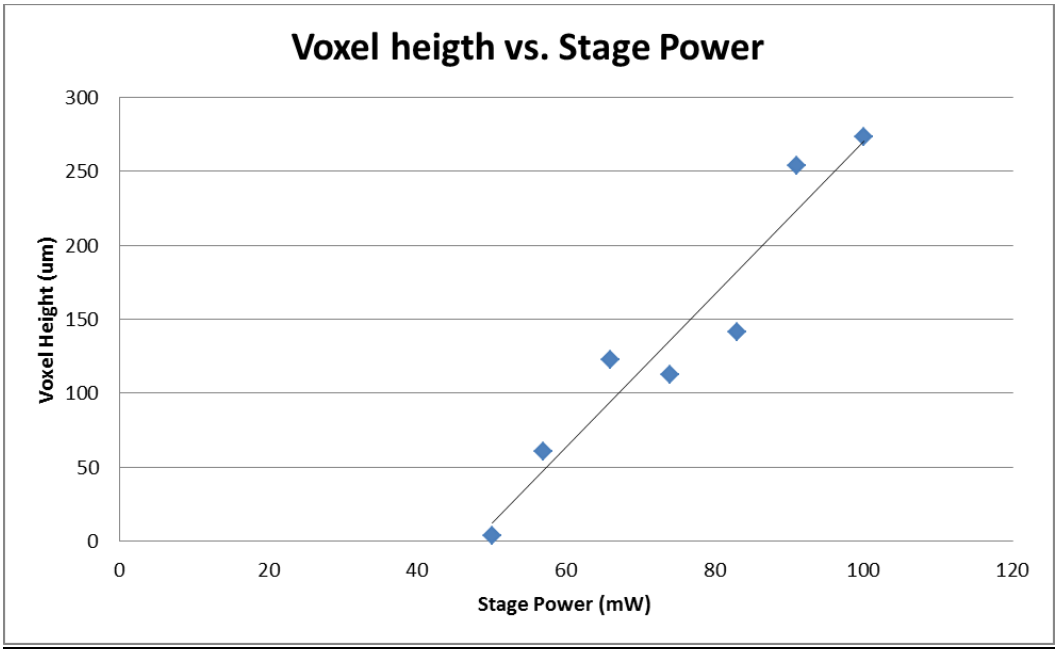

Figure 4-12: Relation between laser power and voxel height of fabricated structures using two-photon polymerization.

References

[1] Gubala, V., Harris, L. F., Ricco, A. J., Tan, M. X., & Williams, D. E. (2011). Point of care diagnostics: status and future. *Analytical chemistry*, *84*(2), 487-515.

[2] Windmiller, J. R., & Wang, J. (2013). Wearable electrochemical sensors and biosensors: a review. *Electroanalysis*, *25*(1), 29-46.

[3] Gubala, V., Harris, L. F., Ricco, A. J., Tan, M. X., & Williams, D. E. (2011). Point of care diagnostics: status and future. *Analytical chemistry*, *84*(2), 487-515.

[3] Windmiller, J. R., & Wang, J. (2013). Wearable electrochemical sensors and biosensors: a review. *Electroanalysis*, *25*(1), 29-46.

[4] Jia, W., Bandodkar, A. J., Valdés-Ramírez, G., Windmiller, J. R., Yang, Z., Ramírez, J., ... & Wang, J. (2013). Electrochemical tattoo biosensors for real-time noninvasive lactate monitoring in human perspiration. *Analytical chemistry*,*85*(14), 6553-6560.

[5] Kim, Y. C., Park, J. H., & Prausnitz, M. R. (2012). Microneedles for drug and vaccine delivery. *Advanced drug delivery reviews*, *64*(14), 1547-1568.

[6] Valdés-Ramírez, G., Li, Y. C., Kim, J., Jia, W., Bandodkar, A. J., Nuñez-Flores, R., ... & Wang, J. (2014). Microneedle-based self-powered glucose sensor.*Electrochemistry Communications*, *47*, 58-62.

[7] Martanto, W., Moore, J. S., Kashlan, O., Kamath, R., Wang, P. M., O'Neal, J. M., & Prausnitz, M. R. (2006). Microinfusion using hollow microneedles.*Pharmaceutical research*, *23*(1), 104-113.

[8] Muller, D. A., Corrie, S. R., Coffey, J., Young, P. R., & Kendall, M. A. (2012). Surface modified microprojection arrays for the selective extraction of the dengue virus NS1 protein as a marker for disease. *Analytical chemistry*, *84*(7), 3262-3268.

[9] Windmiller, J. R., Valdés-Ramírez, G., Zhou, N., Zhou, M., Miller, P. R., Jin, C., ... & Wang, J. (2011). Bicomponent Microneedle Array Biosensor for Minimally-Invasive Glutamate Monitoring. *Electroanalysis*, *23*(10), 2302-2309.

[10] Miller, P. R., Skoog, S. A., Edwards, T. L., Lopez, D. M., Wheeler, D. R., Arango, D. C., ... & Narayan, R. J. (2012). Multiplexed microneedle-based biosensor array for characterization of metabolic acidosis. *Talanta*, *88*, 739-742.

[11] Koeppen, B. M., & Stanton, B. A. (2012). *Renal Physiology: Mosby Physiology Monograph Series*. Elsevier Health Sciences.

[12] Bakker, E., Bühlmann, P., & Pretsch, E. (1997). Carrier-based ion-selective electrodes and bulk optodes. 1. General characteristics. *Chemical Reviews*,*97*(8), 3083-3132.

[13] Lai, C. Z., Fierke, M. A., Stein, A., & Bühlmann, P. (2007). Ion-selective electrodes with three-dimensionally ordered macroporous carbon as the solid contact. *Analytical chemistry*, *79*(12), 4621-4626.

[14] Gittard, S. D., Miller, P. R., Boehm, R. D., Ovsianikov, A., Chichkov, B. N., Heiser, J., ... & Narayan, R. J. (2011). Multiphoton microscopy of transdermal quantum dot delivery using two photon polymerization-fabricated polymer microneedles. *Faraday discussions*, *149*, 171-185.

[15] Burckel, D. B., Washburn, C. M., Raub, A. K., Brueck, S. R., Wheeler, D. R., Brozik, S. M., & Polsky, R. (2009). Lithographically defined porous carbon electrodes. *Small*, *5*(24), 2792-2796.

[16] Xiao, X., Beechem, T. E., Brumbach, M. T., Lambert, T. N., Davis, D. J., Michael, J. R., ... & Polsky, R. (2012). Lithographically defined three-dimensional graphene structures. *ACS nano*, *6*(4), 3573-3579.

[17] Crespo, G. A., Macho, S., & Rius, F. X. (2008). Ion-selective electrodes using carbon nanotubes as ion-to-electron transducers. *Analytical chemistry*, *80*(4), 1316-1322.

[18] Ping, J., Wang, Y., Wu, J., & Ying, Y. (2011). Development of an all-solid-state potassium ion-selective electrode using graphene as the solid-contact transducer. *Electrochemistry Communications*, *13*(12), 1529-1532.

[19] Li, F., Ye, J., Zhou, M., Gan, S., Zhang, Q., Han, D., & Niu, L. (2012). All-solid-state potassium-selective electrode using graphene as the solid contact.*Analyst*, *137*(3), 618-623.

[20] Lai, C. Z., Fierke, M. A., Costa, R. C. D., Gladysz, J. A., Stein, A., & Bühlmann, P. (2010). Highly selective detection of silver in the low ppt range with ion-selective electrodes based on ionophore-doped fluorous membranes. *Analytical chemistry*, *82*(18), 7634-7640.

[21] McCreery, R. L. (2008). Advanced carbon electrode materials for molecular electrochemistry. *Chem. Rev*, *108*(7), 2646-2687.

[22] Pumera, M. (2011). Nanomaterials meet microfluidics. *Chemical Communications*, *47*(20), 5671-5680.

Chapter 5 Electrodeposited Iron as a Biocompatible Material for Microneedle Fabrication

Philip R Miller[1,2], Ryan D Boehm[2], Shelby Skoog[2,3],Thayne L Edwards[1], Mark Rodriguez[1], Susan Brozik[1], Igal Brener[1,4], Thomas Byrd[5], Justin T Baca[5,6], Carlee Ashley[1,] Roger J Narayan[2*], Ronen Polsky[1*]

[1]Sandia National Laboratories, Albuquerque, New Mexico 87185, USA

[2]Joint Department of Biomedical Engineering, University of North Carolina and North Carolina State University, Raleigh, North Carolina 27695-7115, USA

[3]US FDA, Off Sci & Engn Labs, Ctr Devices & Radiol Hlth, Silver Spring, MD 20993 USA

[4]Center for Integrated Nanotechnologies, Sandia National Laboratories, Albuquerque, New Mexico 87185, USA

[5]University of New Mexico School of Medicine, Albuquerque, NM, 87131, USA

[6]Department of Emergency Medicine, University of New Mexico Health Sciences Center, Albuquerque, NM 87131, USA

The following section is a recently accepted manuscript in the journal *Electroanalysis* and is not yet in publication.

Abstract

Electroplated iron was investigated as a novel material for microneedle fabrication due to its recent success as a biocompatible metal in other medical device applications. Hollow polymer microneedles were made using a laser direct write process that involved two-photon polymerization of a commercially available Class 2a biocompatible polymer and subsequent electroplating of this structure with iron. Electroplating bath and deposition conditions were shown to affect the mechanical properties of both iron plated microneedles and iron plated on planar polymer substrates. Conditions for depositing the iron coatings were investigated in terms of grain size, residual strain, and elemental composition for planar iron samples. Fracture strength and puncture mechanics into *ex vivo* porcine skin for iron coated hollow microneedles were examined. Biocompatibility testing was performed using the MTT assay against human epidermal keratinocytes with several concentrations of iron extract to investigate iron as a material used for transdermal applications. Iron coatings proved to significantly improve the strength of the hollow polymer microneedles and sustained structural integrity up to 7 insertions into porcine skin without bending. A commercially available device (Medtronic MiniMed Quick-Serter®) was used for controlled application of microneedles into porcine skin and estimations of insertion forces for the device were made. Plating conditions were optimized such that an adherent, uniform, and high purity iron coating was deposited onto polymer substrates and polymer microneedles without delamination or fracturing of the microneedles upon *ex vivo* insertion into porcine skin.

Keywords: microneedle, electroplating, coating, iron

Introduction

The use of microneedles for drug delivery and sensing has rapidly advanced over the past two decades, offering the possibility of minimally invasive access, self-administration, and efficient drug loading.[1] Microneedle-based devices were initially developed to overcome the limitations the stratum corneum layer of the skin imposes on diffusion of pharmaceutical agents, especially large molecular weight compounds (e.g. vaccines), from the skin surface to deeper tissues, and have most recently been investigated for use in tissue suture and diagnostic applications.[2,3,4] Solid, degradable, and hollow microneedles comprise the main needle geometries used. For sensing applications, hollow microneedles are preferred that can be integrated with a microfluidic diagnostic chip,[5,6] while diffusion-based analyte collection methods have been shown to circumvent issues associated with extraction of interstitial fluid using hollow microneedles.[7,8,9]

Hollow microneedles allow for larger volumes to be delivered compared to coated or degradable needles however special consideration must be taken to prevent clogging after insertion into the skin.[10] An offset bore allows for increased fluid delivery and improved fluid extraction.[11,12] Several fabrication techniques exist that are capable of creating arrays of hollow microneedles with offset bores. Initial efforts concentrated on conventional silicon microfabrication techniques which still remain in common use.[13] Recently, a low cost approach that involves a combination of UV lithography and molding has been reported to create arrays of polymeric hollow microneedles.[14,15] In some scenarios, metals can be deposited as a coating to enhance microneedle strength.[16,17] The majority of the efforts to metal coat microneedles however use nickel which can cause dermatitis.[18] Electroplating is attractive due to the ease of the deposition process and subsequent control over the mechanical properties of the deposited coating.[19] Biocompatible metal coatings such as titanium and 316L stainless steel have found widespread use in medical implants,

but they are difficult to electroplate and require a more sophisticated means for deposition.[20,21]

Iron has been used in electroplating since the 1920's for processing of intaglio plates, coatings for automotive pistons, and induction coils. More recently, iron has been revisited as a degradable biomaterial for use in coronary stents. [22,23] Clinical trials have been performed using iron stents in the descending aorta of pigs without detection of iron overload, due to degradation, in the major organs and also did not exhibit indication of toxicity in the region surrounding the implantation site.[24] Iron stents have been created with an electroforming technique and tested in terms of their mechanical properties, degradation rate, and effect on smooth muscle cell growth with no reduction in cell metabolic activity observed.[25] The mechanical properties, degradation rate, and grain size of electrodeposition-grown iron can be readily controlled by simply varying the electrodeposition parameters.[26,27] In this study, we show that electroplating iron onto hollow microneedles, made with two-photon polymerization, can be used as a facile and biocompatible material to create microneedles for diagnostic and drug delivery applications.

Materials and Methods

Microneedle Fabrication:

Microneedles were prepared in a similar fashion to a previous report.[4] Hollow polymer microneedles were prepared using a laser direct write system utilizing two-photon polymerization. First, a CAD file was created in the desired shape and dimensions of the microneedle and was uploaded to the laser direct writing operating software (GOLD3D). The software sliced the CAD file and assigned writing parameters to optimize the fabrication process. The two photon polymerization effect is achieved using a Ti:Sapphire laser, which was operated at 800 nm, 150 fs, and 76 MHz. A 4× objective was used to focus the beam; write settings of 150 μm s^{-1} write speed, 2 μm *x*- and *y*-axis rastering, as well as 25 μm *z*-step height were used in this study. E-Shell 300 was used as the polymer precursor for both the hollow microneedles and the substrates. Polymer substrates were created in PDMS molds made by laser cutting PMMA into 10 mm × 10 mm × 2 mm pieces and molding them with PDMS. E-Shell 300 was then placed in the molds and cured with a UV lamp. In order to make a fluidic connection between the microfluidic chip and the hollow microneedle, a bore was cut into the substrates with a CO_2 laser to create a bore diameter of approximately 150 μm. Bore patterns were designed in CorelDraw; a single 100 μm circle was drawn and uploaded to the laser cutting software. A well was made on top of the bore-containing substrate such that a microneedle could be written onto the substrate. The well was created with parafilm; once filled with resin, a glass cover slip was placed on top of the spacer. A vacuum was pulled from the bottom of the substrate such that a small amount of resin was pulled into the bore in order to remove air.

Microfluidic Chip Fabrication:

Microfluidic chips were made in a layer-by-layer manner from PMMA sheets and Melinex® double-sided adhesive layers. A CO_2 laser was used to ablate patterns into the PMMA and into the adhesive layers that were used in formation of the fluidic channels. Layers were assembled with a jig and pressed at 1000 psi in order to remove air bubbles from the adhesive layers. O-rings were used between the PMMA layers in order to connect PEEK tubing, which was used to adding fluids to the chip. Hollow microneedles were added to the microfluidic chip by placing a double-sided adhesive on the back of the needles and applying them to the microfluidic chip.

Electroplating of Microneedles:

Hollow microneedles and e-Shell 300 substrates (without microneedles) were used for iron plating experiments. Gold was sputter coated as a seed layer to create the electrical contact for the electroplating process. Microneedles were sputtered with 50 nm of gold while tilted at 45 degrees and with an additional 50 nm after reversing the tilt such that each of the walls was evenly coated. Electroplating masks were created in order to control the surface area of the deposited coatings. This was done to more easily control electroplating conditions and thus material properties of the Fe. Masks were made by laser cutting of the electroplating tape. Patterns made in CorelDRAW were subsequently read by the Universal Laser System. Laser settings of 100% power, 70% write speed, 0.0" stage height, and 300 DPI were used to fabricate the masks. Mask surface areas were 0.1 cm^2 for all of the microneedles and substrates. Iron plating baths used for electroplating were comprised of 400 g/L $FeCl_2$, 80 g/L $CaCl_2$, 1 g/L sodium saccharin, and 0.25 g/L SDS.[22] Baths were adjusted to pH 1 with HCl and NaOH and were prepared regularly. Iron films were deposited with current densities of 5-20 mA/cm^2 against an Ag/AgCl reference and Pt

counter electrode for two hours. Bath temperature was adjusted with a hot plate. In addition, bath pH was monitored over time.

XRD Analysis:

Residual strain within the electroplated iron films was analyzed using X-ray diffraction and the $\sin^2\psi$ method. In brief, scans are performed across the (211) iron peak while monitoring the resulting diffracted intensity over a range of tilt angles (0-50^o) with the assumption that the out-of-plain strain is zero. The $(d-d_o)/d_o$ vs. $\sin^2\psi$ dependence of the tilt was linear, the slope of which was related to the residual stress of the film.

SEM/EDX Imaging:

Electroplated iron microneedles and substrates were imaged using a Carl Zeiss Supra™ 55VP SEM at 10 and 15kV and a working distance of 8.5 mm. All samples were coated with a thin layer of platinum prior to imaging. EDX was used to determine the presence of impurity elements in the iron coatings.

Mechanical Testing:

The fracture forces for deformation of polymer hollow microneedles and iron plated hollow microneedles were investigated. Microneedles were placed in a BOSE Electroforce® 3100 mechanical testing instrument (Bose Corporation, Framingham, MA) with a 20 N load cell. Compressions were run at 0.1mm/s; microneedles were pressed against a metal platen while monitoring the change in force and the displacement upon impact. Microneedles were imaged with a digital microscope or with a scanning electron microscope after compression testing. Thickness measurements were obtained under SEM imaging compressed iron microneedles.

Biocompatibility of Fe Extracts:

Normal adult human primary epidermal keratinocytes (HEKs) were cultured at 37°C with 5% by volume CO_2 in Dermal Cell Basal Medium, which was supplemented with L-glutamine, Extract-P, rh TGF-□, rh insulin, epinephrine, hydrocortisone hemisuccinate, and apo-transferrin (ATCC, Manassas, VA). After growing to 80% confluence, the cells were dissociated with trypsin/EDTA solution for primary cells with subsequent addition of neutralizing solution (ATCC, Manassas, VA). Cells were subsequently resuspended in medium prior to cell seeding. Passage 3 cells were used for all of the experiments.

Cell viability was evaluated using indirect contact cell testing. In this approach, cells were exposed to material extracts according to ISO 10993-5. Electroplated iron films of 4 mm diameter were extracted in HEK culture media at a ratio of 1 mL per 6 cm^2 surface area (ISO 10993-12) in polypropylene tubes. Extractions were performed at 37°C for 24 hours in HEK media (ISO 10993-5). Due to degradation of the material over 24 hours, the extract was filtered using a 0.2 um syringe filter.

HEKs were added to a 96-well plate at a cell density of 10,000 cells per well. After growing cells for 24 hours, HEKs were treated with either media (negative control), media with silver ions (positive control), or test extracts. The filtered extract and a dilution series of the extract (50%, 25%, 10%) using HEK media as the diluent were applied (n=2 per sample). After 24 hours of incubation, cell viability was assessed using the 3-(4,5-dimethylthiazol-2-yl)2,5-diphenyltetrazolium bromide (MTT) assay (CellTiter 96® Non-Radioactive Cell Proliferation Assay, Promega, Madison, WI). Absorbance was measured at a wavelength of 570 nm with a reference wavelength of 650 nm using a 96-well SpectraMax® 190 Absorbance Microplate Reader (Molecular Devices, Sunnyvale, CA). The

data was normalized to the media controls. MTT reduction was expressed as percent viability of the media controls. Cell viability testing was repeated in triplicate.

Puncture Testing:

Porcine skin was used for microneedle penetration studies. The tissue samples were acquired from a local abattoir. The tissue samples were acquired immediately following animal sacrifice and stored at -20^{o}C until use. The porcine skin was thawed in 1X phosphate-buffered saline and then shaved. Hollow iron microneedles with the attached microfluidic chip assembly were anchored to the Medtronic MiniMed Quick-Serter® with double sided Melinex® adhesive. Microneedles were applied to the porcine skin with the Medtronic MiniMed Quick-Serter®. After insertion into the skin, Trypan Blue was injected into the tissue by hand application from a syringe and PEEK tube attachment on the microfluidic chip. After the microneedles were removed, the porcine tissue was embedded in an OCT (optimal cutting temperature) compound and frozen using a metal block that had been cooled with liquid nitrogen. A cyromicrotome, which was operated at -20^{o}C, was used to section porcine skin embedded in OCT. The sections were later imaged using a digital microscope

Results and Discussion

Previously, we developed a laser based (two-photon polymerization-based) fabrication technique for making hollow polymer microneedles.[28] The advantage of this over conventional lithography is that a design can be created in Solidworks and 3D structures can be directly fabricated without a mask or wet chemical etching processes. While highly reproducible structures are readily made with this technique, the materials used in two-photon polymerization are largely limited to photo-cured polymers or photo-reduced metals that lack the mechanical properties of bulk metals. We often observed microneedle tip deformation with repeated ex vivo insertions of the uncoated e-Shell 300 microneedle into porcine skin, especially with the larger internal bore dimensions (~ 200 microns) necessary to increase the extraction volume for sensing. To address these issues, we herein describe electroplating, an inexpensive and facile deposition method, to deposit iron coatings for improving the mechanical integrity of these hollow microneedles.

Figure 5-1A shows an iron microneedle assembled onto a microfluidic chip with PEEK tubing attachment and Figure 5-1B shows an optical image of an iron- plated microneedle. Initial parameters investigated were bath temperature and current density onto 50 nm thick gold sputtered microneedles (see experimental). A bath plating temperature of 25^{o}C showed darkening in some areas of deposited films and delamination, indicative of a highly stressed coating. Electroplated coatings on polymers have been known to suffer from delamination due to poor adhesion of the seed layer and/or difference in stresses between the layers due to formation of surface oxides. Previous reports have shown that plating conditions affect the properties of deposited iron films; however, these properties have not been optimized for depositing adherent coatings onto the polymer substrates used here. Increasing bath temperatures using a current density of -10 mA cm^{-2} resulted in more ductile films, which exhibited strong adhesion to the substrate without

delamination under stress tests. Figure 5-2 shows scanning electron micrographs of iron-coated microneedles that were compressed at 0.1mm s^{-1}. The SEM images reveal very different modes of failure for various plating temperatures. Microneedles plated at 75°C deform via peeling and bending of the iron layer. Microneedles plated at a lower bath temperature of 25°C failed via fracture, with very little bending of the iron layer. The results from these compressions tests indicate iron films plated at lower temperatures are susceptible to fracturing and are undesirable, potentially fragmenting into pieces within dermal tissue upon insertion. For microneedles that were plated at cooler temperatures, fracture was typically observed at the base of the needle; shear against the grain between the needle walls and the substrate was noted. Of the needles that underwent fracture, the

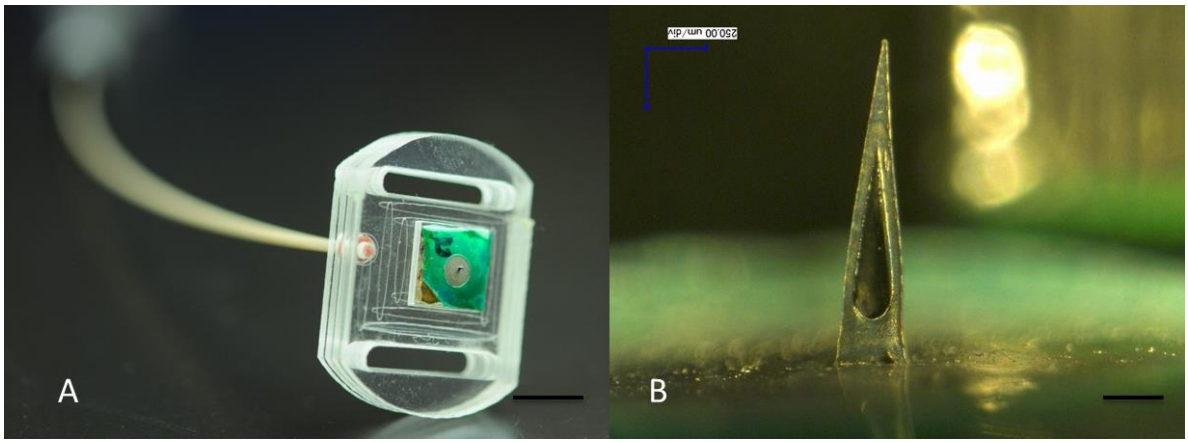

Figure 5-1:(A) Photograph of a hollow iron microneedle attached to a 10 mm x 10mm e-shell 300 substrate within a laminate microfluidic chip that was attached to 1/16″ PEEK tubing, and B a microphotograph of an iron-plated hollow microneedle. Scale bar for figure A and B is 10 mm and 250 μm respectively.

needles appeared structurally sound with no delamination or deformation at the tip.

The grain size and morphology of the electroplated coatings were investigated with scanning electron microscopy, as seen in Figure 5-3 and 5-4. Previous studies have investigated the effect of iron chloride bath plating conditions on electroplated iron films.[29,30] These studies revealed that increased bath temperatures resulted in an increase in

grain size and current efficiency due to enhanced diffusion of the iron ions, which exhibit greater mobility at higher temperatures, in solution. Hardness values of the coatings decreased at higher bath temperatures; higher temperatures also promoted crystal growth as opposed to nucleation. It is important to note that previous studies involved plating of iron coatings onto polished metal substrates while the microneedles and polymer substrates used in this study have surface undulations, which likely affect the uniformity of the coatings. In an attempt to improve coating adhesion, we investigated the grain size and morphology of iron plated at -10mA cm^{-2} while varying bath temperatures between 25°C and 87°C onto flat gold-coated polymer substrates (gold coating thickness ~ 100 nm). A bath temperature of 87°C was the initial condition used in this study due to the fact this this temperature is commonly used in electroplating studies. The grain size, determined by SEM analysis, for these plating conditions was 1.69 ± 0.063 m. The plating density was then held constant while the bath temperature was reduced. Decreasing grain size was observed with decreasing bath temperatures; bath temperatures of 25°C, 50°C, and 65°C were associated with grain sizes of 1.10 ± 0.214 um, 0.62 ± 0.164 um, and 0.18 ± 0.149 um, respectively. Bath temperatures above 25°C produced adherent, gray/silver toned coatings with no dark oxide deposits while dark oxide deposits were noted in room temperature-plated coatings. Iron plated on polymer substrates with metal seed layers exhibited similar grain sizes and morphologies to iron plated on metal substrates. Room temperature plating revealed two distinct regions; one region type with nano-wire like structures and another region type with thin undulating flakes. Iron coatings deposited at 87°C produced two distinct regions, one with well-defined crystal growth and another with a varying and non-crystalline surface morphology. Bath temperatures of 50°C and 65°C produced uniform coatings with well-defined crystallinity.

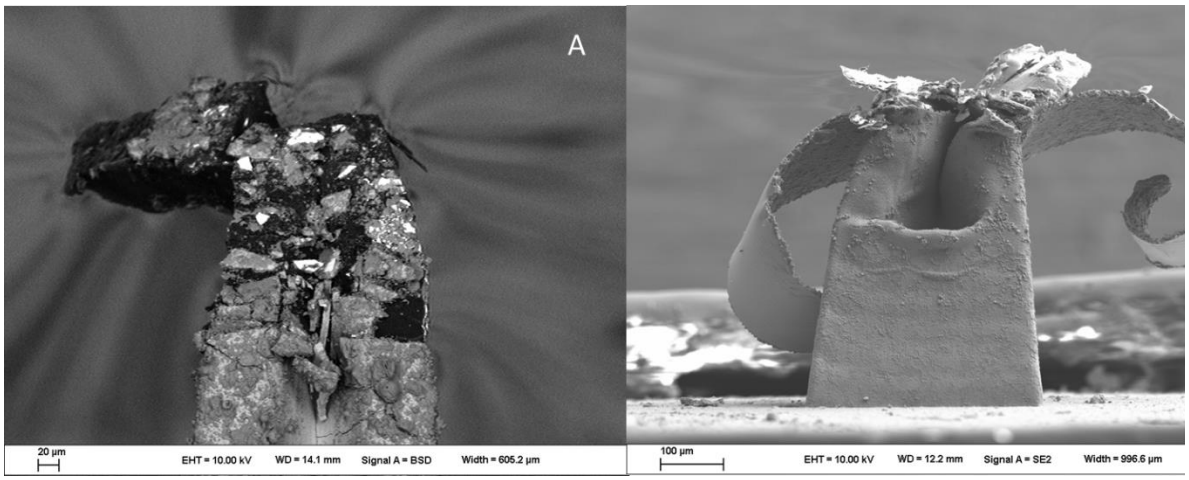

Figure 5-2: SEM images comparing iron plated on microneedle at different plating conditions, showing the effect of processing conditions on the mechanical properties of the plated films. Figure 2A was plated a lower temperature (25^{o}C) and Figure 2B was plated at higher temperatures (75^{o}C); a constant current density (-10mA/cm^{2}) and bath composition were used for processing of both films.

Elemental characterization was performed to investigate the purity of the iron coatings. Previous reports indicate stringent control of temperature and plating current density is necessary to produce high purity films.[31] Impurities impede grain growth, leading to smaller grains and more stressed films. EDX plots of deposited iron coatings at varying bath-plating temperatures are presented in Figure 5-5. Samples plated at 25^{o}C and 87^{o}C show high amounts of oxygen, while samples plated at 50^{o}C and 65^{o}C indicate lower oxide formation. Plating at 25^{o}C and 87^{o}C also showed a small amount of chloride, which is a product of burning. Carbon observed in these samples and can be attributed to impurities resulting from saccharin decomposition, which is used as a stress-reducing agent in the plating. A platinum peak was seen throughout the samples and was a result of a thin coating prior to SEM and EDX imaging to improve the conductivity of substrates. Coatings plated at 50^{o}C and 65^{o}C showed moderate levels of oxygen, while having little or no other elemental impurities.

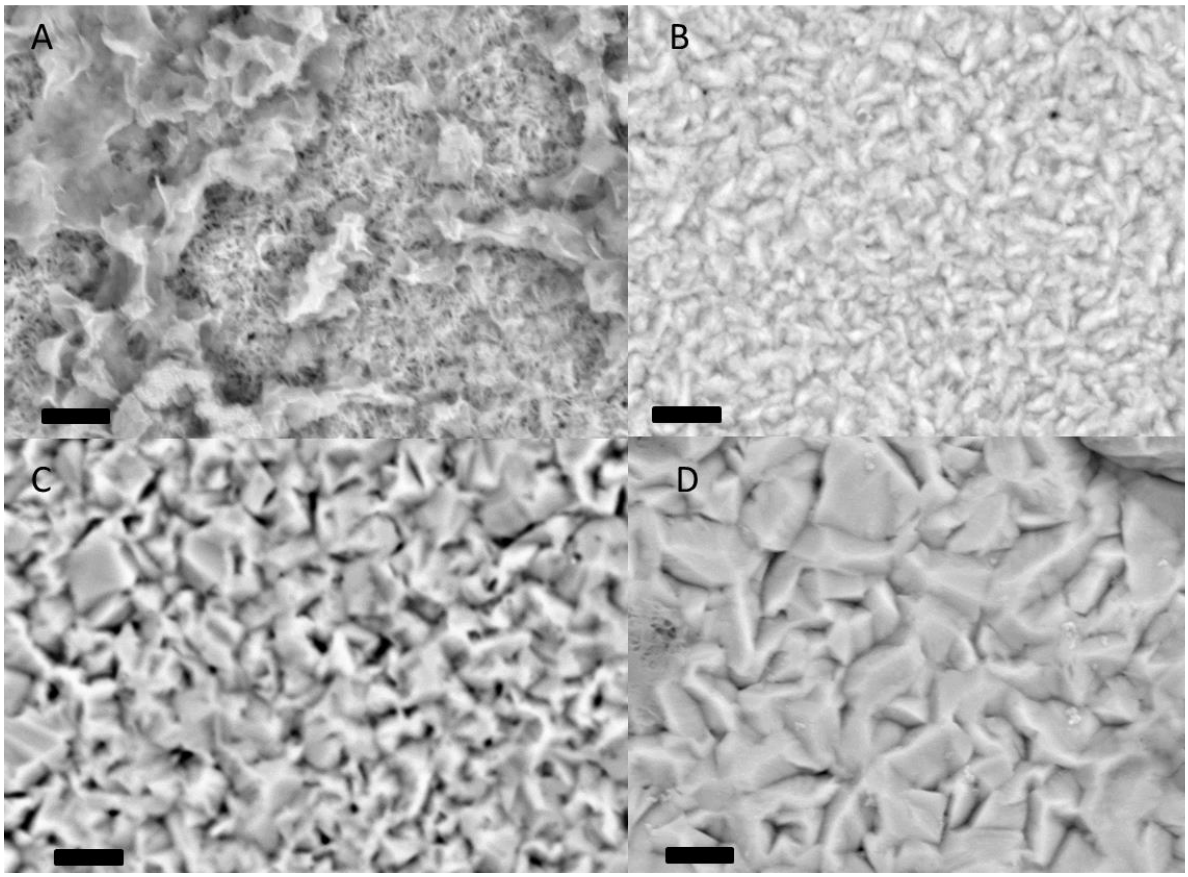

Figure 5-3: Scanning electron micrographs of iron films deposited at different temperatures (A: 25°C, B: 50°C, C: 65°C, and D: 87°C) at a constant current density of -10mA/cm^2. Scale bar=1 □m.

SEM imaging and puncture testing confirmed that the iron films contained residual stresses. Quantification of the degree of residual stress was examined with XRD analysis to further understand the effect of bath plating parameters on the properties of iron-plated polymers (Figure 5-6). Residual strain measurements were made by monitoring the d-spacing at various tilt angles (X(o)), assuming that X(o)=0 where X(o) is perpendicular to the surface of the film). Plotting sin^2(x) versus change in d-spacing produces a line, the slope of which corresponds to the strain of the film. Gold coated (thickness=100n m) polymer substrates were initially analyzed to ensure that the initial seed layer contained no residual strain. Broad Au (311) peaks were seen throughout the X-tilt angle, indicating a nanocrystalline structure; the lack of a 2-theta peak shift indicated little to no residual

stress was present. As seen in Figure 5-6A, XRD scans of all of the Fe films showed distinct Fe (211) peaks. Room temperature plating showed significant shifts in d-spacing, resulting in a film with 0.21% tensile strain, which is considered a highly stressed film since absolute strain values above 0.1% are not associated with potential instrumental error. Increasing the bath temperature to 50^{o}C reduced residual stress by more than half (0.09%) that of room temperature plating. Increasing the bath temperature to 65^{o}C continued to reduce the residual film strain to a value of 0.07%, producing the least stressed coated of all the tested samples. Since a bath of 65^{o}C produced films with the least amount of strain, other plating densities were investigated at this temperature to determine if increasing the plating current density could be undertaken (to increase plating rates and iron purity) while maintaining an unstressed film. Iron films plated at 65^{o}C and -15mA cm^{-2} produced strain values above those of the 50^{o}C scans (0.1%), indicating that an increase in current density caused an increase in film strain.

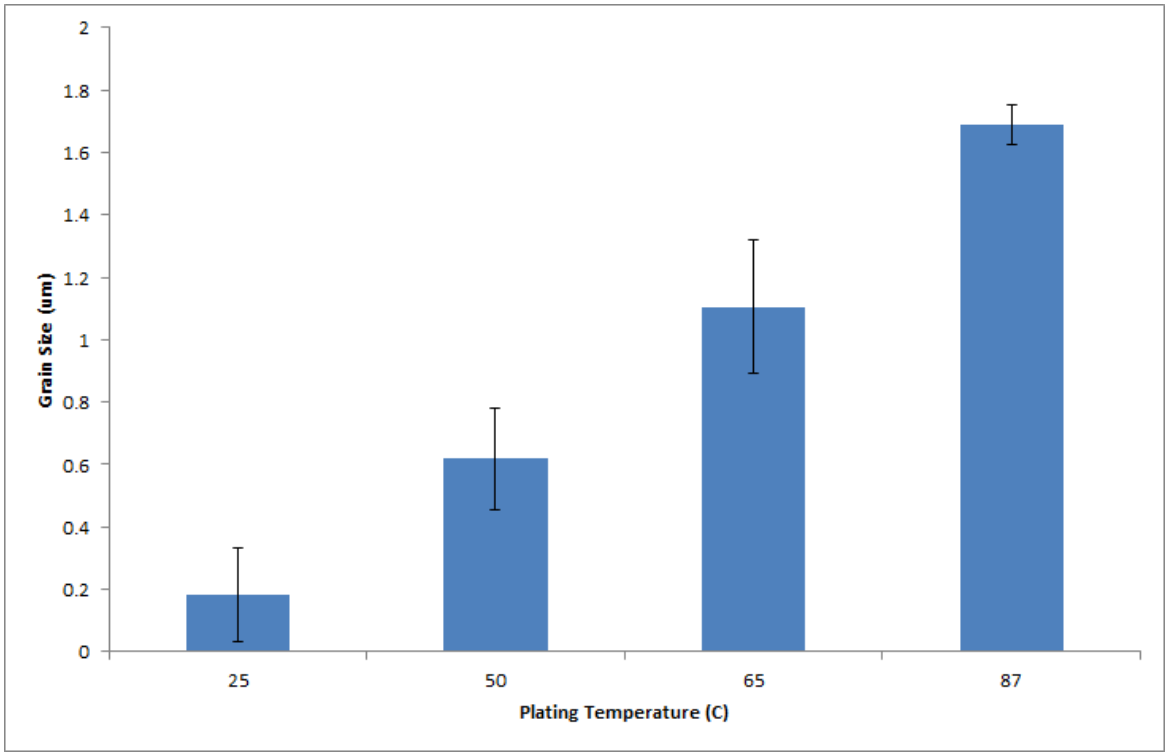

Figure 5-4: Grain size of electroplated iron coatings onto planar polymer substrates at a constant plating density of -10mA/cm^2 at several bath temperatures.\

Iron coatings were investigated in relation to microneedle fracture strength presented in Figure 5-7. Hollow microneedles were made in a three-sided pyramidal shape and were 1500 ⍰m, 350 ⍰m, and 175 ⍰m in height, base, and bore size, respectively. Microneedles were compressed at a rate of 0.1 mm/s between two metal plates while monitoring the change in displacement and force. The hollow polymer microneedles coated with only the initial 100 nm gold seed layer deformed at 0.04 ± 0.03 N. It should be noted that polymer microneedles without iron coatings always plastically deformed when compressed and never fractured. The 50^{o}C iron coating produced microneedles that fractured at 0.7 6± 0.08 N. The 65^{o}C coating produced a coating slightly weaker, fracturing at 0.61 ± 0.17 N. The reduction in microneedle fracture strength can be attributed to the softer nature of the coatings plated at a higher bath temperature. Microneedles tested at 65^{o}C bath temperature deformed similarly to the initial microneedles tested in Figure 5-2B

in that coating deformed via bending rather than fracturing, which we believe is a beneficial feature for transdermal usage. A sample that was prepared using increased plating current density (-15mA cm^{-2} plated in a 65°C bath temperature) was tested; the fracture strength of this coating was higher than the other tested coatings. This result can be attributed to both the increased plating density and stressed plating parameters.

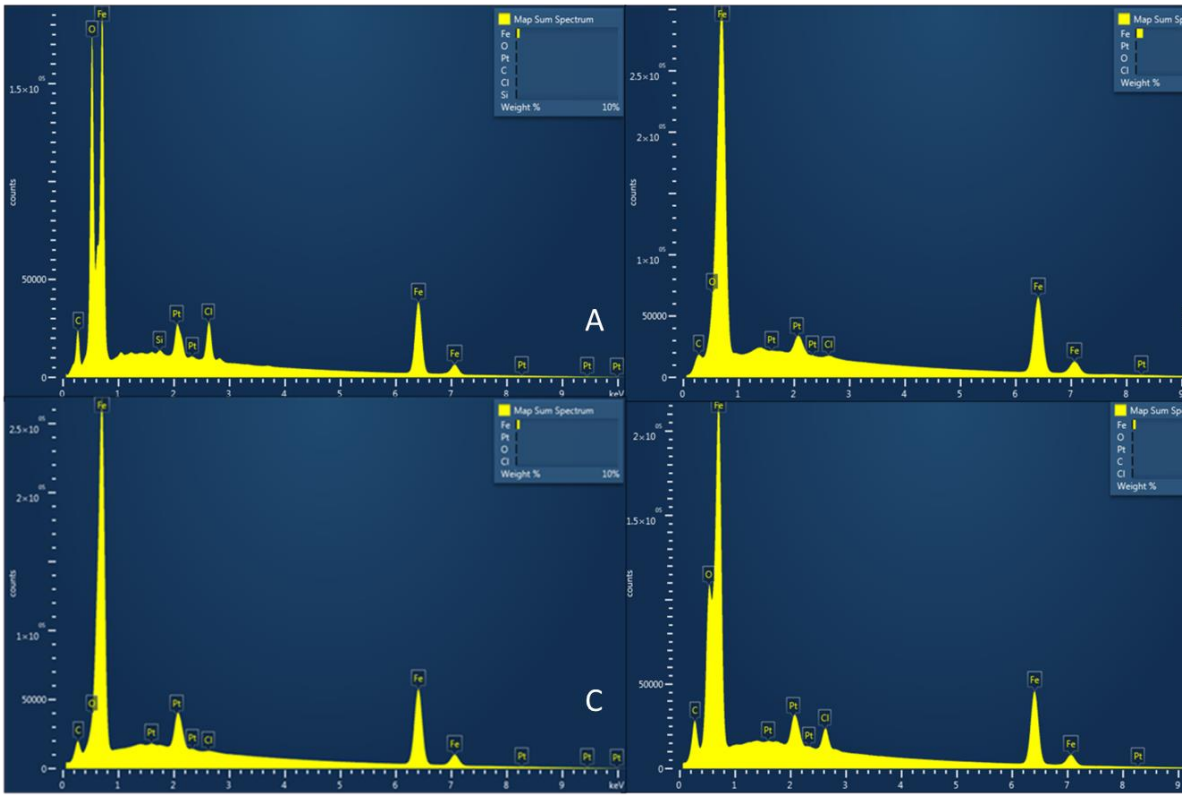

Figure 5-5: EDX profiles of iron films deposited at different temperatures (A: 25°C, B: 50°C, C: 65°C, and D: 87°C) and at a constant current density of -10mA/cm^2.

As previously mentioned, the biocompatibility of iron and electroplated iron has been tested in both clinical studies and with cell testing; however, these cell tests have focused primarily on smooth muscle cells due to the intended use of electroformed iron as a coronary stent material. To our knowledge, the biocompatibility of electroplated iron has not been characterized for transdermal applications. Cell viability was evaluated using indirect contact cell testing, in which cells were exposed to iron extracts according to ISO 10993-5. Fluid extracts were taken from electroplated iron coupons incubated in cell

growth medium for 24 hours at 37°C. Undiluted electroplated iron extracts were tested along with diluted iron extracts against human epidermal keratinocytes using the MTT assay (Figure 5-8), which has been used previously to validate the biocompatibility of several microneedle materials.[32] Iron extracts were tested at 10%, 25%, 50%, and 100% purity and were compared to tissue culture wells and silver ions as the negative and positive controls, respectively. Pure extracts exhibited 71% viability, with diluted iron extracts approaching nearly 100% viability for the remainder of the tested extracts.

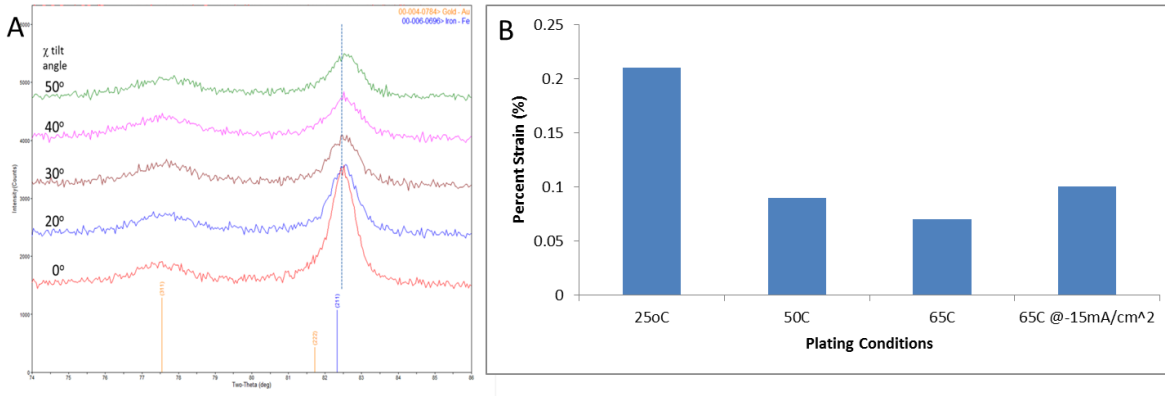

Figure 5-6: XRD scans of varying tilt angle (0-50 degrees) of iron plated at 25°C and -10mA/cm^2 (A) and resulting residual strain of iron films plated at various plating and bath conditions (B).

Several groups have demonstrated the benefit of applying microneedles and microneedle arrays with a controlled velocity to increase the permeability of skin.[33] These devices are typically custom made such that the impact velocity of the microneedles can be carefully controlled. Our initial results indicated that controlled application of microneedles was beneficial; however, we selected a more straightforward method for application of microneedles. The Medtronic MiniMed Quick-Serter® is used for controlled delivery of an insulin needle in an automated and controlled manner into the skin of a patient. Since our device sat higher on the platform than the Medtronic infusion set, the device (Figure 5-9D) was slightly modified with a spacer such that plunger could fully extend once the trigger was initiated. PMMA rings were used as the spacer and were laser cut in the same manner

as the microfluidic chip; these rings were attached to the device to create a spacing such that the actuating spring was nearly fully extended when the device (microneedle with microfluidic chip) was applied to the skin. The inserter has a single spring that is activated by a double push-button activator. Using a video camera, we estimated the velocity of the Medtronic MiniMed Quick-Serter® insertion process to be 0.5 m/s. When used with the Medtronic MiniMed Quick-Serter®, hollow iron microneedles were capable of being inserted *ex vivo* into porcine skin up to 7 times without fracturing. Microneedles were imaged before and after insertion (Figure 5-9A); little change in structure was noted in the microneedles after *ex vivo* penetration of porcine skin. Trypan blue was injected to show needle penetration depths within the tissue after cryosectioning shown in Figure 5-8. Future studies are needed to correlate bore size with extraction efficiency of interstitial fluid.

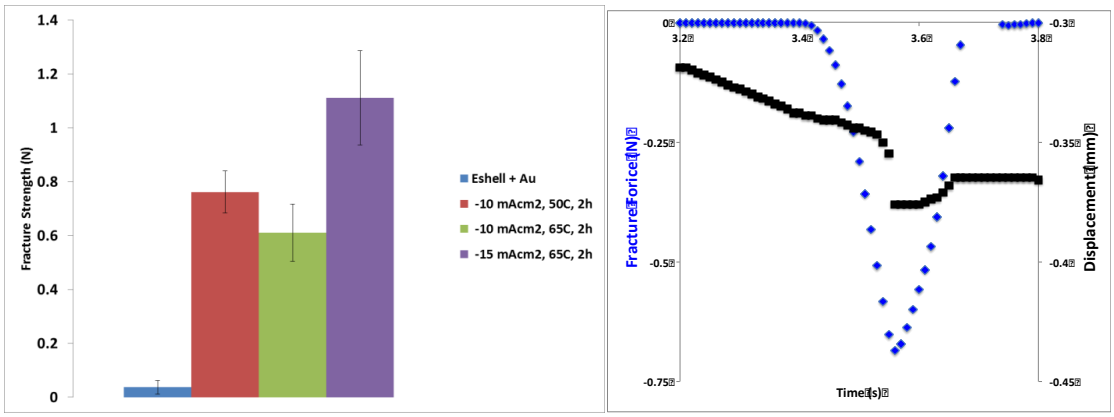

Figure 5-7: Mechanical testing of hollow iron plated microneedles at different plating conditions (A) and a typical result from a compression study using a hollow iron microneedle plated at -10 mA/cm^2 and a bath temperature of 65^{o}C for two hours.

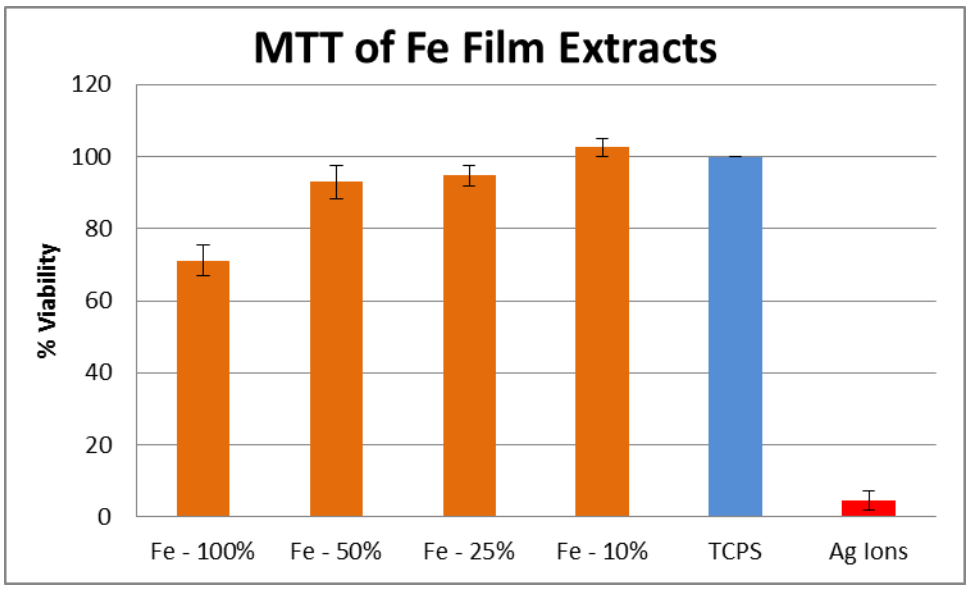

Figure 5-8: Results from MTT assay of electroplated Fe extracts incubated in growth medium for 37°C for 24 hours for several concentrations of the extract tested against human epidermal keratinocytes.

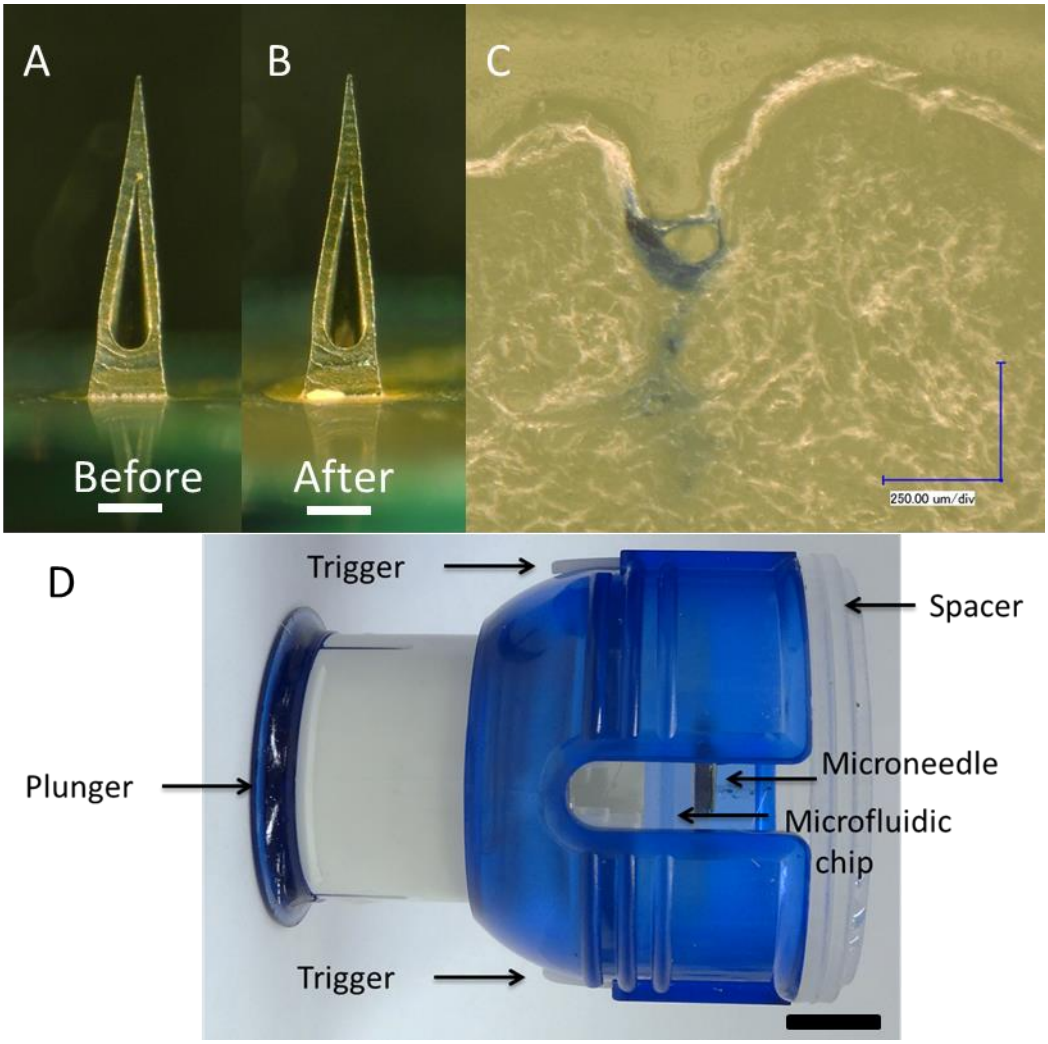

Figure 5-9: Optical images of before and after insertion of iron-plated microneedles using the Medtronic Quick-Serter® (A and B, scale bar: 250 m). Optical images of a cyrosectioned portion of porcine skin that had been injected with Trypan Blue through a hollow iron microneedle (C) and the Medtronic MiniMed Quick-Serter® (D); scale bar=10 mm.

Conclusions

Electrodeposition of iron was investigated as a biocompatible coating for hollow microneedles and to improve microneedle stiffness. The mechanical properties of the deposited coatings were investigated by modifying the plating conditions. Optimized plating conditions (65^{o}C and -10mA/cm^{2}) produced an adherent, uniform, and high purity iron coating on polymer substrates and on hollow polymer microneedles without delamination. Iron-plated microneedles were capable of being inserted into *ex vivo* porcine skin multiple times without fracturing. Controlled insertion was performed using the Medtronic MiniMed Quick-Serter®, which applied microneedles *ex vivo to* porcine skin at ~0.5 m/s.

Acknowledgements

We would like to thank Amy Allen for her help with the scanning electron micrographs, Graham Yelton for his insight with electroplating, as well as Steve Jett and Tamara Howard for access to the cryosectioning system. Sandia is a multiprogramming laboratory operated by Sandia Corporation, a Lockheed Martin Company, for the United States Department of Energy's National Nuclear Security Administration under Contract DE-AC04-94AL85000. The authors acknowledge the Sandia National Laboratories' Laboratory Directed Research & Development (LDRD) program.

References

[1] Kim, Y. C., Park, J. H., & Prausnitz, M. R. (2012). Microneedles for drug and vaccine delivery. *Advanced Drug Delivery Reviews*, *64*(14), 1547-1568.

[2] Yang, S. Y., O'Cearbhaill, E. D., Sisk, G. C., Park, K. M., Cho, W. K., Villiger, M., ... & Karp, J. M. (2013). A bio-inspired swellable microneedle adhesive for mechanical interlocking with tissue. *Nature Communications*, *4*, 1702.

[3] Jina, A., Tierney, M. J., Tamada, J. A., McGill, S., Desai, S., Chua, B., ... & Christiansen, M. (2014). Design, Development, and Evaluation of a Novel Microneedle Array-based Continuous Glucose Monitor. *Journal of Diabetes Science and Technology*, *8*(3), 483-487.

[4] Jin, J., Reese, V., Coler, R., Carter, D., & Rolandi, M. (2014). Chitin microneedles for an easy-to-use tuberculosis skin test. *Advanced Healthcare Materials*. 3 (3), 349–353.

[5] Miller, P. R., Xiao, X., Brener, I., Burckel, D. B., Narayan, R., & Polsky, R. (2014). Microneedle-based transdermal sensor for on-chip potentiometric determination of K+. *Advanced Healthcare Materials*. 3 (6), 876–881.

[6] Windmiller, J. R., Zhou, N., Chuang, M. C., Valdés-Ramírez, G., Santhosh, P., Miller, P. R., ... & Wang, J. (2011). Microneedle array-based carbon paste amperometric sensors and biosensors. *Analyst*, *136*(9), 1846-1851.

[7] Chua, B., Desai, S. P., Tierney, M. J., Tamada, J. A., & Jina, A. N. (2013). Effect of microneedles shape on skin penetration and minimally invasive continuous glucose monitoring in vivo. *Sensors and Actuators A: Physical*, *203*, 373-381.

[8] Vazquez, P., Herzog, G., O'Mahony, C., O'Brien, J., Scully, J., Blake, A., ... & Galvin, P. (2014). Microscopic gel–liquid interfaces supported by hollow microneedle array for voltammetric drug detection. *Sensors and Actuators B: Chemical*, *201*, 572-578.

[9] Invernale, M. A., Tang, B. C., York, R. L., Le, L., Hou, D. Y., & Anderson, D. G. (2014). Microneedle electrodes toward an amperometric glucose-sensing smart patch. *Advanced Healthcare Materials*. 3 (3), 338–342.

[10] Norman, J. J., Choi, S. O., Tong, N. T., Aiyar, A. R., Patel, S. R., Prausnitz, M. R., & Allen, M. G. (2013). Hollow microneedles for intradermal injection fabricated by sacrificial micromolding and selective electrodeposition. *Biomedical Microdevices*, *15*(2), 203-210.

[11] Martanto, W., Moore, J. S., Couse, T., & Prausnitz, M. R. (2006). Mechanism of fluid infusion during microneedle insertion and retraction. *Journal of Controlled Release*, *112*(3), 357-361.

[12] Mukerjee, E. V., Collins, S. D., Isseroff, R. R., & Smith, R. L. (2004). Microneedle array for transdermal biological fluid extraction and in situ analysis. *Sensors and Actuators A: Physical*, *114*(2), 267-275.

[13] Gardeniers, H. J., Luttge, R., Berenschot, E. J., De Boer, M. J., Yeshurun, S. Y., Hefetz, M., ... & van den Berg, A. (2003). Silicon micromachined hollow microneedles for transdermal liquid transport. *Journal of Microelectromechanical Systems, 12*(6), 855-862.

[14] Ceyssens, F. Chaudhri B. P., Van Hoof C., Puers R. (2013). Fabrication process for tall, sharp, hollow, high aspect ratio polymer microneedles on a platform. *Journal of Micromechanics and Microengineering,* 23, 075023.

[15] Wang, P. C., Wester, B. A., Rajaraman, S., Paik, S. J., Kim, S. H., & Allen, M. G. (2009, September). Hollow polymer microneedle array fabricated by photolithography process combined with micromolding technique. In*Engineering in Medicine and Biology Society, 2009. EMBC 2009. Annual International Conference of the IEEE* (pp. 7026-7029). IEEE.

[16] Davis, S. P., Landis, B. J., Adams, Z. H., Allen, M. G., & Prausnitz, M. R. (2004). Insertion of microneedles into skin: measurement and prediction of insertion force and needle fracture force. *Journal of Biomechanics*, *37*(8), 1155-1163.

[17] Shikida, M., Hasada, T., & Sato, K. (2006). Fabrication of a hollow needle structure by dicing, wet etching and metal deposition. *Journal of Micromechanics and Microengineering*, *16*(10), 2230.

[18] Calnan, C. D. (1956). Nickel dermatitis*. *British Journal of Dermatology*, *68*(7-8), 229-236.

[19] Schlesinger, M., & Paunovic, M. (Eds.). (2011). *Modern electroplating* (Vol. 55). John Wiley & Sons.

[20] Uda, T., Okabe, T. H., Waseda, Y., & Awakura, Y. (2006). Electroplating of titanium on iron by galvanic contact deposition in NaCl–$TiCl_2$ molten salt. *Science and Technology of Advanced Materials*, *7*(6), 490-495.

[21] Philippe, L., Heiss, C., & Michler, J. (2008). Electroplating of stainless steel. *Chemistry of Materials*, *20*(10), 3377-3384.

[22] Izaki, M. (2011). Electrodeposition of iron and iron alloys. *Modern Electroplating*,*4*, 461-481.

[23] Moravej, M., Prima, F., Fiset, M., & Mantovani, D. (2010). Electroformed iron as new biomaterial for degradable stents: Development process and structure–properties relationship. *Acta Biomaterialia*, *6*(5), 1726-1735.

[24] Peuster, M., Hesse, C., Schloo, T., Fink, C., Beerbaum, P., & von Schnakenburg, C. (2006). Long-term biocompatibility of a corrodible peripheral iron stent in the porcine descending aorta. *Biomaterials*, *27*(28), 4955-4962.

[25] Moravej, M., Purnama, A., Fiset, M., Couet, J., & Mantovani, D. (2010). Electroformed pure iron as a new biomaterial for degradable stents:< i> In vitro</i> degradation and preliminary cell viability studies. *Acta Biomaterialia*, *6*(5), 1843-1851.

[26] Myung, N. V., Park, D. Y., Urgiles, D. E., & George, T. (2004). Electroformed iron and FeCo alloy. *Electrochimica Acta*, *49*(25), 4397-4404.

[27] Moravej, M., Amira, S., Prima, F., Rahem, A., Fiset, M., & Mantovani, D. (2011). Effect of electrodeposition current density on the microstructure and the degradation of electroformed iron for degradable stents. *Materials Science and Engineering: B*, *176*(20), 1812-1822.

[28] Doraiswamy, A., Jin, C., Narayan, R. J., Mageswaran, P., Mente, P., Modi, R., ... & Chichkov, B. (2006). Two photon induced polymerization of organic–inorganic hybrid biomaterials for microstructured medical devices. *Acta Biomaterialia*, *2*(3), 267-275.

[29] Yoshimura, S., Yoshihara, S., Shirakashi, T., & Sato, E. (1994). Preferred orientation and morphology of electrodeposited iron from iron (II) chloride solution. *Electrochimica Acta*, *39*(4), 589-595.

[30] Myung, N. V., Park, D. Y., Urgiles, D. E., & George, T. (2004). Electroformed iron and FeCo alloy. *Electrochimica acta*, *49*(25), 4397-4404.

[31] Brongersma, S. H., Kerr, E., Vervoort, I., Saerens, A., & Maex, K. (2002). Grain growth, stress, and impurities in electroplated copper. *Journal of Materials Research*, *17*(03), 582-589.

[32] Miller, P. R., Gittard, S. D., Edwards, T. L., Lopez, D. M., Xiao, X., Wheeler, D. R., ... & Narayan, R. J. (2011). Integrated carbon fiber electrodes within hollow polymer microneedles for transdermal electrochemical sensing. *Biomicrofluidics*, *5*(1), 013415.

[33] Verbaan, F. J., Bal, S. M., Van den Berg, D. J., Dijksman, J. A., Van Hecke, M., Verpoorten, H., ... & Bouwstra, J. A. (2008). Improved piercing of microneedle arrays in dermatomed human skin by an impact insertion method. *Journal of Controlled Release*, *128*(1), 80-88.

Chapter 6 Flexible Hollow Microneedle Arrays Fabricated with an Electromolding Method

Philip R Miller[1,2], Matt Mormon[1], Ryan D Boehm[2], Igal Brener[1], Roger J Narayan[2*], Ronen Polsky[1*]

[1]Sandia National Laboratories, Department of Biosensors and Nanomaterials, Albuquerque, New Mexico 87185, USA

[2]Joint Department of Biomedical Engineering, University of North Carolina and North Carolina State University, Raleigh, North Carolina 27695-7115, USA

Abstract

A novel fabrication method was developed for the creation of flexible hollow metal microneedle arrays made using reusable molds. In this method, micromolding and electroplating were utilized with a process we refer to as electromolding. Master structures were made with two-photon polymerization utilizing laser direct write then molded with conventional micromolding techniques. Molds were coated with a seed layer of Ti/Au then electroplated into for creation of the hollow microneedles. The method was investigated for creating hollow microneedles with an offset bore, mold replication and reusability, flexibility of the microneedle substrate, microneedle fracture strength, and insertion into ex-vivo porcine skin.

Introduction

Wearable sensors have gone from a next generation idea to commercially available devices for monitoring everything from sleep patterns to daily activity.[1,2] While these devices are largely limited to measuring vital signs, microneedles are an emerging wearable technology for analyzing physiological changes within the body, both locally and systemically.[3,4] Microneedle technology was initially developed for transdermal drug delivery but is becoming an attractive means for transdermal sensing due to its unique ability to acquire interstitial fluid without imposing significant pain to the user.[5,6] A variety of microneedle designs have been used for sensing applications however hollow microneedles overcome limitations of fouling that are potentially seen with solid microneedles and have been incorporated into a device to continuously measure glucose in human subjects for 72 hours.[7,8] While hollow microneedles offer unique benefits compared to other microneedles types for sensing applications they pose a greater fabrication challenge than solid microneedles, which are easier to fabricate due to their simpler geometry, and more sophisticated systems are necessary for creation of hollow microneedles thus driving up their cost. Recently, Normal et al suggested a set of parameters for making hollow microneedles that accounts for their fabrication challenges, cost of materials and equipment, and required microneedle geometry for suitable performance.[9] Additionally, as described by Norman et al and others, not all hollow microneedles designs perform equally and improved performance has been shown with having the bore off-set from the tip, meaning bore placement not being concentric about the tip, thus adding additional fabrication challenges.[10] In his report a technique for single hollow microneedle fabrication was developed but arrays of hollow microneedles are required for sensing applications due to lack of fluid extraction with smaller array sizes.[11] In addition to the proposed hollow microneedle requirements, we envision that hollow

microneedles arrays must have some degree of flexibility in order to conform to the surface of the skin and have a suitable level of biocompatibility due the in intended duration these devices will reside in the skin.

A variety of techniques exist for making hollow microneedle arrays from a range of different materials, each with its own inherent strengths and weaknesses. The first hollow microneedle arrays were made from standard silicon microfabrication techniques, which also pioneered the first solid microneedles, with either an in-plane or out of place configuration.[12,13,14] While these methods created microneedles with an offset bore placement the resulting structures were brittle, expensive, and have some limitations of control over the desired geometry. Since that time a few other stand-alone fabrication methods were used for microneedle fabrication. Microstereolithography was used for creation of hollow microneedles and dozens of arrays could be fabricated within a single batch, however resolution and material compatibility limit this technique.[15] Recently, Yung et al used micro-injection molding for creation of hollow microneedles arrays made from polymer (POM).[16] Injection molding is an industrial fabrication technique for scalable production of parts however tips sharpness and control of microneedle geometry still limits this fabrication system. Due to the limitations of these techniques multiple groups have sought new methods for making hollow microneedles using a combination of fabrication methods. For instance, Davis et al created hollow microneedles via electroplating into polymer substrates containing conical voids made via laser micromachining.[17] Upon selectively dissolving the polymer, arrays of metal hollow microneedles were used to deliver insulin to diabetic rats. Other groups have used a similar technique for electroplating into predefined voids or over solid microneedles that were later cut for creation of the bore.[18,19] While these techniques all create hollow microneedles they're limited in their ability to create an off-set bore with a flexible substrate.

Due to the limitations with fabricating hollow microneedles some groups have used solid microneedles made from hydrogels in order to extract fluid for analysis from the skin of both rats and humans.[20,21] These devices are novel in that they don't require a particular geometry to function since the material naturally wicks fluid upon contact. The hydrogel offer a high degree of biocompatibility and their strength can be tailored based on the polymer precursors to improve insertion into skin however they're currently limited in the volume of fluid they can extract from the skin and sensor integration.

A few groups have also explored a molding methodology for creation of hollow microneedles that lend towards scalability and facile production. Wang et al created arrays of hollow microneedles by UV curing SU-8 into predefined PDMS molds for creation syringe style needles.[22] The tips of the molds were slanted to produce a sharp tip and multiple masks were used to selectively fabricate the bore. Arrays were inserted into ex vivo porcine skin and were capable of injecting a dye into the skin. In another novel approach Matteucci et al used a technique for making hollow polymeric microneedles with offset bores via a molding method that allowed for the master to be reused up to 10 times.[23,24] In this technique inverse microneedle masters were made with a pillar rising from within each microneedle mold. When the molds were filled with a PMMA-based copolymer the pillars blocked a portion of the mold, which formed the microneedle bore however a sanding step was needed to remove excess material to form a continuous lumen. While this technique provided a novel methodology for hollow microneedle fabrication insertion tests, mechanical characterization, flexibility of the array, and biocompatibility have yet to be performed. Based on the limitations of previous techniques our group investigated a method for fabricating hollow metal microneedle arrays on a flexible substrate from reusable masters and reusable molds with an offset bore.

Materials and Methods

Master Structure Fabrication:

Master structures were designed in Solidworks© as a four sided-pyramid measuring 550um in height and 250um in its base. An inward facing ledge was placed on one face of the pyramid shaped microneedles for creation of the microneedle bore. Ledges sizes were adjusted in terms of their depth within in the microneedle and ranged from 20um to 60um. The upward facing wall of the 20um ledge was perpendicular to the microneedle substrate and ledges smaller than this were expected to not sufficiently block the initial seed layer for creation of the bore so they were not tested. Dimensions of the ledge cutout were held at 60um (width) and 50um (height) while the ledge depth was adjusted. Master structures were fabricated using a two-photon lithography system utilizing laser direct write.[26,27] Solidworks© files were converted to STL files and sliced with a 10um step height and 1.5um raster spacing. A Ti-Sapphire laser was used to initiate the two-photon polymerization process and masters were fabricated using laser write speed of 100um/sec and a power of 370mW (measured at the output of laser). The laser operated at 800nm, 76MHz, and 150fs pulse duration. Masters were fabricated onto polymer substrates made via a microstereolithography system as previously described and both masters and their substrates were made from a commercially available class 2a biocompatible UV curable polymer (Eshell 300).[25] Fabricated structures were developed in ethanol and post-cured with a UV lamp to ensure complete polymerization. Master structures were then coated with 100nm of gold using a SEM sputter coater depositing at ~0.1nm/sec.

Master Micromolding:

Master structures were micromolded with PDMS by using Sylgard 184 at a ratio of 10:1 or 20:1. Structures were placed in a prior to curing of the PDMS such that air bubbles

were removed from the face and ledge of the microneedle masters and then were baked in an oven at 100F to cure the PDMS.

Electroforming:

PDMS molds were coated with a metal multi-layer of 10nm titanium and 100nm gold using an e-beam evaporator to create the initial seed layer. Following seed layer deposition metal coated PDMS molds were electroplated using pulsed chronoamperometry with a VoltaLab potentiostat against an Ag/AgCl reference and Pt wire counter electrode. Either nickel or iron baths were used to electroform the microneedles. Contents for the nickel bath were 300 g/L nickel sulfamate, 11g/L nickel chloride, 30g/L boric acid, and 4g/L SDS and were heated to 37^{o}C while stirring. Contents for the iron bath were 120g/L iron sulfate, 45g/L boric acid, and 0.5g/L ascorbic acid and were kept at 25^{o}C while stirring. Baths were remade for each sample. Both constant plating and pulse plating methods were explored for the electroforming process. Prior to the deposition of the bulk of the metal film an initial plating process took place for 15min at -1.0V. The sample was then spun such that the electrical connector from the potentiostat was connected to the thicker layer of nickel, which created a more robust connection. Constant plating was performed by applying a potential of -1000mV for between 2 and 8 hours. For pulsed plating, potentials were cycled between -1.0V for 3 seconds and -0.5V for 6 seconds for 4000-10000 repetitions. Electroforms were removed from PDMS molds by hand.

Insertion Test:

Porcine skin was used for microneedle penetration studies and tissue samples were acquired from a local abattoir. The tissue samples were acquired immediately following animal sacrifice and stored at -20^{o}C until use. The porcine skin was thawed in 1X

phosphate-buffered saline and then shaved. Hollow metal microneedle arrays were attached to a microfluidic chip made with a previously described technique. [26] Microneedles were applied to the porcine skin with the Medtronic MiniMed Quick-Serter® at a rate of 0.5m/s.[27] Following insertion into the skin, Trypan Blue was injected into the tissue by hand application from a syringe and PEEK tube attachment on the microfluidic chip. The tissue samples were cleaned with an ethanol wipe and imaged using a camera.

Mechanical Testing**:**

The fracture forces for deformation of the hollow metal microneedles were tested using the BOSE Electroforce® 3100 mechanical testing instrument (Bose Corporation, Framingham, MA) with a 20 N load cell. Compressions were run at 0.1mm/s; microneedles were pressed against a metal platen while monitoring the change in force and the displacement upon impact.

SEM/EDX Imaging:

Hollow metal microneedles were imaged using a Carl Zeiss Supra™ 55VP SEM at 10 and 15kV and a working distance of 8.5 mm. All samples were coated with a thin layer of platinum prior to imaging. EDX was used to determine the elemental composition of the deposited metals.

Digital Imaging:

Optical images of hollow microneedles, molds and cross-sections of molds, and master structures were taken with a Keyence Digital Microscope. All other optical images were taken with a digital camera.

Results and Discussion

Two-photon polymerization utilizing laser direct write was created to improve upon previous fabrication systems by allowing the polymerization process to happen within the resin as opposed to at the surface of the resin as seen in traditional UV-based stereolithography systems.[28] The multi-photon process lends towards high spatial resolution and can create structures with sub 100nm resolution.[29] This technique has been used by our group for the creation of hollow microneedles with well-defined control of microneedle geometry however scaling this system for fabrication of large arrays of microneedles is troublesome.[30] The main issues facing this technique is fabrication time due to the single focal spot, alignment between bores in the substrate and bores of the microneedles, and yield of the successfully created microneedles since one poorly produced structure can ruin an entire array. Components such as multi-spot two-photon polymerization have been incorporated into this fabrication technology to increase its scalability, where multiple spots (4 x 4 array) can be fabricated at the same time, however alignment between the substrate and microneedles is still an issue for hollow microneedles.[31,32] These factors influenced a new method to be created for fabrication of arrays of hollow microneedles with the particular features previously listed (e.g. off-set bore, sharp tip). We choose to take advantage of the resolution and feature compatibility of 2PP-LDW to make master structures, which could then be turned into hollow microneedles following a molding step. Our goal was to create a method that was scalable, used biocompatible materials, created microneedles with the desired geometries, and the master structure could be fabricated via other, cheaper fabrication systems thus reducing the overall cost.

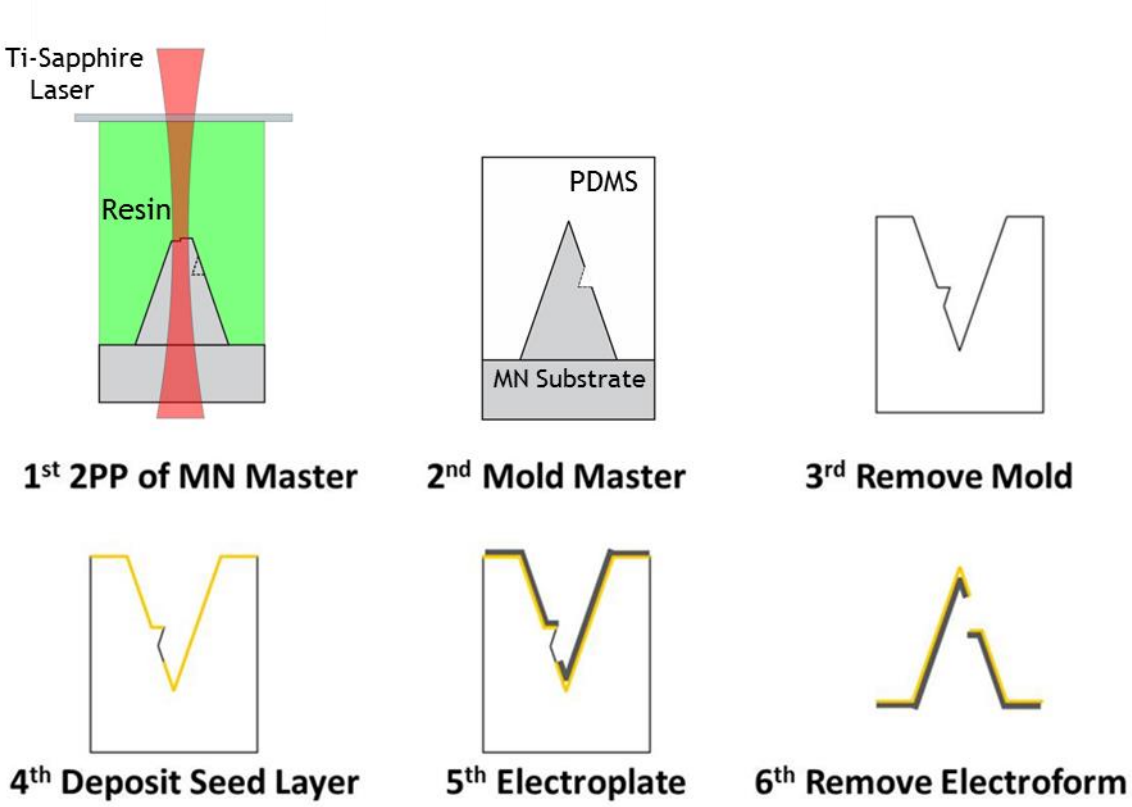

Figure 6-1: Cross-sectional schematic of electromolding process for hollow microneedle fabrication. Microneedle master first created with two-photon polymerization utilizing laser direct write, PDMS micromolding of the master creates the mold, E-beam deposition of seed layer creates conductive coating and void behind inward facing ledge for the hollow microneedle bore, and followed by electroplating and removal from mold.

Kim et al demonstrated a method that contributed to the motivation for this study and showed that replication of high aspect ratio structures could be created via electroplating into PDMS molds.[33] Molds of high aspect ratio structures fabricated with LIGA were made with PDMS and coated with a seed layer then electroplated for creation of the metallic replica. The technique demonstrated a rapid method for mass replication of structures however the approach showcased only uniform structures without selectively placed voids. Additionally, reusability of the molds following the electroplating step was not investigated. We sought to extend this technique for making hollow microneedles and creation of the bore was the first aspect investigated. Figure 6-1 shows a schematic of the

proposed fabrication process, which we refer to as electromolding, using an inward facing ledge for creation of the microneedle bore. Due to the directional nature of evaporative metal deposition Kim et al ensured the side walls of their molds were coated by tilting and rotating the sample during seed layer deposition. We chose to use the directionality of metal evaporation to our advantage and designed features on the microneedle master to either block or catch some portion of the seed layer to create a void in the seed layer for the microneedle bore. A four sided pyramidal microneedle structure was chosen due to the simply geometry amenable to micromolding and the angled walls would be easily coated with the seed layer deposition. Microneedle master designs using vertical sidewalls suffered from inconsistent coating. Two different microneedle master structures were designed; one with an inward facing ledge on one of the pyramidal microneedle faces, designed to block a portion of the seed layer and the second having an outward facing structure, designed to catch some portion of the seed layer (Figure 6-2). After fabricating each of the microneedles it became apparent that the inward facing ledge was a simpler structure to fabricate repeatedly for creating the off-set bore and the outward facing structure didn't provide sharp enough angles to avoid deposition of the seed layer in the void and was a structure that would be very difficult to replicate with another, cheaper fabrication system. Based on these results only the inward facing ledge design was studied.

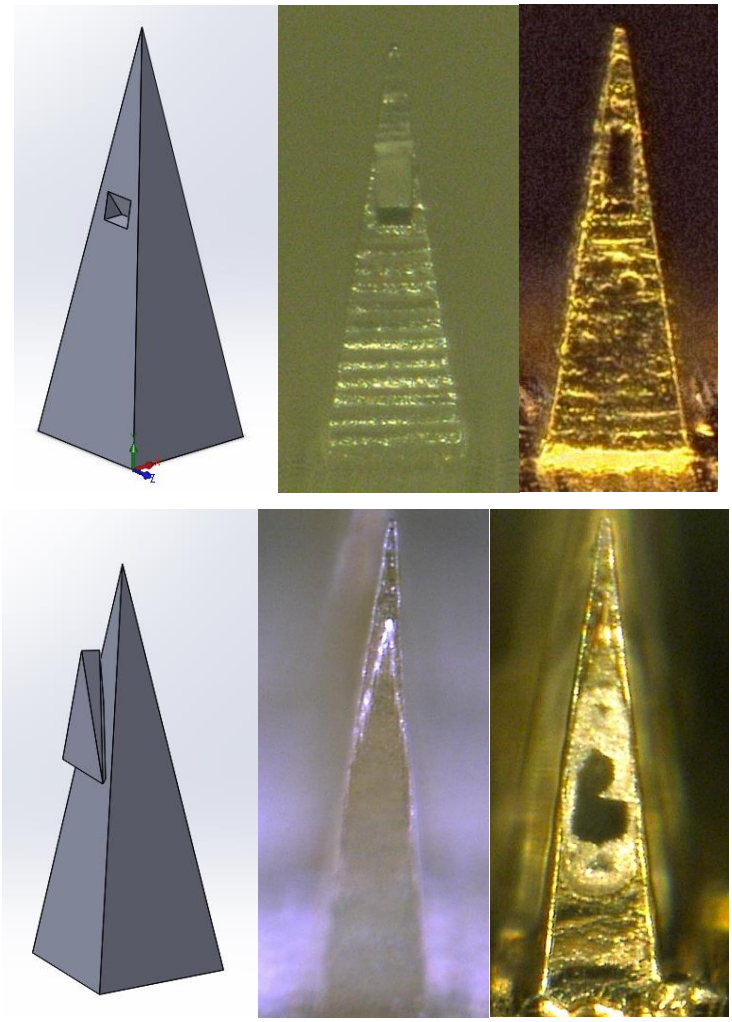

Figure 6-2: Comparison between the two ledge designs (inward and outward facing for the progression from STL design to microneedle master to electroformed hollow microneedle array.

Seed layer material and thickness were then investigated. The Kim et al study used a thick (2um) seed layer of either of Cu or Ti/Au and due to coppers known cytotoxicity Ti/Au was chosen for this study since this layer will primarily be interacting with the dermal tissue during use. PDMS molds were coated with varying thicknesses and 5nm/350nm, 10nm/100nm, , and 15nm/500nm Ti/Au were tested for their ability to remain adherent to the mold, film electrical resistance, and removal from mold post electroplating without tearing off portions of PDMS. Electrical resistance measurements were performed using an Ohm meter across the length of the mold (2cm) and showed no significant difference (10-20

Ohm) in resistance for each of the seed layer thicknesses tested. The 10nm/100nm Ti/Au thickness was chosen to try and reduce the amount of seed layer deposited behind the ledge thus retaining the largest bore size possible. Each of the seed layer thicknesses created uniform metal deposition on the molds and were capable of being removed without destroying the mold or pulling any noticeable portion of PDMS from the mold. Additionally, electroforms stayed adhered to the molds during the plating process and didn't delaminated due to the plating process.

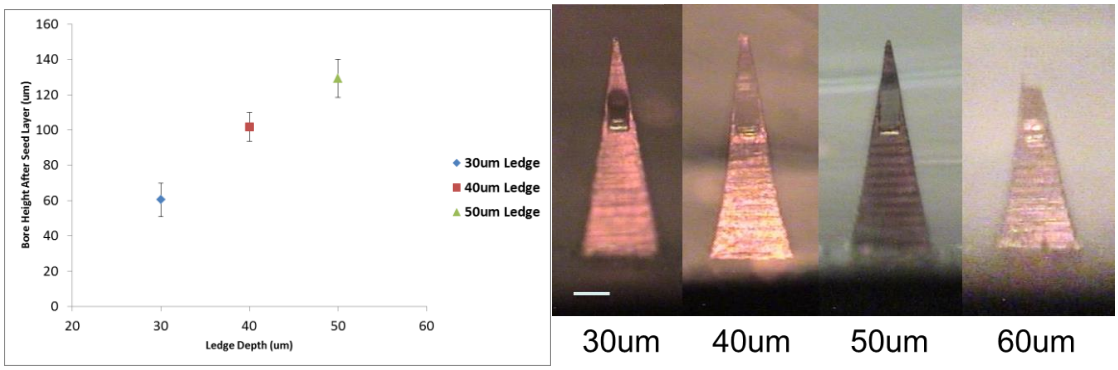

Figure 6-3: Resulting bore height within mold following Ti/Au seed layer deposition with varying ledge sizes (A) and optical images of voids from seed layer within molds (B), scale bar 100um.

During the seed layer thickness experiments inward facing ledges were used with varying ledge depths and were shown to effect the size of the resulting bore. Ledge depths that resulted in perpendicular faces created smaller bores as seen in Figure 6-3 compared to deeper ledges. Since these ledges were not angled back, away from the incoming e-beam seed layer deposition most of the ledge was covered with the seed layer and reduced the size of the microneedle bore. Based on these results we sought to adjust the ledge depth of the inward facing ledge and investigate the resulting seed layer void. Ledge sizes of 30um, 40um, 50um, and 60um were incorporated into master microneedle structures and PDMS micromolded. Figure 6-4 shows optical images taken from within a single microneedle mold detailing the size of each of the ledges. It was noticed that the size

of the microneedle ledges did not exactly reflect the input size of the ledge designed in Solidworks© and the figure shows the relation between input ledge size and resulting mold leg size. In 2PP-LDW, as is with other rapid prototyping techniques; the input size of the structure doesn't always directly reflect size of the fabricated part. In this case we believe that the fabrication parameters are typically optimized for fabrication time and the mechanical shutter can lag behind the path of the beam especially when making small structures as seen with the ledges.

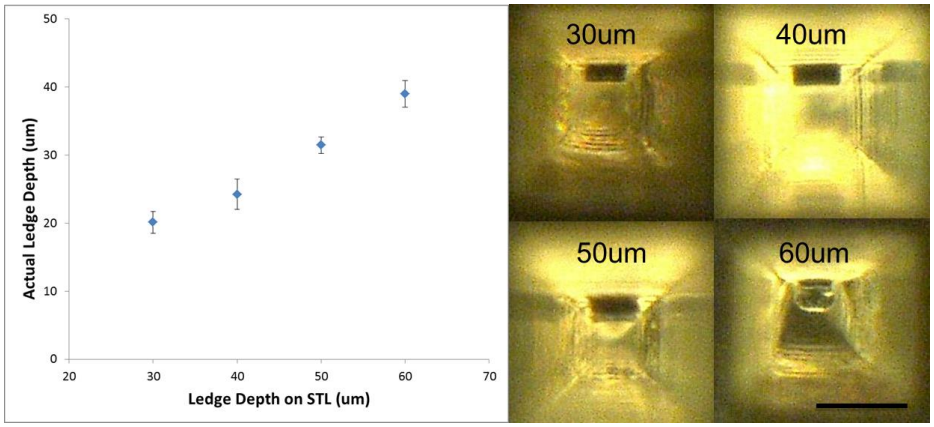

Figure 6-4: Comparison of designed ledge size to actual fabricated ledge size (A) and in-mold images of molds made from microneedle masters (B), scale bar 100um.

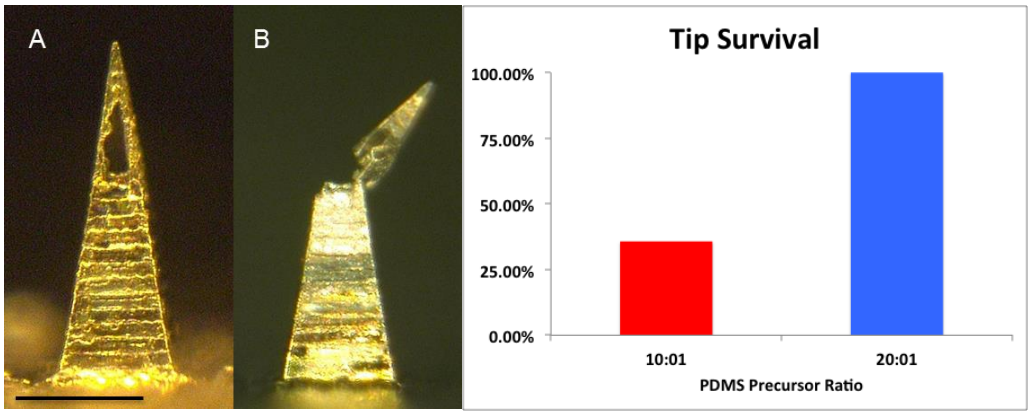

Figure 6-5: Optical image of a hollow microneedle made from a 50um ledge PDMS mold with a ratio of 20:1 PDMS precursor (A) and 10:1 PDMS precursor (B) with details regarding the percentage of microneedle tips that survive the demolding process (C). Scale bar of 250um for image A and B.

Ledge size effect on resulting seed layer void was investigated as seen in Figure 6-3. PDMS molds were created from microneedle masters having each of the bore sizes (30um, 40u 50um, and 60um) and coated with 10nm/100nm Ti/Au. Molds were then cut directly beside the microneedle mold on the ledge side and were imaged to determine the effect of the ledge size on resulting seed layer void. As anticipated increasing the ledge size created larger voids however the 60um ledge had no seed layer deposited on the tip. Upon investigation it was apparent that at this size the microneedle could no longer withstand solvent developing following 2PP-LDW fabrication and caused the microneedle master the bend at the ledge due to the lack of supporting polymer. This ledge size was not investigated following this result. Each ledge size resulted in a consistent void with bore void heights ranging from 60um to 130um depending on the ledge size. The 30um, 40um, and 50um ledge size were studied moving forward due to the size of their resulting void.

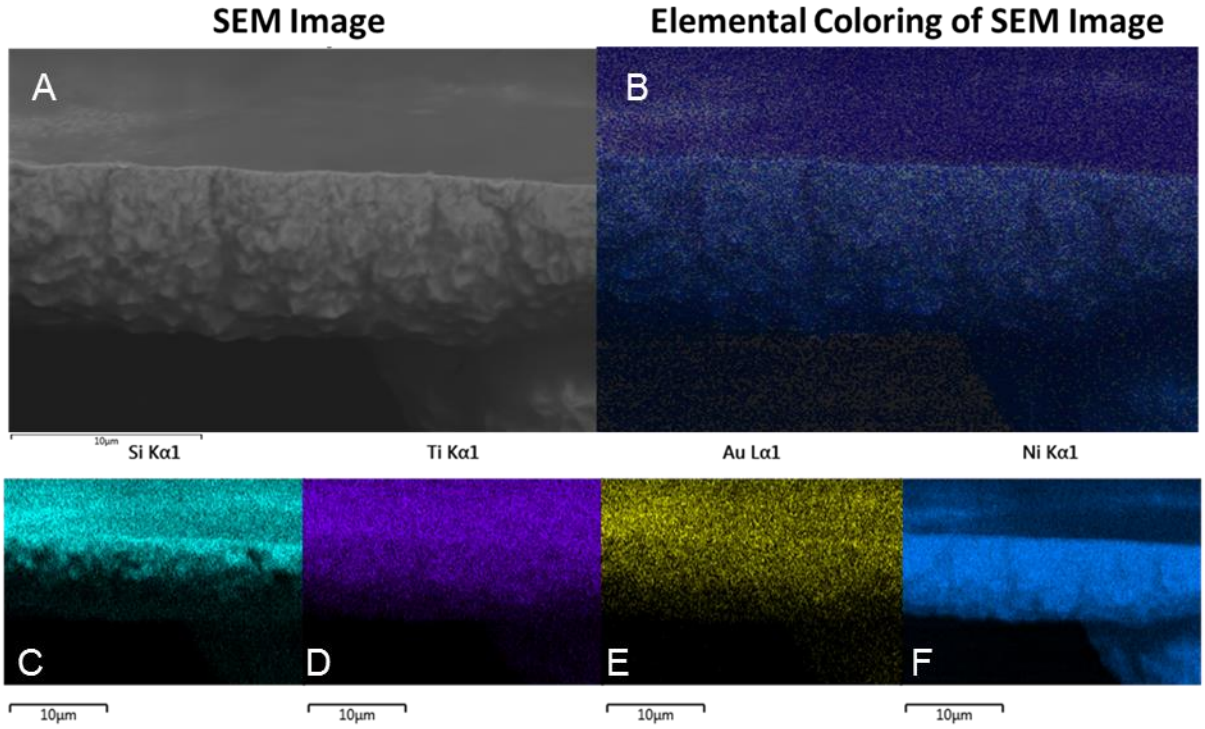

Figure 6-6: SEM images electroformed hollow microneedle bore edge of (A) with elemental coloring overlay (B) and each individual element characterized (C-F).

It became apparent during fabrication of the hollow microneedles that some of the microneedle tips were not surviving the mold removal process. Upon imaging within the molds following the electroplating step metal was noticed at the tip of the mold indicating that either a suitable amount of metal was not deposited at that area or something was causing tip to shear from the rest of the microneedle. Two aspects were investigated to improve tip survivability and first the PDMS mold precursor ratio was adjusted to create a more elastic mold. Previous groups have studied the effect of adjusting the ratio of cross-linker to polymer precursor on resulting Young's Modulus and Brown et al showed adjusting the ratio from 10:1 to 50:1 the modulus was reduced from 1783kPa to 48 kPa.[34] We studied cross-linker to polymer precursor ratios of 10:1, 20:1, 30:1, and 50:1. Molds resulting from the 50:1 PDMS precursor ratio did not survive removal from the laminate molds they were cast in and tore into pieces upon removal. Molds with 30:1 ratio were capable of surviving the casting removal process however were difficult to handle and caused island formation of the seed layer due to their elasticity which made establishing an electrical connection difficult. Compared to the 10:1 PDMS mold ratio the 20:1 mold ratio were elastic however not too deformable to effect the electrical stability of the seed layer. Tip survival, meaning intact tip upon mold removal, was compared for each of the molds and the 20:1 mold resulted in no tip deformation when 50um ledges were electroplated for 6000 cycles of 3 second pulse of -0.1V followed by 6 second pulse of -0.5V in a heated nickel bath against a Ag/AgCl reference and Pt wire counter electrode as seen in Figure 6-5. The second method to improve tip survivability was adjusting the electroplating parameters. Initial tests used constant potential plating to form the hollow microneedles. While this technique was effective for forming the microneedles overplating was noticed at the edges of the ledge and mold, which in some cases caused closure of the bore from within the mold. A pulsed electroplating technique was investigated to improve distribution of plating

salts across the surface of the microneedle mold since points and edges preferentially plate and result in non-uniform surfaces. Additionally, we believe that due to the depth of the microneedle tips metal salts replenish slower compared to the substrate or portions of the microneedle mold towards the base. Pulsed electroplating techniques cycle the reducing potential or current between values that deposit the metal and one that does not so as to allow the redistribution of ions to take place across the sample.[35] Comparison between constant plating at -1.0V and pulsing between -1.0V and -0.5V (a potential not capable of electroplating either bath) resulted in less over deposition of hollow microneedles and contributed to stronger tips due to the lack of tip deformation using this technique. Additionally, resulting current densities during pulsed deposition (-25mA/cm^2) were comparable previous reports that showed less residual stress within pulsed electroplated films compared to constant plating conditions at the same current density.[36] A short series of pulses from a deposition scan can be seen in Figure 6-11and shows uniform pulse generation and stability between the on and off pulses indicating optimizes pulse parameters.

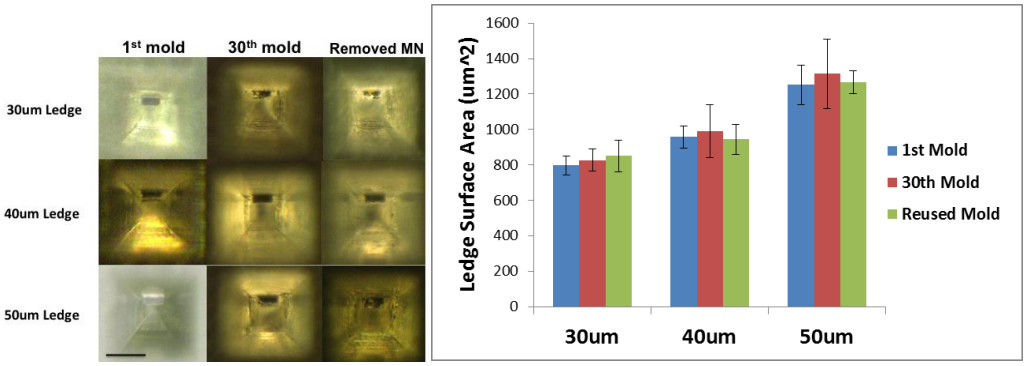

Figure 6-7: Optical images from within microneedle molds for the 30um, 40um, and 50um ledge size for the first mold, thirtieth mold, and molds that had the microneedle removed (top). All images correspond to the 100um scale bar. Comparison of ledge surface area for each ledge size for the first month, thirtieth mold, and a removed microneedle (bottom).

As we began creating hollow microneedles using the electromolding method it was

noticed that the molds seemed unaffected by the process and experiments were performed to determine whether they were damaged at all. Upon removal of the a microneedle from the mold SEM and EDX color mapping was used to determine whether any portion of the PDMS mold was removed and stayed on the microneedle. Figure 6-6 shows cross-sectional SEM images and false colored elemental images from the bore of an electromolded hollow microneedle. Cross-sections were imaged to estimate layer thickness of each of the deposited coatings (titanium, gold, nickel) and any residual material (silicon) left from the molding process. EDX elemental mapping showed the three distinct metal layers from the seed layer and electroplating process and a very thin layer of silicon on the surface of the Ti layer resulting from contact with the mold. While this imaging technique is not designed to be quantitative the color intensity of the silicon layer was comparable to that of the titanium layer, which was deposited at 10nm. This result suggests that removal of the microneedles from the mold doesn't significantly destroy the molds and motivated experiments on reusing the molds. Initial experiments performed with previously used molds resulted in hollow microneedles that mimicked the first batch made and further experiments are needed to determine the number of times the molds can be reused before producing unacceptable microneedles.

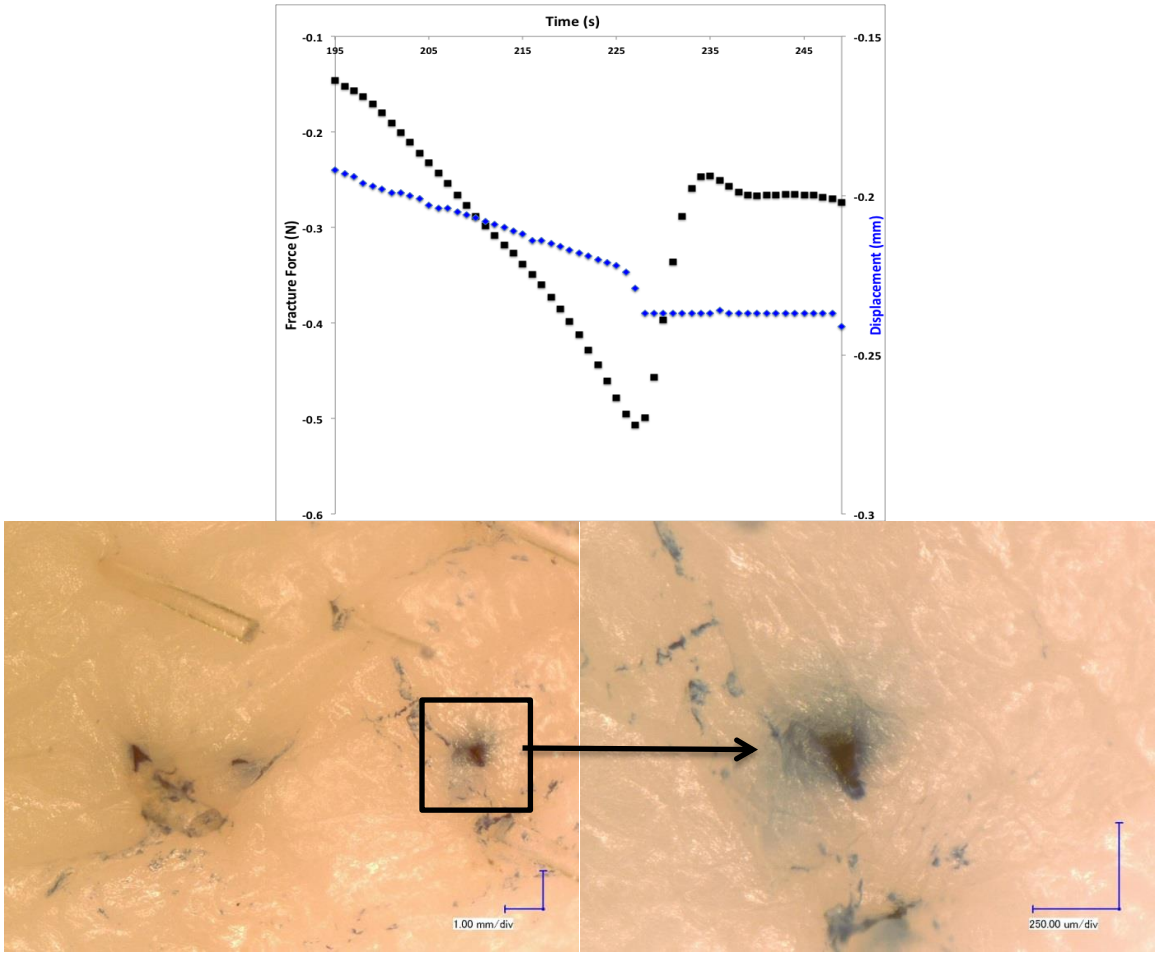

Figure 6-8: Mechanical compression testing of hollow microneedles made via electroforming (top) and optical images of trypan blue injections into ex-vivo porcine skin with electromolded hollow microneedle array.

Experiments were performed to determine what effects if any happens to the mold following reuse and after numerous replications of the master microneedle structures. Optical images of the ledge within the mold were taken after the initial mold, after microneedle removal, and following 30 replications of the master as seen in Figure 6-7. Ledge integrity was investigated due to its role in creation of the microneedle bore and once the ledge loses its structure the mold no longer becomes effective in producing microneedles with the required features. Using each of the ledge sizes (30um, 40um, 50um) molds were imaged before and after electromolding and the no damage was noticed to the

ledge of the mold following microneedle removal. Each ledge size had a comparable degree of surface area, measured using the Keyence Microscope measurement tool, from the first mold to the thirtieth and after electroform removal indicating a potential high degree of scalability for this technique.

Electromolded hollow microneedles were tested in terms of the mechanical properties and their functionality in penetrating porcine skin. Compression tests were performed using the BOSE Electroforce 3100 system by compressing a microneedle while monitoring both the displacement of the platens and the resulting force. Microneedles were compressed using a previous method and resulted in consistent fracture forces and average fracture of 0.58N for microneedles made with 6000 pulses between -1.0V for 3 seconds and -0.5V for 6 seconds (Figure 6-8). Functionality testing of the microneedles was performed by insertion and injection experiments with *ex vivo* porcine skin. Hollow microneedle arrays were attached to a laminate microfluidic chip and were inserted into the porcine skin using a controlled velocity of ~0.5m/s by the Medtronic MiniMed Quick-Serter. Once in the skin trypan blue with injected via hand pressure applied to a syringe connected to the microfluidic chip. Porcine skin samples were cleaned with an alcohol swipe and imaged for their insertion sites as seen in Figure 6-8. In the image shown a 3x1 microneedle array was applied to the skin with injection sites seen for each microneedle. Upon removal from the skin microneedles remained intact and were capable of multiple injections prior to tip deformation.

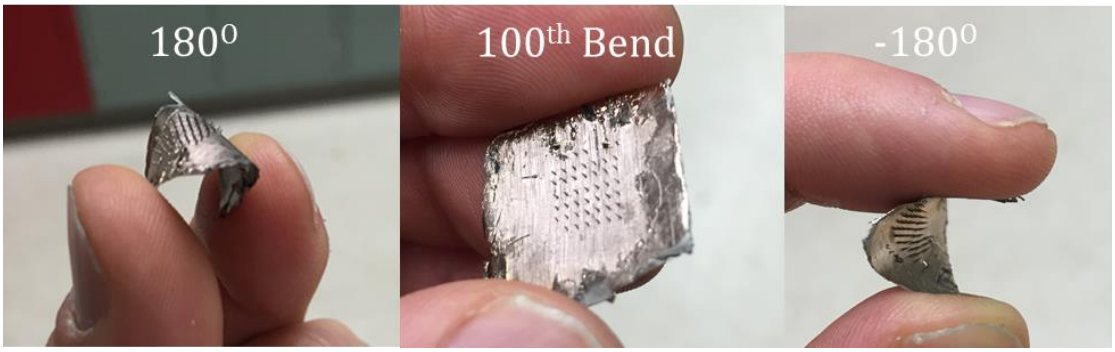

Figure 6-9: Optical images detailing the flexibility of the electroformed parts by flexing the microneedle substrate in multiple directions and after 100 bends in each of the directions shown. Microneedle array substrates are 20mm x 20mm.

It anticipated that a flexible substrate would benefit hollow microneedle functionality for sensing applications due to the elastic nature of the skin and dynamic movements seen over the course of a day by the end used. Due to these facts electromolded hollow microneedle arrays were tested for their ability to withstand multiple types of deformation that may be seen during the course of use. As seen in Figure 6-9 arrays were bent such edges of the microneedle substrate were bent over the microneedles or under them via hand bending. Electroformed microneedle arrays were capable of deforming with the direction of the bend without fracturing or tearing of the microneedles or their substrate and following these movements the array returned to its original shape even after 100 bends in each direction tested. These results indicate that the metal multilayer substrate provides a strong substrate for the microneedle array while offering a degree of flexibility that may be beneficially to use during dynamic movements.

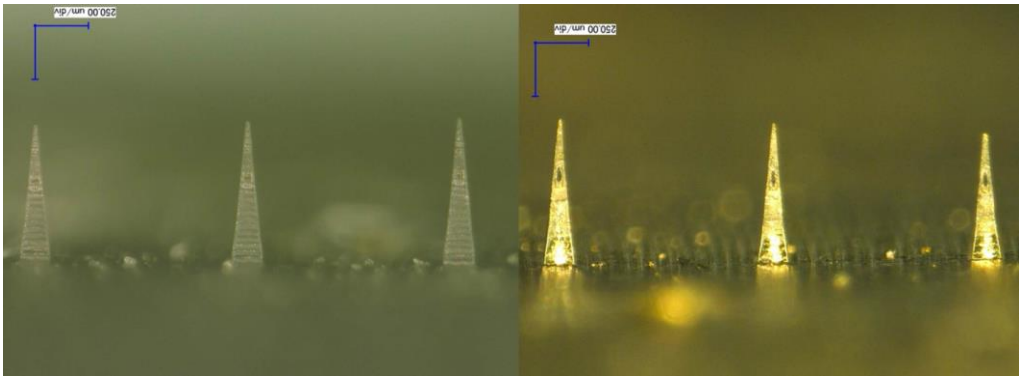

Figure 6-10: Optical images of an array microneedle master structures (left) and electromolded microneedles made using a perpendicular ledge.

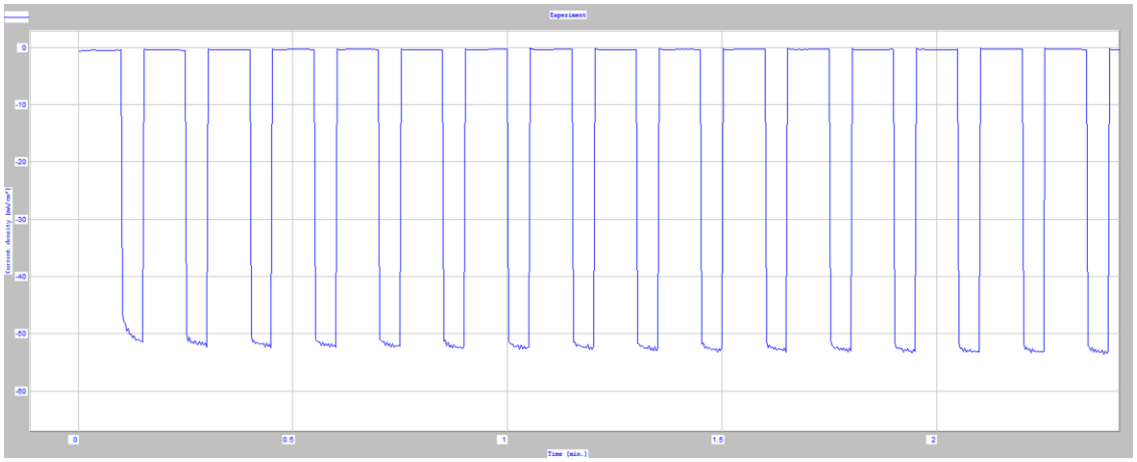

Figure 6-11: Representative electrochemical profile of pulsed electrodeposition over a short number of pulses (16) of nickel onto microneedle molds.

Conclusion

A novel fabrication method was presented that created flexible hollow microneedle arrays from a reusable master and reusable molds. Two-photon polymerization utilizing laser direct write was used for creation of microneedle master structures. Molds were made from master structures and electroplated into for formation of the hollow microneedles. Features used for creation of the microneedle bore were investigated for the type of ledge structure used, their ability to be molded, and size of resulting seed layer void. Molds were capable of being reused, molded up to thirty times without damaging, and not losing significant portions of material when microneedles were removed. Electroformed microneedles were tested their tip fracture strength and for delivery into ex vivo porcine skin. The electroforming method presented showcases a scalable method for creation of flexible hollow microneedle arrays.

References

[1] Takacs, J., Pollock, C. L., Guenther, J. R., Bahar, M., Napier, C., & Hunt, M. A. (2014). Validation of the Fitbit One activity monitor device during treadmill walking. *Journal of Science and Medicine in Sport*, *17*(5), 496-500.

[2] Takacs, J., Pollock, C. L., Guenther, J. R., Bahar, M., Napier, C., & Hunt, M. A. (2014). Validation of the Fitbit One activity monitor device during treadmill walking. *Journal of Science and Medicine in Sport*, *17*(5), 496-500.

[3] Keum, D. H., Jung, H. S., Wang, T., Shin, M. H., Kim, Y. E., Kim, K. H., ... & Hahn, S. K. (2015). Microneedle Biosensor for Real-Time Electrical Detection of Nitric Oxide for In Situ Cancer Diagnosis During Endomicroscopy. *Advanced healthcare materials*.

[4] Our microneedle sensor review

[5] Kim, Y. C., Park, J. H., & Prausnitz, M. R. (2012). Microneedles for drug and vaccine delivery. *Advanced drug delivery reviews*, *64*(14), 1547-1568.

[6] El-Laboudi, A., Oliver, N. S., Cass, A., & Johnston, D. (2013). Use of microneedle array devices for continuous glucose monitoring: a review.*Diabetes technology & therapeutics*, *15*(1), 101-115.

[7] Invernale, M. A., Tang, B. C., York, R. L., Le, L., Hou, D. Y., & Anderson, D. G. (2014). Microneedle Electrodes Toward an Amperometric Glucose-Sensing Smart Patch. *Advanced healthcare materials*, *3*(3), 338-342.

[8] Jina, A., Tierney, M. J., Tamada, J. A., McGill, S., Desai, S., Chua, B., ... & Christiansen, M. (2014). Design, Development, and Evaluation of a Novel Microneedle Array-based Continuous Glucose Monitor. *Journal of diabetes science and technology*, *8*(3), 483-487.

[9] Norman, J. J., Choi, S. O., Tong, N. T., Aiyar, A. R., Patel, S. R., Prausnitz, M. R., & Allen, M. G. (2013). Hollow microneedles for intradermal injection fabricated by sacrificial micromolding and selective electrodeposition.*Biomedical microdevices*, *15*(2), 203-210.

[10] Mukerjee, E. V., Collins, S. D., Isseroff, R. R., & Smith, R. L. (2004). Microneedle array for transdermal biological fluid extraction and in situ analysis.*Sensors and Actuators A: Physical*, *114*(2), 267-275.

[11] Zimmermann, S., Fienbork, D., Stoeber, B., Flounders, A. W., & Liepmann, D. (2003, June). A microneedle-based glucose monitor: fabricated on a wafer-level using in-device enzyme immobilization. In *TRANSDUCERS, Solid-State Sensors, Actuators and Microsystems, 12th International Conference on, 2003*(Vol. 1, pp. 99-102). IEEE.

[12] Gardeniers, H. J., Luttge, R., Berenschot, E. J., De Boer, M. J., Yeshurun, S. Y., Hefetz, M., ... & van den Berg, A. (2003). Silicon micromachined hollow microneedles for transdermal liquid transport. *Microelectromechanical Systems, Journal of*, *12*(6), 855-862.

[13] Paik, S. J., Byun, S., Lim, J. M., Park, Y., Lee, A., Chung, S., ... & Chun, K. (2004). In-plane single-crystal-silicon microneedles for minimally invasive microfluid systems. *Sensors and Actuators A: Physical*, *114*(2), 276-284.

[14] Henry, S., McAllister, D. V., Allen, M. G., & Prausnitz, M. R. (1998). Microfabricated microneedles: a novel approach to transdermal drug delivery.*Journal of pharmaceutical sciences*, *87*(8), 922-925.

[15] Miller, P. R., Gittard, S. D., Edwards, T. L., Lopez, D. M., Xiao, X., Wheeler, D. R., ... & Narayan, R. J. (2011). Integrated carbon fiber electrodes within hollow polymer microneedles for transdermal electrochemical sensing. *Biomicrofluidics*, *5*(1), 013415.

[16] Yung, K. L., Xu, Y., Kang, C., Liu, H., Tam, K. F., Ko, S. M., ... & Lee, T. M. (2012). Sharp tipped plastic hollow microneedle array by microinjection moulding. *Journal of Micromechanics and Microengineering*, *22*(1), 015016.

[17] Davis, S. P., Martanto, W., Allen, M. G., & Prausnitz, M. R. (2005). Hollow metal microneedles for insulin delivery to diabetic rats. *Biomedical Engineering, IEEE Transactions on*, *52*(5), 909-915.

[18] Kim, K., Park, D. S., Lu, H. M., Che, W., Kim, K., Lee, J. B., & Ahn, C. H. (2004). A tapered hollow metallic microneedle array using backside exposure of SU-8. *Journal of Micromechanics and Microengineering*, *14*(4), 597.

[19] Lee, K., Lee, H. C., Lee, D. S., & Jung, H. (2010). Drawing Lithography: Three-Dimensional Fabrication of an Ultrahigh-Aspect-Ratio Microneedle. *Advanced Materials*, *22*(4), 483-486.

[20] Donnelly, R. F., Mooney, K., Mccrudden, M. T., Vicente-Pérez, E. M., Belaid, L., González-Vázquez, P., ... & Woolfson, A. D. (2014). Hydrogel-Forming Microneedles Increase in Volume During Swelling in Skin, but Skin Barrier Function Recovery is Unaffected. *Journal of pharmaceutical sciences*, *103*(5), 1478-1486.

[21]Romanyuk, A. V., Zvezdin, V. N., Samant, P., Grenader, M. I., Zemlyanova, M., & Prausnitz, M. R. (2014). Collection of Analytes from Microneedle Patches.*Analytical chemistry*, *86*(21), 10520-10523.

[22] Wang, P. C., Paik, S. J., Kim, J., Kim, S. H., & Allen, M. G. (2011, January). Hypodermic-needle-like hollow polymer microneedle array using UV lithography into micromolds. In *Micro Electro Mechanical Systems (MEMS), 2011 IEEE 24th International Conference on* (pp. 1039-1042). IEEE.

[23] Perennes, F., Marmiroli, B., Matteucci, M., Tormen, M., Vaccari, L., & Di Fabrizio, E. (2006). Sharp beveled tip hollow microneedle arrays fabricated by LIGA and 3D soft lithography with polyvinyl alcohol. *Journal of Micromechanics and Microengineering*, *16*(3), 473.

[24] Matteucci, M., Fanetti, M. A. T. T. I. A., Casella, M. I. C. H. E. L. E., Gramatica, F., Gavioli, L. U. C. A., Tormen, M., ... & Di Fabrizio, E. N. Z. O. (2009). Poly vinyl alcohol re-usable masters for microneedle replication. *Microelectronic Engineering*, *86*(4), 752-756.

[25]Miller, P. R., Gittard, S. D., Edwards, T. L., Lopez, D. M., Xiao, X., Wheeler, D. R., ... & Narayan, R. J. (2011). Integrated carbon fiber electrodes within hollow polymer microneedles for transdermal electrochemical sensing.*Biomicrofluidics*, *5*(1), 013415.

[26] Miller, P. R., Xiao, X., Brener, I., Burckel, D. B., Narayan, R., & Polsky, R. (2014). Microneedle-Based Transdermal Sensor for On-Chip Potentiometric Determination of K+. *Advanced healthcare materials*, *3*(6), 876-881.

[27] Iron plating manuscript, accepted *Electroanalysis,* publication details coming

[28] Cumpston, B. H., Ananthavel, S. P., Barlow, S., Dyer, D. L., Ehrlich, J. E., Erskine, L. L., ... & Perry, J. W. (1999). Two-photon polymerization initiators for three-dimensional optical data storage and microfabrication. *Nature*, *398*(6722), 51-54.

[29] Wollhofen, R., Katzmann, J., Hrelescu, C., Jacak, J., & Klar, T. A. (2013). 120 nm resolution and 55 nm structure size in STED-lithography. *Optics express*,*21*(9), 10831-10840.

[30] Doraiswamy, A., Jin, C., Narayan, R. J., Mageswaran, P., Mente, P., Modi, R., ... & Chichkov, B. (2006). Two photon induced polymerization of organic–inorganic hybrid biomaterials for microstructured medical devices. *Acta Biomaterialia*, *2*(3), 267-275.

[31] Obata, K., Koch, J., Hinze, U., & Chichkov, B. N. (2010). Multi-focus two-photon polymerization technique based on individually controlled phase modulation.*Optics express*, *18*(16), 17193-17200.

[32] Gittard, S. D., Nguyen, A., Obata, K., Koroleva, A., Narayan, R. J., & Chichkov, B. N. (2011). Fabrication of microscale medical devices by two-photon polymerization with multiple foci via a spatial light modulator. *Biomedical optics express*, *2*(11), 3167-3178.

[33] Kim, K., Park, S., Lee, J. B., Manohara, H., Desta, Y., Murphy, M., & Ahn, C. H. (2002). Rapid replication of polymeric and metallic high aspect ratio microstructures using PDMS and LIGA technology. *Microsystem Technologies*,*9*(1-2), 5-10.

[34] Brown, X. Q., Ookawa, K., & Wong, J. Y. (2005). Evaluation of polydimethylsiloxane scaffolds with physiologically-relevant elastic moduli: interplay of substrate mechanics and surface chemistry effects on vascular smooth muscle cell response. *Biomaterials*, *26*(16), 3123-3129.

[35] Chandrasekar, M. S., & Pushpavanam, M. (2008). Pulse and pulse reverse plating—Conceptual, advantages and applications. *Electrochimica Acta*, *53*(8), 3313-3322.

[36] Hadian, S. E., & Gabe, D. R. (1999). Residual stresses in electrodeposits of nickel and nickel–iron alloys. *Surface and Coatings Technology*, *122*(2), 118-135.

Chapter 7 Development of an Automated Electrochemical Immunoassay for a Wearable Microneedle-Based Diagnostic Device

Philip R Miller[1,2], Matthew Moorman[1], Thayne Edwards[1], Igal Brener[1], Roger J Narayan[2*], Ronen Polsky[1*]

[1]Sandia National Laboratories, Department of Biosensors and Nanomaterials, Albuquerque, New Mexico 87185, USA

[2]Joint Department of Biomedical Engineering, University of North Carolina and North Carolina State University, Raleigh, North Carolina 27695-7115, USA

Abstract

An automated, cartridge-based electrochemical immunoassay was developed for a cardiac biomarker for wearable sensor applications. Commercially available screen printed electrodes were incorporated into a laminate microfluidic chip and a liquid based reagent storage system was investigated. Liquid plug sizes were studied for their ability to separate and store reagents, wash the fluidic channels, and perform the electrochemical assay. A common biomarker was investigated and detected at a clinically relevant concentration and discussions into incorporation of the assay with wearable device were presented.

Introduction

Rapid clinical analysis of biological fluid is a promise of point-of-care (POC) diagnostics and as this technology has matured commercial devices such as Abbott's handheld i-STAT has been developed, which is capable of detecting a myriad of analytes within minutes with the appropriate sensor cartridge.[1] A new subset of POC technology is wearable electronics, which provide "on-body" analysis of health parameters and clinically relevant analytes thus creating unique capabilities not seen in hand-held devices.[2] Additionally, the use of wearable diagnostics is beginning to be seen in commercialized devices such as Dexcom's G4, which can measure glucose for 7 days with a self-implantable subcutaneous sensor.[3] Less invasive wearable devices have been developed by the Rogers group who pioneered a system that mimics the elastic modulus of the epidermis that incorporates sensors for monitoring strain, electrophysiology, and temperature and for energy harvesting and storage when worn on internal organs.[4,5] These wearable sensors (epidermal electronics) work by directly contacting the skin with sensors that are either embedded within the patch or on the skin side of the patch. While these devices have been shown to work in a range of applications and conform beautifully to the skin they are currently restricted to detecting analytes, which diffuse through the skin or can be analyzed via direct contact with the skin.

Microneedles have extensively been shown to improve diffusion across the skin for drug delivery studies and can act as a means to acquire interstitial fluid for sensing applications.[6,7] Previous sensing reports have focused on small biomolecule detection (glucose, lactate, pH, potassium, etc.) with microneedles themselves acting as the sensor/biosensor or using the microneedles to extract fluid for detection elsewhere.[8,9,10] However large biomolecule detection (proteins, viruses, etc.) has only been investigated

with microneedles for off-body detection.[11] In this technique pioneered by the Kendall group, solid microneedles act as a means to both access the interstitial space and selectively adhere and extract analytes via surface functionalization of the microneedles with antibodies. In this approach, solid microneedles are worn for a period of time to allow the analytes to interact with antibodies on the surface of the microneedles that selectively bind to the analytes. Microneedles are then removed and analysis is performed off the body with conventional diagnostic techniques. While these devices are highly capable of acquiring particular analytes, detection is still reliant on off-body analysis, which limits unique applications that wearable diagnostics devices offer such as remote sensing and sense-act-treat systems.

A major challenge of on–body diagnostics is the automation of complex biological assays to provide quantitative clinical data on the user's condition. Biomarkers pose one of the most challenging biomolecules to detect in this manner due to complex assays, which are required for their detection. Traditionally, biomarkers are detected via an immunoassay where multiple antibodies are used to selectively bind to the analyte of interest and produce a signal for detection.[12] Multiple steps are required for these assays with intermediate washing steps thus making the automation of such an assay complicated. Many sophisticated microfluidics chips have been created to perform these assays autonomously however there level of sophistication lends towards costly fabrication and complicated use.[13,14,] Linder et al developed a "plug-in cartridge" device that stored the reagents in a tube spaced by air bubbles or "plugs" and delivered them to a microfluidic chip to perform the assay without the use of valves and with only a syringe pump to control the entire process.[15] This low cost method was capable of diagnosing HIV in a clinical sample in only 13min and air spacers allowed the reagents to be stored in close proximity to each

other without mixing. A similar air spacer method was used for the multiplexed detection of cancer biomarkers PSA and AFP.[16] These markers were detected at a low limit of detection and performed on commonly available screen-printed carbon electrodes. Zhang et al adapted the preloaded reagent method for use with finger pricking for a hand held device for the pretreatment, amplification, and detection of the nucleic acid single nucleotide polymorphism.[17] Using a similar technique we will adapt a reagent flow and storage method to incorporate this detection method for a proposed wearable device for the detection of a relevant cardiac biomarker.

Materials and Methods

Fluidic Chip Fabrication:

Microfluidic chips were made using a laminate chip technology as previously described for integration with microneedles for sensing applications.[18] In this technique alternating layers of PMMA and an adhesive were assembled and cut via a CO_2 laser cutting system. Creation of the fluidic pathways was done via laser cutting patterns into the adhesive layers and creation of the fluidic connections alignment holes was done via laser cutting into the PMMA layers. Patterns for all cuts were designed in CorelDraw before exporting to the laser cutting software. Screen-printed carbon electrodes that had been modified for the flow through immunoassay or for characterization of the fluidic spacer and fluidic pathway design were added to the fluidic chip by cutting a plastic spacer of a similar thickness to the SPCE such that the electrode could fit within one of the layers. O-rings were used as connectors for the fluidic tubing connectors and were sandwiched between layers of the chip such that they were suspended and ensured a leak-free connection. Each of the layers was adding to a jig such that the layers were aligned accurately and were then pressed at 500psi for 2 minutes to ensure a proper seal.

Microneedle Fabrication:

Arrays of hollow microneedles were made via an Electromolding technique as previously described.[19] In this technique microneedles are made via electroplating into a PDMS mold and the mold was created from a master structure made via two-photon polymerization utilizing laser direct write. The microneedle masters were designed in a four-sided pyramidal style with one of the faces having an inward facing ledge, which acted as the means for creation of the hollow bore. Once the master structure was molded a seed layer of 10nm titanium and 100um gold with deposited with e-beam evaporation. The ledge

structure blocked deposition of a portion of the seed layer creating a void in the seed layer, which later created the bore after electroplating. The electroplating process used a watts bath and pulsed between -1.0V for 3 seconds and -0.5V for 6 seconds versus and Ag/AgCl reference and counter electrode for 6000 pulses. Arrays of hollow microneedles were adhered to the device via a two-sided Mylar adhesive, the same used for attaching layers the PMMA of the fluidic chip.

Screen-Printed Carbon Electrode (SPCE) Characterization and Functionalization:
SPCEs were purchased from DropSens. Activation of the electrodes was performed to clean their surfaces and to enhance their electrochemical activity and was performed in 0.1M H_2SO_4 by running 5 cyclic voltammogams from -1.1V to 0.5V at 100 mV/sec against a pseudo silver reference and carbon counter electrode residing on the SCPE. Electrodes were characterized using potassium ferricyanide in 1X PBS at pH 7.4 and modification of the electrode surface was done with diazonium chemistry. Diazoniums were made in-situ by adding 0.1mM, 1mM, or 2mM aminobenzonic acid and sodium nitrite into 0.1M H_2SO_4 for five minutes under sonication at room temperature. Deposition of the diazoniums onto SCPEs was performed via cyclic voltammograms from 0.2V to -0.6V at 100mV/sec versus the on-chip electrode pseudo Ag and a carbon counter electrode. Following depositions electrodes were washed with 100% ethanol and Di H_2O. Primary anti-myoglobin antibodies were bound to the diazonium modified SCPEs via EDC/NHS chemistry where a 100mM EDC and 25mM NHS in 0.1 MES Buffer pH 5.0 was applied to the electrodes for 1 hour then washed with the same buffer without the EDC or NHS. Immediately following, 2ppm primary antibody in 1X PBS pH 7.4 was applied to the electrodes for 1 hour to bind the antibodies to the surface of the electrode and then were washed with 1X PBS. BSA was used

to block unbound sites at 0.1wt/% in 1X PBS pH 7.4 for 30 minutes and was then washed with 1X PBS. Antibody modified electrodes were stored in 1X PBS pH 7.4 at 4°C until used.

Washing Experiments:

Washing experiments were performed using trypan blue followed by alternating 10cm plugs of 1X PBS and 4cm fluorinert. Plugs were pulled through a fluidic chip containing a SCPE and collected. Optical intensity measurements were performed on each of the collected 1X PBS plugs at 585nm using a nanodrop UV-Vis and compared to the stock trypan blue solution.

Automated Immunoassay Preparation and Testing:

Automated immunoassays were performed via plugging assay cartridges into fluidic chips housing antibody modified SPCEs. Reagents were stored in Tefzel tubing (1/16″ ID) marked on their exterior with a marker alternating at 10cm and 4cm lengths for the reagent and fluorinert spacer respectively. Reagents were pulled into the tubes by hand such that the assay was stored in the tube. Reagents that included the biomarker, secondary IgG, and washing plugs were filled in 10cm segments and the Fluorinert fluidic spacer were filled in 4mm segments. Detection plugs were made via filling tubes with a conductivity solution that contained both the peroxide and TMB mediator. Assay plugs were pulled through the fluidic chips via a syringe pump operating at 5ul/min. Once the assay plug was pulled through the fluid chip the detection plugs was applied and allowed to be pulled through the fluidic chamber. Detections were made by applying a potential of -0.2V during flow of the detection solution for 60 seconds versus the on-chip pseudo silver reference and carbon counter electrode.

Results and Discussion

Development of a wearable device for performing an automated immunoassay requires integration of multiple components to control the flow of reagents, extraction of biological fluid, sensing of the fluid, and housing for each of these systems. A laminate fabrication method was explored for creation of the microfluidic chip as the layer-by-layer assembly was amenable towards integrating a commercially available screen-printed carbon electrode between the layers as seen in the schematic in Figure 7-1. The chip was designed with an inlet and outlet port to deliver the reagents from the preloaded cartridges to perform the assay and clean the fluidic pathway following each reagent passage. An advantage to this fluidic fabrication system is the design turnaround time, facile assembly, and creation of lightweight devices due to the materials used.

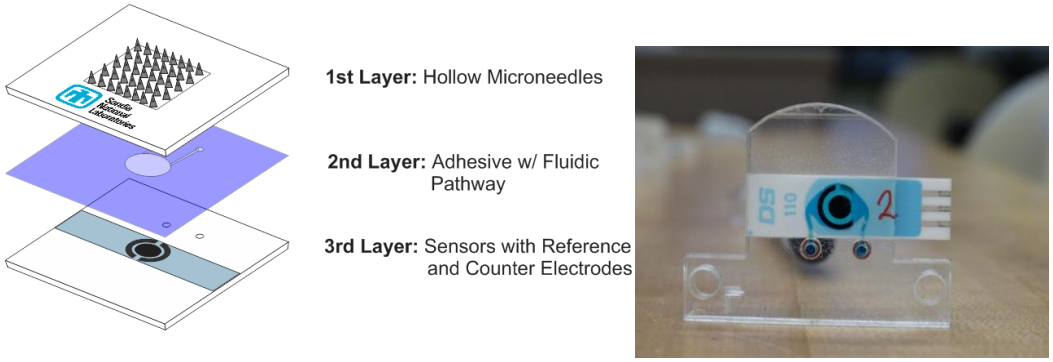

Figure 7-1: Screen-printed carbon electrode within a laminate microfluidic chip (right). SCPE substrate dimensions 10mm x 34mm. Trypan blue solution flown through channel to show fluidic connections and configuration of fluidic pathway. Schematic of the microfluidic chip with integrated SPCE drawn in CorelDraw (left).

Screen-printed carbon electrodes (SPCE) were chosen for the electrode material due to their successful history as an electrode for biosensor applications and for their commercial availability.[20] SPCEs in this study were first investigated for their electrochemical activity against on-chip pseudo silver reference and carbon counter electrode as seen in Figure 7-2. Cyclic voltammograms were performed using 5mM potassium ferricyanide, a common redox reversible molecule for characterizing electrodes,

in 1X PBS pH 7.4 and showed the SPCEs needed to be cleaned prior to use (Figure 7-8) based on redox peak heights that were poorly defined and because redox peak spacing was larger than the expected for carbon electrodes indicating poor electrode transfer kinetics (~210mV). Activation of carbon electrodes is a common method for improving their electrochemical response by removing surface impurities and an electrochemical technique was performed using cyclic voltammograms in 0.1M sulfuric acid as seen in Figure 7-8. Following electrochemical cleaning the SPCEs were retested in potassium ferricyanide at scan rates from 10 to 100mV/sec, which resulted in peak spacing of 165mV at 100mV/sec (compared to 210mV for un-cleaned electrodes) and less redox peak potential shifts compared to un-cleaned samples as seen in Figure 7-4. Figure 7-4b shows redox peaks currents plotted against the square root of the scan rate and the resulting plots were linear indicating a diffusion-controlled reaction. For all of the experiments moving forward electrodes were cleaned in this manner.

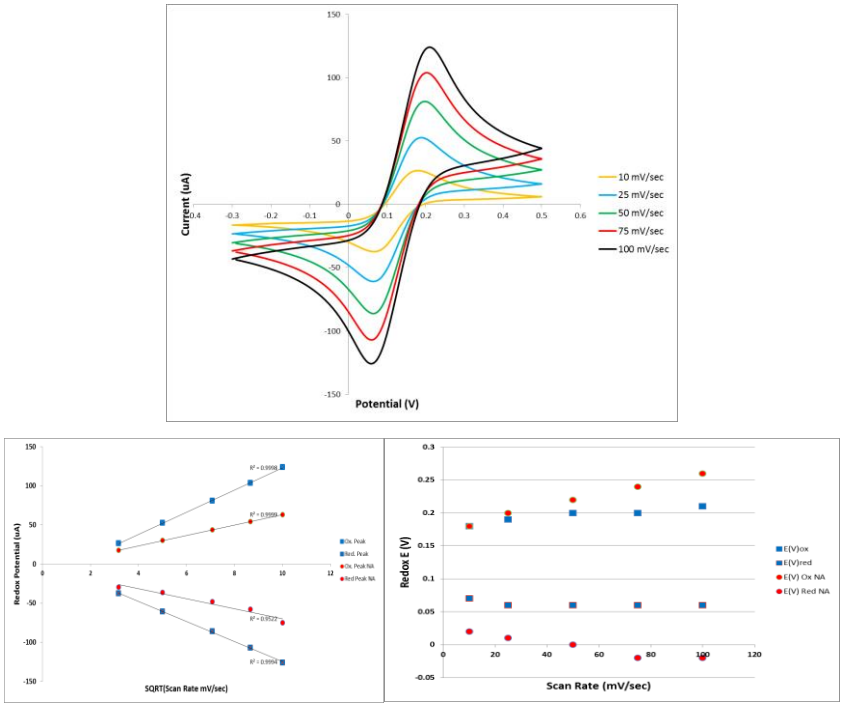

Figure 7-2: Electrochemical characterization of screen printed carbon electrodes in the presence of 5mM potassium ferricyanide in 1X PBS pH 7.4 with on-chip reference and counter electrode at varying scan speeds (top) and plot of potassium ferricyanide redox peak currents versus scan rate (bottom left) and redox peak potential versus scan rate (bottom right) on activated and non-activated electrodes.

Screen-printed carbon electrodes were integrated into laminate microfluidic chips to perform the automated on-chip electrochemical immunoassay and previous groups have incorporated screen-printed carbon electrodes into fluidic chips for detection of biomarkers with automated assays however not with laminate chips to our knowledge. Initial experiments were performed to determine the optimal fluidic pathway for delivery of the reagents necessary to perform the assay. Many of the previous studies used small width (~100um) meandering channels due to the issue of wettability of larger channel configurations, which can cause wetting of only one of the sides of the channel and restricts passage of reagents across the entire surface of the electrode.[16] These methods use an air spacer for separating the reagents such that no cross-contamination of the reagents occurs during cartridge loading, storage, or assembly of the assay. The reagents can be delivered

across the surface of the electrode such that a sandwich assay can be built automatically via delivery from a syringe pump. The initial channel design with meandering channel resulted in poor electrochemical response when tested using cyclic voltammograms in a solution of 5mM potassium ferricyanide as seen in Figure 7-3. A small oxidation peak was noticed with no resulting reduction wave that is typically seen with the reversible molecule. We believe a couple issues are causing this effect. First, the assembly process for the laminate chip involves compressing the layers to 500psi to ensure a proper bond, which compromises the electrical connections to the electrodes and second the adhesive may be interfering with the surface chemistry of the electrochemical reactions. In the previous reports that used meandering channels, the fluidic pathways was fabricated using PDMS and O-zone was used to bond the PDMS fluidics to the electrodes thus negating the pressing step seen in our technique. An alteration of the fluidic pathway was next performed as seen in Figure 7-3b and a single channel with a wider fluidic pathway (2mm) was explored that included a portion of the working, reference, and counter electrodes however electrochemical characterization showed poor redox activity, again suggesting that the fluidic configuration wasn't suitable for electrochemical measurements. A fluidic pathway that encompassed each of the three electrode electrodes was investigated as seen in Figure 7-3c. The electrochemical response of this fluidic channel produced a redox response that resembled the response seen with SCPEs in solution without being housed in a fluidic chip. While the electrochemical results of this fluidic configuration were positive, improper wetting was seen when an air spacer was used to separate the reagents while flowing sequential plugs through the fluidics. In light of this fact we investigated a fluidic spacer instead of the air spacer to continuously wet of the fluidic channel during delivery of the reagents.

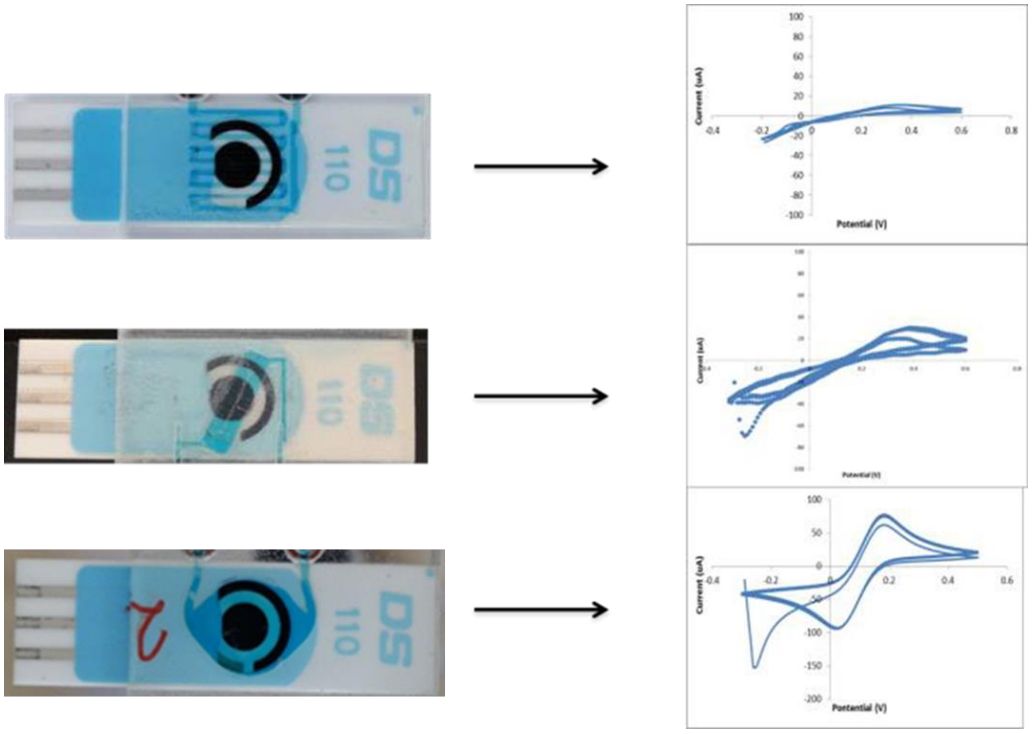

Figure 7-3: Comparison of fluidic channel patterns of a SCPE on a microfluidic chip to resulting electrochemical signal in 5mM potassium ferricyanide in 1X PBS pH 7.4.

Fluorinert is a fluorocarbon fluid that has been used in various microfluidic applications for biosensor and bioassay applications and since it's immiscible in aqueous solutions it was investigated as a spacer for separating the reagents and for keeping the fluidic chamber wet during the assay. Additionally, we believe the immiscibility of fluorinert will help clean the channel following the washing plug and reduce the number of washing plugs necessary to perform the assay thus reducing the total time required to perform the assay. Initial tests were performed with two different flourinerts, FC-40 and FC-72, and electrochemical measurements verified that each type of fluorinert had no electrochemical response when tested with cyclic voltammetry on the SPCEs as seen in Figure 7-5. Tefzel tubing was filled with alternating fluorinert and reagent plugs containing the PBS/ferricyanide mixture was then flown through the microfluidic chip and over the screen printed carbon electrode as seen schematically in Figure 7-5. Chronoamperometric scans

were run at +1.0V while the solutions were pulled through the chip at 5ul/min using a syringe pump and the resulting current was monitored. Immediately the FC-72 evaporated when the solution reached the surface of the electrode and was not studied from that point forward. We believe the large difference in boiling point (56^0C vs. 165^0C) attributed to this result. For these tests the microneedle array was not attached to the microfluidic chip such that visualization of the flow of reagents could be monitored while optimizing the fluidic spacer. A typical result of the flow through experiments using FC-40 is seen in Figure 7-9. Current intensity increased as the potassium ferricyanide/PBS solution entered the fluidic chamber due to the salinity of the solution, which allows current to pass between the electrodes and the current dropped once the fluorinert pushed the reagent solution off the fluidic chip due to the electrical resistance seen with FC-40.[21] Initial tests showed that not all fluorinert plugs cleared the electrode chamber and plug length was investigated. Three plug lengths were investigated (1, 2, and 4cm) which corresponded to 2uL, 4uL, and 8uL with the microfluidic chamber volume being approximately 6ul in total volume measured from fluid entering the fluidics to exiting the outlet port. A plug was considered successful if ferricyanide/PBS plug entered the fluidic chamber and caused a maintained increase in current and then a sharp decrease in current, which was also maintained, at the entrance of the fluorinert plug. When the plug lengths were shortened to less than the volume of the fluidic chamber the fluorinert plugs were susceptible of not passing through the chamber and needed additional fluorinert plugs to enter prior to being able to be removed. Increasing the length of the fluorinert plug such that the plug volume was larger than the volume of the chamber caused plugs to flow into the chamber and out without leaving behind residual spacer fluid as seen in Figure 7-4.

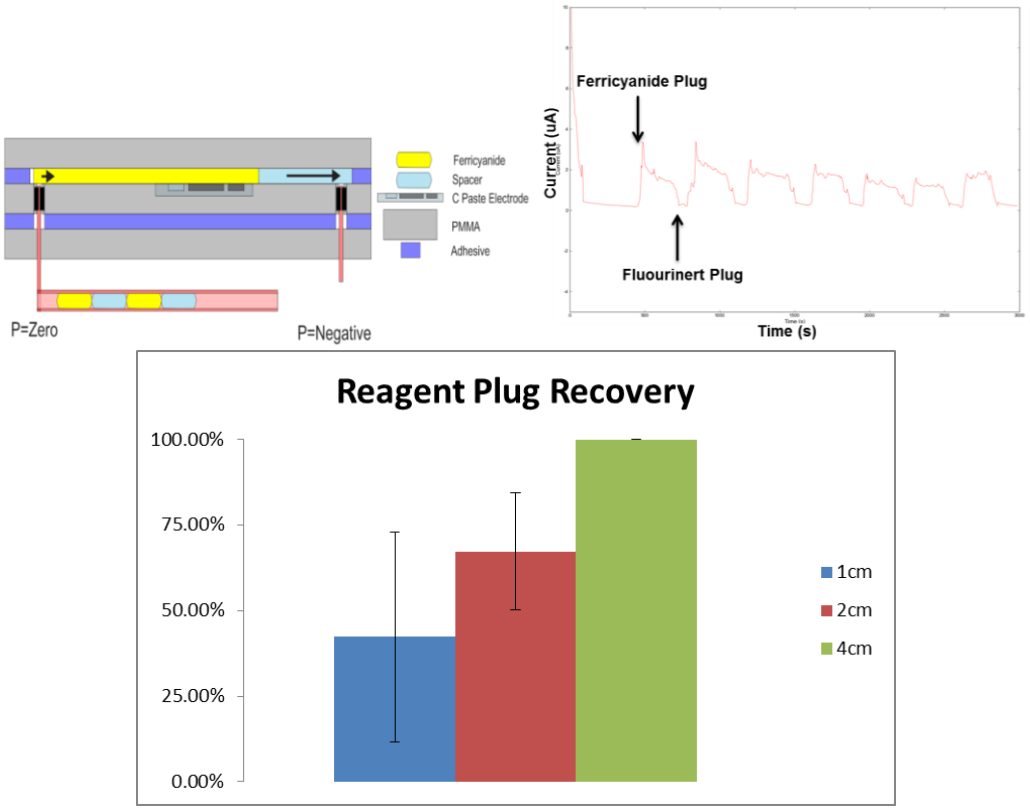

Figure 7-4: Electrochemical characterization of fluidic plugs within fluidic chip. Alternating plugs of 10cm 5mM potassium ferricyanide in 1X PBS and 4cm of fluorinert while 1V is applied across the working electrode. Plugs are pulled through fluidic chamber at 5ul/min.

An essential component to the automated immunoassay is washing of the electrode surface and fluidic chamber between each incubation step such that the prior reagents are no longer present. Failure to remove residual material can cause an increase in the detection signal due to residual target analyte in the fluidic chamber and the number of washing plugs was investigated for their ability to remove residual dye from the electrode chamber. Trypan blue was used as a test material to determine how well the alternating 1X PBS and fluorinert plugs removed the dye from the fluidic chamber. The chamber was initially filled with the trypan blue solution than a cartridge containing alternating plugs of 1X PBS pH 7.4 at 10cm in length and fluorinert FC-40 at 4cm in length were flown into the fluidic chamber at 5ul/sec (Figure 7-5). PBS plugs were collected as they left the microfluidic chip following washing of the chamber and were measured for their optical

density compared to the stock solution of trypan blue. Following a single passage of the washing plug (1X PBS and fluorinert) the optical density of the wash plugs resembled that of the 1X PBS control indicating that one sequence of the wash plugs cleaned the fluidic chamber of the dye. During visual inspection, the fluorinert plug acted as a physical cleaner of the fluidic chamber since the aqueous dye solution was immiscible in fluorinert and was pushed from the reservoir without any noticeable residual dye. Slight increases in optical density were noticed on the third and fourth run however upon visual inspection this was attributed to dye remaining in the space around the O-ring of the outlet side of the fluidic chip thus this increase in optical density was not from residual dye within the channel and wouldn't lead to improper results of the immunoassay. One sequence of 10cm of 1X PBS and 4cm of fluorinert were chosen as the optimal washing amount and was used throughout the following experiments.

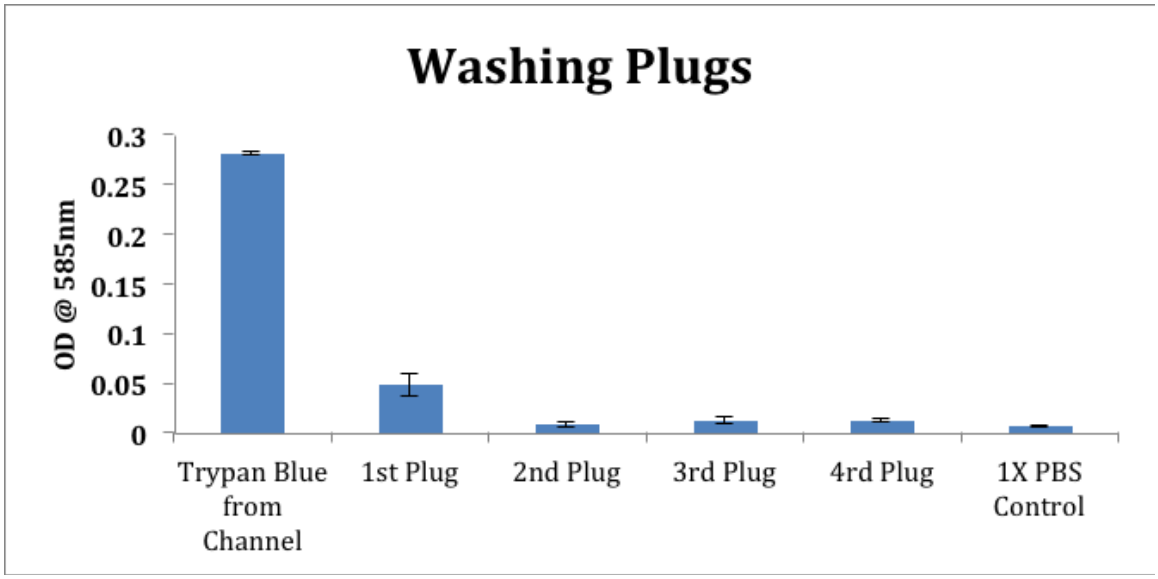

Figure 7-5: Washing experiments of alternating 1X PBS and fluorinert after flowing trypan blue through the chamber. Optical intensity of plugs measured at 585nm.

Surface modification of the screen printed carbon electrode was necessary for adherence of the primary antibody and was investigated next. Groups have previously studied the synthesis, deposition, and characterization of aryl diazoniums for sensing

applications and we sought a carboxyl terminated diazonium for this application due to convenient EDC/NHS chemistry used to bond biomolecules to the surface of a functionalized electrode.[22] This diazonium was made in-situ in an acidic solution and deposited electrochemically onto screen-printed carbon electrodes as schematically in Figure 7-6a and the electrochemical reduction via cyclic voltammetry as seen in Figure 7-6b. Diazonium precursor concentrations effect deposition and surface cover so the initial experiments studied making the in-situ carboxyl diazonium with 0.1mM, 1mM, or 2mM for both the aminobenzoic acid and sodium nitrite in a standard solution of 0.1M sulfuric acid. Electrochemical reduction was performed using one cyclic voltammogram as seen in Figure 7-5b and as anticipated larger precursor concentrations lead to larger reduction peaks, indicative of more surface coverage. To determine how each of the precursor concentrations affected the surface coverage, blocking of modified screen printed carbon electrodes were tested in 5mM potassium ferricyanide and compared to unmodified electrodes as seen in Figure 7-6c. The goal of these experiments was to find a precursor concentration that blocked a portion of the electrode however did not completely block the electron transfer process, which can restrict the immunoassay signal thus reducing detection capabilities. Based on the blocking tests 1mM of each of the precursors was chosen since it had roughly 50% blockage relative to the unmodified electrode. This concentration and procedure for deposition of the in-situ carboxyl diazonium was used throughout the following experiments. Consistency of the carboxyl diazonium was also investigated to ensure that comparable surface coverage was seen throughout each of the electrodes modified. When studying the modified SPCEs the average reduction potential was -25.52uA $\pm$ 0.21. The data derived for these calculations was taken from multiple batches of the in-situ diazonium created and indicates that there was little fluctuation in batch-to-to preparation of the surface chemistry.

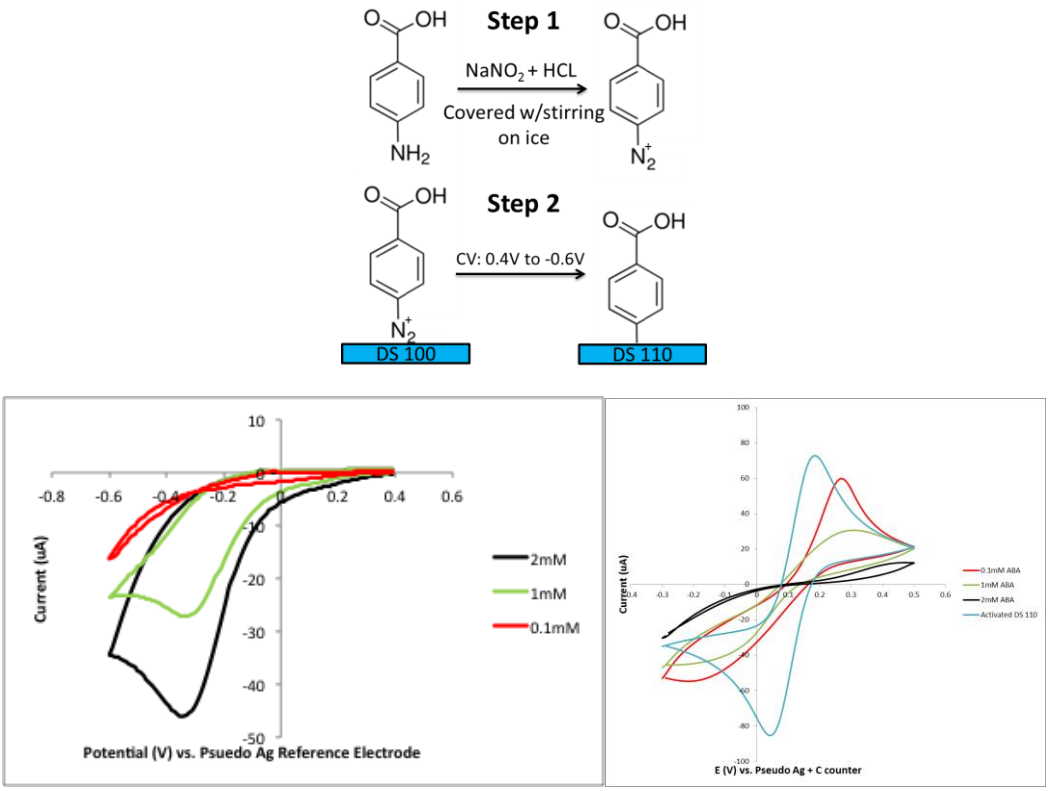

Figure 7-6: Schematic of in-situ carboxyl diazonium synthesis and electrochemical deposition (top). Overlay of electrochemical reduction via one cyclic voltammogram of in-situ diazonium on SCPE (vs pseudo silver reference electrode and carbon counter electrode) at 100mV/sec (bottom left) and blocking measurements of deposited in-situ carboxyl diazoniums on SPCEs at varying concentrations of diazonium precursor in 5mM potassium ferricyanide in 1X PBS (bottom right).

For the automated immunoassay a tube was loaded such that reagent plugs were 10cm in length and fluorinert spacer plugs were 4cm as seen in the schematic in Figure 7-7. All plugs were loaded by hand via a 1mL syringe and tubing was marked with a marker at measured intervals so that the required volume per plug was properly loaded and tubes were stored at 4°C until use. Reagent filled tubes were connected to fluidic chips containing the primary antibody functionalized screen printed carbon electrodes with the outlet fluidic port attached to a syringe pump. The tubing connected to the syringe pump was filled with water so less pressure was needed to pull the reagent plugs through the fluidic chip. The fluidic chip was preloaded with 1X PBS to keep the surface bound antibodies hydrated and

the chamber walls wet to avoid bubble formation during operation. An extraction rate of 20ul/min was applied to the fluid system until the plugs began moving then the extraction rate was changed to 5ul/min for the rest of the assay. Previous groups using a similar flow through electrochemical assay didn't incorporate the detection solution within the reagent-loaded tubing. In our experience when the detection solution (TMB and H2O2) was loaded into the tubing it became oxidized as it passed the section of tubing where the secondary antibody previously resided. We believe some portion of the secondary IgG with HRP tag stuck to the side of the tubing and caused the oxidation seen due to the color change from clear to blue. To avoid this issue we created a reagent tube and a detection tube, which was attached to the fluidic chip once the reagent tube was pulled through. Without changing the flow rate the tubes were exchanged and the electrochemical detection was performed while pumping at 5ul/min. We investigated modifying the interior of the tubing with BSA to attempt to restrict adhesion of the secondary antibody from the tubing walls however the restrictive effect wasn't enough to stop oxidation of the detection solution. The biomarker, myoglobin, was chosen as the test analyte due to its history as a protein indicative of both cardiac and skeletal muscle damage.[23,24] A clinically relevant concentration (100ppb) was tested relative to the control using chronoamperometric scans at -0.2V until the current stabilized. Resulting detection currents of the biomarker assay were -2.89uA compared to -0.95uA for the control indicating a discernable difference for detection. These results indicate that the stored reagents could perform the assay with suitable cleaning of the fluidics between reagents plugs in an automated fashion. Due to optimization of the plug lengths total procedure time was 21.5 minutes.

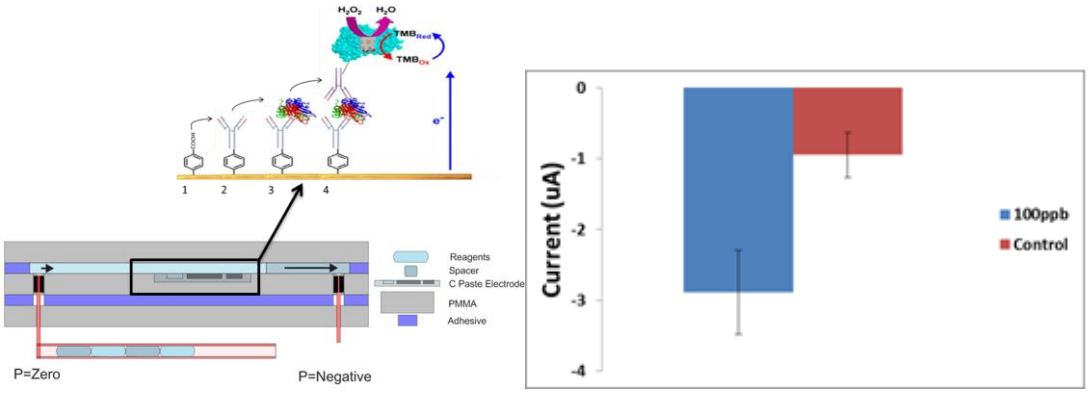

Figure 7-7: Schematic of cross-section of device with reagents flowing through channel with zoomed in schematic of sandwich assay progression from surface modification to electrochemical detection of biomarker (A). Electrochemical detection of biomarker with flow through assay detected at -1V compared to control.

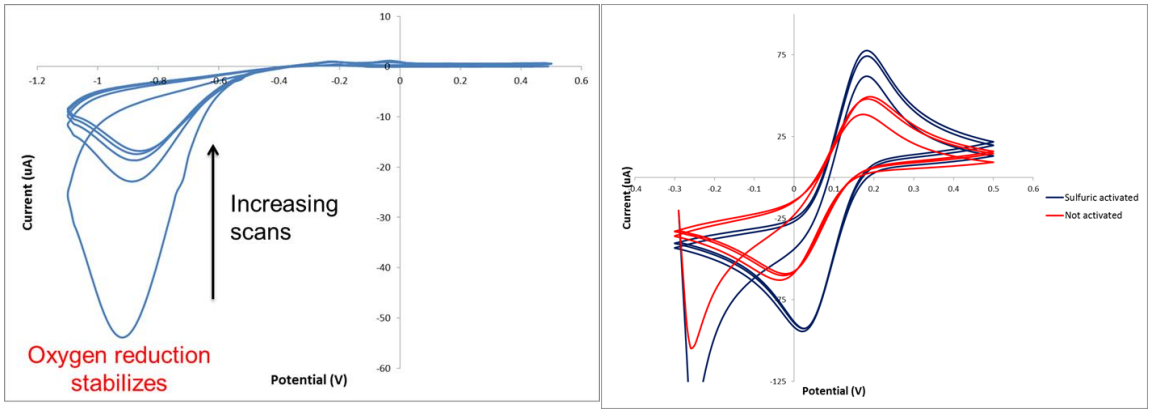

Figure 7-8: Cyclic voltammograms of electrochemical cleaning procedure in 0.1M sulfuric acid against on-chip pseudo silver reference and carbon counter electrode at 100mV/sec from -1.1V to 0.5V (left). Overlays of cyclic voltammograms performed in 5mM potassium ferricyanide for cleaned and uncleaned SCPEs (right).

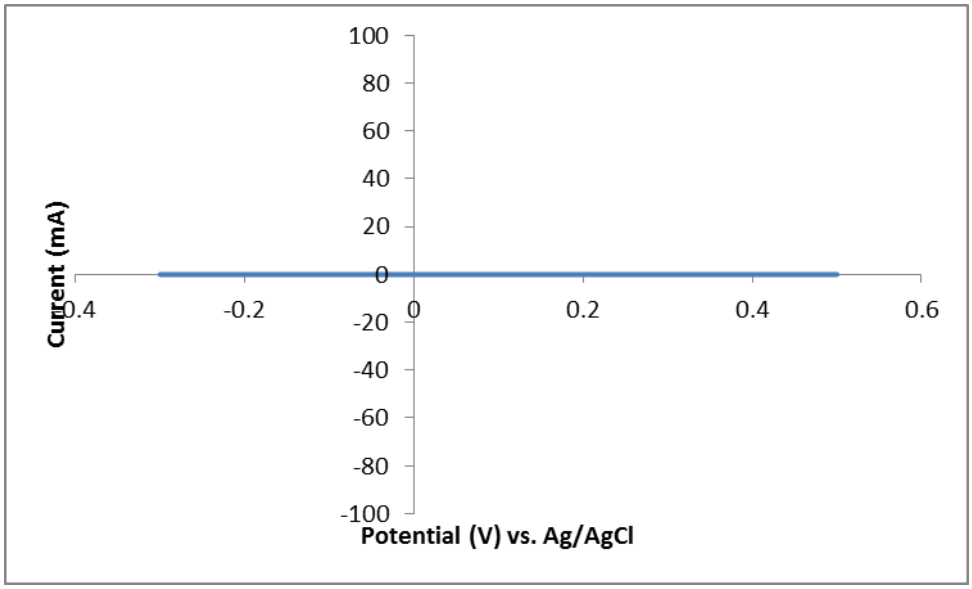

Figure 7-9: Electrochemical response of fluorinert (FC-40). Cyclic voltammogram was run through the same potential window as the potassium ferricyanide solution (-0.3V to 0.5V at 100mV/sec) versus a Ag/AgCl reference and Pt wire counter electrode.

Conclusion

An automated electrochemical immunoassay was developed for application in wearable sensing of clinically significant biomarkers. A laminate microfluidic chip was designed and created such that it incorporated a commercially available screen printed carbon electrode with inlet and outlet ports. Fluidic pathways were created such that the electrochemical properties were optimized. Screen-printed carbon electrodes were electrochemically modified with a carboxyl diazonium such that an antibody could be adhered for creation of an automated immunoassay. The automation of the immunoassay was performed by loading the reagents into a tube and separating each of the reagents by a fluorocarbon fluid. Lengths of the fluorocarbon spacer and the washing solutions were optimized to reduce the amount of the solution necessary to perform the assay. Once the conditions for the device were optimized a clinically relevant concentration of cardiac biomarker was quantified. Future studies will focus on incorporating a hollow microneedle array onto the chip and controlling the extracted fluid and reagents for the assay.

References

[1] Papadea, C., Foster, J., Grant, S., Ballard, S. A., Cate, J. C., Southgate, W. M., & Purohit, D. M. (2002). Evaluation of the i-STAT portable clinical analyzer for point-of-care blood testing in the intensive care units of a university children's hospital. *Annals of Clinical & Laboratory Science*, *32*(3), 231-243.

[2] Gatzoulis, L., & Iakovidis, I. (2007). Wearable and portable eHealth systems.*Engineering in Medicine and Biology Magazine, IEEE*, *26*(5), 51-56.

[3] Garcia, A., Rack-Gomer, A. L., Bhavaraju, N. C., Hampapuram, H., Kamath, A., Peyser, T., ... & Cobelli, C. (2013). Dexcom G4AP: an advanced continuous glucose monitor for the artificial pancreas. *Journal of diabetes science and technology*, *7*(6), 1436-1445.

[4] Kim, D. H., Lu, N., Ma, R., Kim, Y. S., Kim, R. H., Wang, S., ... & Rogers, J. A. (2011). Epidermal electronics. *science*, *333*(6044), 838-843.

[5] Dagdeviren, C., Yang, B. D., Su, Y., Tran, P. L., Joe, P., Anderson, E., ... & Rogers, J. A. (2014). Conformal piezoelectric energy harvesting and storage from motions of the heart, lung, and diaphragm. *Proceedings of the National Academy of Sciences*, *111*(5), 1927-1932.

[6] Kim, Y. C., Park, J. H., & Prausnitz, M. R. (2012). Microneedles for drug and vaccine delivery. *Advanced drug delivery reviews*, *64*(14), 1547-1568.

[7] El-Laboudi, A., Oliver, N. S., Cass, A., & Johnston, D. (2013). Use of microneedle array devices for continuous glucose monitoring: a review.*Diabetes technology & therapeutics*, *15*(1), 101-115.

[8] Mukerjee, E. V., Collins, S. D., Isseroff, R. R., & Smith, R. L. (2004). Microneedle array for transdermal biological fluid extraction and in situ analysis.*Sensors and Actuators A: Physical*, *114*(2), 267-275.

[9] Miller, P. R., Skoog, S. A., Edwards, T. L., Lopez, D. M., Wheeler, D. R., Arango, D. C., ... & Narayan, R. J. (2012). Multiplexed microneedle-based biosensor array for characterization of metabolic acidosis. *Talanta*, *88*, 739-742.

[10] Miller, P. R., Xiao, X., Brener, I., Burckel, D. B., Narayan, R., & Polsky, R. (2014). Microneedle-Based Transdermal Sensor for On-Chip Potentiometric Determination of K+. *Advanced healthcare materials*, *3*(6), 876-881.

[11] Corrie, S. R., Fernando, G. J., Crichton, M. L., Brunck, M. E., Anderson, C. D., & Kendall, M. A. (2010). Surface-modified microprojection arrays for intradermal biomarker capture, with low non-specific protein binding. *Lab on a Chip*, *10*(20), 2655-2658.

[12] Van Weemen, B. K., & Schuurs, A. H. W. M. (1971). Immunoassay using antigen—enzyme conjugates. *FEBS letters*, *15*(3), 232-236.

[13] Lee, B. S., Lee, J. N., Park, J. M., Lee, J. G., Kim, S., Cho, Y. K., & Ko, C. (2009). A fully automated immunoassay from whole blood on a disc. *Lab on a Chip*, *9*(11), 1548-1555.

[14] Sista, R. (2007). *Development of a digital microfluidic lab-on-a-chip for automated immunoassay with magnetically responsive beads*. ProQuest.

[15] Linder, V., Sia, S. K., & Whitesides, G. M. (2005). Reagent-loaded cartridges for valveless and automated fluid delivery in microfluidic devices. *Analytical chemistry*, *77*(1), 64-71.

[16] Yang, F., Zuo, X., Li, Z., Deng, W., Shi, J., Zhang, G., ... & Fan, C. (2014). A Bubble-Mediated Intelligent Microscale Electrochemical Device for Single-Step Quantitative Bioassays. *Advanced Materials*, *26*(27), 4671-4676.

[17] Zhang, L., Zhang, Y., Wang, C., Feng, Q., Fan, F., Zhang, G., ... & Jiang, X. (2014). Integrated Microcapillary for Sample-to-Answer Nucleic Acid Pretreatment, Amplification, and Detection. *Analytical chemistry*, *86*(20), 10461-10466.

[18] Miller, P. R., Xiao, X., Brener, I., Burckel, D. B., Narayan, R., & Polsky, R. (2014). Microneedle-Based Transdermal Sensor for On-Chip Potentiometric Determination of K+. *Advanced healthcare materials*, *3*(6), 876-881.

[19] Publication forthcoming

[20] Hart, J. P., Crew, A., Crouch, E., Honeychurch, K. C., & Pemberton, R. M. (2005). Some recent designs and developments of screen-printed carbon electrochemical sensors/biosensors for biomedical, environmental, and industrial analyses. *Analytical letters*, *37*(5), 789-830.

[21] http://multimedia.3m.com/mws/media/64888O/fluorinert-electronic-liquid-fc-40.pdf

[22] Gooding, J. J. (2008). Advances in interfacial design for electrochemical biosensors and sensors: aryl diazonium salts for modifying carbon and metal electrodes. *Electroanalysis*, *20*(6), 573-582.

[23] McCord, J., Nowak, R. M., McCullough, P. A., Foreback, C., Borzak, S., Tokarski, G., ... & Weaver, W. D. (2001). Ninety-minute exclusion of acute myocardial infarction by use of quantitative point-of-care testing of myoglobin and troponin I. *Circulation*, *104*(13), 1483-1488.

[24] Vassallo, J. D., Janovitz, E. B., Wescott, D. M., Chadwick, C., Lowe-Krentz, L. J., & Lehman-McKeeman, L. D. (2009). Biomarkers of drug-induced skeletal muscle injury in the rat: troponin I and myoglobin. *Toxicological sciences*, kfp166.

Conclusion

The presented work details advances in microneedle-based sensing systems and novel fabrication and coatings for the creation of hollow microneedles and hollow microneedle arrays. Prior work showed the technology was feasible as a sensing modality however lacked the sophistication to detect entities beyond glucose. This thesis investigated incorporating electrochemical sensors and biosensors with hollow microneedles for detecting a range of analytes including lactate, pH, ascorbic acid, hydrogen peroxide, potassium, and myoglobin for a range of applications such as point-of-care devices and athletic monitoring among others. Carbon was the choice electrode material and was studied in the form of carbon fibers, carbon paste, porous carbon, porous graphene, and commercially available screen-printed carbon electrodes and modified via electrochemical and chemical surface coatings, enzyme incorporation, ion selective membranes, and complex sandwich assays for the mentioned analytes. Two rapid prototyping systems were used for creation of the hollow microneedles, microstereolithography and two-photon polymerization utilizing laser direct write, and material strength and toxicity were determined for the materials used in these systems. Metal coatings were deposited and characterized on hollow polymer microneedles and planar substrates for their residual stress, grain size, toxicity against dermal cell types, and ability to puncture porcine tissue. A novel electromolding method was created to increase the scalability of hollow microneedle array production and creation of flexible microneedle substrates that better conform to the skin than previous designs. Lastly, a cartridge system was created for the autonomous storage and assembly of a sandwich assay for myoglobin but could be tailored for a range of biomarkers. Futures projects will need to study the functionality of these devices on humans in both inactive and active states, determine what biomolecules and biomarkers exist in the dermal space and if correlations can be made with clinical established intravenous levels, effective lifetime of the devices, developed valves for controlling detection solution and reagents if necessary, material toxicity over time, and usability and acceptance of the device on the end user.